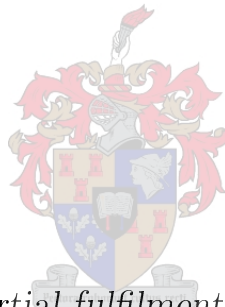


A multibody modelling workflow to investigate anterior cruciate ligament biomechanics

by

Jacobus Everhardus van Niekerk



Thesis presented in partial fulfilment of the requirements for the degree of Master of Engineering (Mechanical) in the Faculty of Engineering at Stellenbosch University

Supervisor: Dr. J.H. Müller

Co-supervisor: Prof. G. Venter

December 2019

Declaration

By submitting this thesis electronically, I declare that the entirety of the work contained therein is my own, original work, that I am the sole author thereof (save to the extent explicitly otherwise stated), that reproduction and publication thereof by Stellenbosch University will not infringe any third party rights and that I have not previously in its entirety or in part submitted it for obtaining any qualification.

Date: December 2019

Copyright © 2019 Stellenbosch University
All rights reserved.

Abstract

A multibody modelling workflow to investigate anterior cruciate ligament biomechanics

J.E. van Niekerk

*Department of Mechanical and Mechatronic Engineering,
University of Stellenbosch,
Private Bag X1, Matieland 7602, South Africa.*

Thesis: MEng (Mech)

December 2019

Anterior cruciate ligament (ACL) injury often occurs in high intensity sports involving contact or sudden changes of direction. Knee biomechanics change due to ACL injury and cause other ligaments and structures such as the medial collateral ligament (MCL) and the menisci to be at risk of concurrent injury. Presented in this study is a joint-level model of a human knee that was developed using a multibody modelling workflow and experimental data from the Open Knee(s) project.

The model was developed in MSC Adams and simulated knee biomechanics between 0° and 30° of flexion for an intact and ACL deficient (ACLd) knee. Three different loading conditions were applied to the joint: (1) 100 N anterior-posterior (AP) tibial drawer, applied in 10 N increments, (2) 10 Nm varus-valgus (VV) torque, applied in 2.5 Nm increments and (3) 5 Nm internal-external (IE) tibial torque, applied in 1 Nm increments. These loading conditions were applied individually as isolated degree of freedom loads, and simultaneously as combined degree of freedom loads. Loading conditions were applied to measure model predicted joint kinematics, ligament forces and tibiofemoral and meniscofemoral contact force. A sensitivity analysis was performed to investigate the sensitivity of modelling output to changes in modelling parameters. One parameter was changed at a time.

Kinematic output was validated against experimental tibiofemoral testing data and had root mean square (RMS) errors of less than 4.50 mm for position and less than 6.5° for orientation. Predicted model outputs were the most sensitive to changes in the zero-load length (ZLL) of ligaments ($> 30\%$ change in output parameter for 20% change in ZLL). Changes in compliant contact stiffness also resulted in changes in predicted output, but to a lesser extent than

changes in ZLL ($< 20\%$ change in output for 50% change in contact stiffness). The model was least sensitive to changes in ligament stiffness ($< 10\%$ change in output for a 30% change in ligament stiffness). For the intact knee, the greatest force in the ACL was predicted for a combination of anterior tibial loading, valgus torque and internal tibial torque (151 N). For the ACLd knee, the model predicted that AP and IE laxity increased by 343% and 28% respectively when a 100 N tibial drawer load was applied. For a combination of 100 N tibial drawer load, 10 Nm valgus torque and 5 Nm internal tibial torque, AP and IE laxity increased by 261% and 37% respectively. ACL deficiency resulted in an increase in MCL force (56 N at 30° flexion) and meniscus contact force for tibial drawer loading (33.9 N and 14.7 N at 30° flexion on the medial and lateral sides respectively). The increase in meniscus contact force coincided with joint motion that has been reported to result in meniscus injury.

This study developed a multibody model of the knee using a multibody modelling approach. The model showed how anterior-posterior laxity, internal-external tibial rotation, meniscal contact force and MCL force increased due to ACL deficiency. The model was most sensitive to changes in the ligament zero-load length and least sensitive to changes in ligament stiffness. The model confirmed previous findings describing the mechanism of meniscal ramp lesions, and the predicted meniscomfemoral contact force was similar to what was measured experimentally and predicted by other models.

Uittreksel

'n Multi-liggaam model vir die ondersoek van anterior kruisligament biomeganika

(“A multibody modelling workflow to investigate anterior cruciate ligament biomechanics”)

J.E. van Niekerk

*Departement Meganiese en Megatroniese Ingenieurswese,
Universiteit van Stellenbosch,
Privaatsak X1, Matieland 7602, Suid Afrika.*

Tesis: MIng (Meg)

Desember 2019

Anterior kruisligament (ACL) beserings kom dikwels voor in hoë intensiteit sportsoorte wat kontak of skielike rigtingveranderinge behels. Knie-biomeganika verander as gevolg van 'n ACL-besering en veroorsaak dat ander ligamente en strukture, soos die mediale kollaterale ligament (MCL) en die menisci, die risiko loop vir gepaartgaande besering. In hierdie studie word 'n multiliggaam-model ('multibody model') van 'n menslike knie aangebied wat ontwikkel is met behulp van eksperimentele data van die 'Open Knee(s)' projek.

Die model is ontwikkel in MSC Adams en was gebruik om knie-biomeganika tussen 0° en 30° fleksiehoeke vir 'n ongeskonde en ACL-lose (ACLd) knie te ondersoek. Drie verskillende lastoestande was op die knie toegepas: (1) 100 N anterior-posterior (AP) tibiale las ('tibial drawer'), aangewend in inkremente van 10 N, (2) 10 Nm varus-valgus (VV) draaimoment, aangewend in inkremente van 2.5 Nm en (3) 5 Nm interne-eksterne (IE) tibiale draaimoment, aangewend in 1 Nm inkremente. Hierdie lastoestande is afsonderlik toegepas as geïsoleerde vryheidsgraad belading, en gesaamentlik as gekombineerde vryheidsgraad beladings. Lastoestande is toegepas om die voorspelde gewrigs-kinematika, ligamentkragte, tibiofemorale en meniscofemorale kontakkrage te meet. 'n Parametriese studie is uitgevoer om die sensitiwiteit van modelleringsuitsette vir veranderinge in modelleringsparameters te ondersoek. Een parameter is op 'n slag verander.

Kinematiese uitset is gevalideer op grond van eksperimentele tibiofemorale toetsdata en het 'root mean square' (RMS) foute van minder as 4.5 mm vir posisie en minder as 6.5° vir oriëntasie. Voorspelde modeluitsette was die sensitiefste vir veranderinge in die nulbelastinglengte ('zero-load length', ZLL) van ligamente ($> 30\%$ verandering in die uitsetparameter vir 20% verandering van die ZLL). Veranderinge in die kontakstyfheidparameter het ook gelei tot veranderinge in die voorspelde uitset, maar tot 'n mindere mate as veranderinge in ZLL ($< 20\%$ verandering in uitset vir 50% verandering in kontakstyfheidparameter). Die model was die minste sensitief vir veranderinge in ligamentstyfheid ($< 10\%$ verandering in uitset vir 30% verandering in ligamentstyfheid). Vir die ongeskonde knie is die grootste krag in die ACL voorspel vir 'n kombinasie van anterior tibiale las, valgus-draaimoment en interne tibiale draaimoment (151 N), wat groter is as wat in die literatuur gemeld word. Vir die ACLd-knie het die model voorspel dat die laksheid ('laxity') van AP translasie en IE rotasie onderskeidelik met 343% en 28% toegeneem het toe 'n anterior tibiale las van 100 N aangewend is. Vir 'n kombinasie van 100 N tibiale las, 10 Nm valgus-draaimoment en 5 Nm interne tibiale draaimoment, het AP en IE-laksiteit onderskeidelik met 261% en 37% toegeneem. ACL-tekort het gelei tot 'n toename in MCL-krag (56 N by 30° fleksie) en meniscus-kontakkrag vir die aangewende anterior tibiale las (33.9 N vir die mediale en 14.7 N vir die laterale meniscus by 30° fleksie). Die toename in die kontakrag van die menisci het gepaard gegaan met die kniebewegings wat na bewering tot meniscus besering lei.

Hierdie studie het 'n multi-liggaam model van die knie ontwikkel. Die model het voorspel hoe anterior-posterior laksheid, interne-eksterne tibiale rotasie, meniscus kontakrag en MCL-krag toegeneem het as gevolg van 'n anterior kruisligament-tekort. Die model was die mees sensitief vir veranderinge in die nulbelastinglengte van ligamente en die minste sensitief vir veranderinge in die ligamentstyfheid. Die model kon die meganisme van meniscus skeure ('meniscal ramp-lesions') wat in die literatuur beskryf is bevestig, en die voorspelde krag was soortgelyk aan wat eksperimenteel gemeet is en deur ander modelle voorspel is.

Acknowledgements

I would like to express my sincere gratitude to the following people:

To Dr. Cobus Müller, my supervisor, for his advice and guidance throughout this study. Thank you for continuing to provide feedback and suggesting improvements in my work, despite being on a different continent for the latter half of the year.

To Prof. Gerhard Venter, my co-supervisor, for his advice and suggestions while writing this document. Thank you for making time to provide feedback on my work and for being available to answer my queries.

To Llewellyn and Ebard, my fellow BERG students, for numerous ‘kantoor krieket’ innings. You guys made the struggles and frustrations of modelling worthwhile.

To Jan, for keeping me company during long runs in Jonkershoek, while I ponder about how to get my model working.

To Ananja, for your continuous love and support. Thank you for motivating me to do my best.

And finally, to my parents, Everhard and Nina, and my brother, Dawie, for their love and support (emotionally and with food). Thank you for giving me the opportunity to further my studies.

Contents

Declaration	i
Abstract	ii
Uittreksel	iv
Acknowledgements	vi
Contents	vii
List of Figures	ix
List of Tables	xi
1 Introduction	1
1.1 Background	1
1.2 Motivation	1
1.3 Objectives	2
1.4 Scope	2
2 Literature review	4
2.1 Anatomy and functions of the knee joint	4
2.2 Mechanisms of ACL injury	10
2.3 Computational techniques for modelling the knee joint	11
2.4 Current state of the art multibody models	19
3 Materials and methods	21
3.1 Open Knee(s) project dataset	21
3.2 Computational model formulation	23
3.3 Using the model to simulate ACL biomechanics	33
3.4 Parametric study	36
3.5 Model validation	39
4 Results	40
4.1 Model validation	40

CONTENTS

viii

4.2	Ligament wrapping	41
4.3	Knee kinematics	42
4.4	Ligament forces	48
4.5	Contact forces	51
4.6	Loading of the menisci in the ACL deficient knee	52
4.7	Parametric study	54
5	Discussion	57
5.1	Model validation	57
5.2	Ligament wrapping	58
5.3	Knee kinematics	60
5.4	Ligament forces	62
5.5	Contact forces	65
5.6	Loading of the menisci in the ACL deficient knee	68
5.7	Parametric study	69
5.8	Model limitations	70
6	Conclusion	72
6.1	Objectives	72
6.2	Future work	73
	Appendices	74
A	MRI settings	75
B	Estimation of experimental uncertainty	78
C	RMS errors	79
D	Parametric study	81
	List of References	85

List of Figures

2.1	Lateral view of the right lower limb	5
2.2	Anterior view of the extended right knee	6
2.3	Parasagittal section trough the extended right knee	7
2.4	Anterior view of the right knee at full extension	8
2.5	Posterior view of the extended right knee	9
2.6	The six degrees of freedom of the knee	9
2.7	Force-elongation relationship for a ligamentous fibre	11
2.8	A schematic representation of an analytical model of the knee	12
2.9	A multibody model of the knee	13
2.10	A finite element model of the knee	15
3.1	Model coordinate system in terms of the KJCS	24
3.2	Ligament wrapping of the MCL	26
3.3	Model input and output boundary conditions	30
3.4	A sample of experimental data filtering	31
3.5	Schematic comparison between the experiment and the model	33
3.6	Desired loading profile for 30° AP drawer testing	35
3.7	Desired loading profile for isolated loading testing	36
3.8	Desired loading profile for combined loading testing	37
3.9	Schematic representation of model validation	39
4.1	RMS errors of simulating 30° AP drawer with ligament wrapping . .	43
4.2	Joint position for 30° AP drawer test data	44
4.3	Joint orientation for 30° AP drawer test data	45
4.4	Kinematic range of motion for ACLi and ACLd knees for 30° AP drawer simulation	46
4.5	Kinematic range of motion for ACLi and ACLd knees for isolated loading and combined loading simulations	47
4.6	Ligament forces for 30° AP drawer simulation	48
4.7	Change in ligament forces from 0° to 30° flexion for ACLi and ACLd knees at POIs for isolated loading testing	49
4.8	Change in ligament forces from 0° to 30° flexion for ACLi and ACLd knees at POIs for combined loading testing	50

4.9	Change in contact forces from 0° to 30° flexion for ACLi and ACLd knees at POIs for isolated loading testing	51
4.10	Change in contact forces from 0° to 30° flexion for ACLi and ACLd knees at POIs for combined loading testing	53
4.11	Meniscomfemoral contact forces for 30° AP drawer testing	54
4.12	Model sensitivity to changes in tibiofemoral contact stiffness	55
4.13	Model sensitivity to changes in ACL zero-load length	56
4.14	Model sensitivity to changes in MCL zero-load length	56
5.1	Medial view of the knee models showing wrapping of the MCL	59
D.1	Model sensitivity to changes in ACL stiffness	81
D.2	Model sensitivity to changes in PCL stiffness	82
D.3	Model sensitivity to changes in MCL stiffness	82
D.4	Model sensitivity to changes in LCL stiffness	83
D.5	Model sensitivity to changes in PCL zero-load length	83
D.6	Model sensitivity to changes in LCL zero-load length	84

List of Tables

3.1	Specimen characteristics	21
3.2	Ligament parameters	27
3.3	Compliant contact parameters	29
3.4	Solver parameters	32
3.5	Points of interest for isolated and combined loading tests	37
3.6	Parameters in sensitivity analysis	38
4.1	RMS errors of simulations	41
4.2	CPU time of simulating 30° AP drawer with ligament wrapping	42
A.1	General purpose MRI scan settings	75
A.2	Cartilage MRI scan settings	76
A.3	Connective tissue MRI scan settings	77
B.1	Tolerances of experimental measurement devices	78
C.1	RMS errors of individual 30° AP drawer simulations	79
C.2	RMS errors of individual isolated loading simulations	80
C.3	RMS errors of individual combined loading simulations	80

Chapter 1

Introduction

1.1 Background

Anterior cruciate ligament (ACL) injury often occurs in high intensity sports involving contact or sudden changes of direction. It is believed that twisting on an extended weight-bearing knee is the most likely cause of injury (Martini *et al.*, 2012). Rapid valgus and internal rotation (Markolf *et al.*, 1995, 2008) of the knee causes overextension of the ACL and combined with high loading, results in rupture or tear. ACL injury is of multifactorial nature as the anatomical structures, joint laxity and neuromuscular control all contribute to what results in injury (Kiapour *et al.*, 2014; Shultz *et al.*, 2015). Studies have shown that non-contact ACL injury is more common for females than males (Shultz *et al.*, 2015), however, the mechanism for rupture is believed to be the same. This is due to a combination of anatomical features (Faber *et al.*, 2001; Tillman *et al.*, 2002) and neuromuscular behaviour (Chappell *et al.*, 2007).

It has been well established that ACL injury changes natural knee kinematics. This increases the risk of cartilage degeneration or the premature development of osteoarthritis (Lohmander *et al.*, 2007; Guess and Stylianou, 2012). Corrective surgery to repair a torn ACL is difficult and the recovery process can take up to eight months after reconstructive surgery to return to normal gait patterns (Knoll *et al.*, 2004). ACL reconstructive surgery techniques include suture of the torn ligament and reconstructing the ligament using autografts or allografts (Macaulay *et al.*, 2012; Cerulli *et al.*, 2013).

1.2 Motivation

Cadaver (*in vitro*) studies have enabled researchers to determine quasi-static loading conditions that result in increased ACL load (Markolf *et al.*, 1995, 2008), but *in vivo* measurements of ACL force are yet to be made. Musculoskeletal models enable estimation of ligament forces, that can be used to investigate the relationship between joint kinematics and joint kinetics. More

specifically, models can be used to predict how knee biomechanics change as a result of ligament deficiency by subjecting the modelled knee to specific external loads.

Furthermore, musculoskeletal models can be used to determine the influence of ligament deficiency on structures surrounding the torn ligament (Markolf *et al.*, 1995; Weiss and Gardiner, 2001). This use of computational models is motivated by the fact that ACL injury is often accompanied by damage to other ligaments and structures, such as the MCL, the menisci, or the cartilage surrounding ACL attachment sites (Sakane *et al.*, 1999; Lohmander *et al.*, 2007; Chahla *et al.*, 2016; Guess and Razu, 2017; Ohori *et al.*, 2017).

Finally, models can assist with surgical decision making, as the changes in knee biomechanics can be quantified for the variation of graft material stiffness or ligament attachment location.

1.3 Objectives

The aim of this research was to develop a joint-level multibody model of the human knee joint that includes the anterior and posterior cruciate ligaments, the medial and lateral collateral ligaments, the femoral and tibial cartilage, as well as the medial and lateral menisci. The model was used to investigate the mechanics of the ACL and the effect of ACL deficiency on structures surrounding the ACL, joint kinematics and joint kinetics. Therefore, the research objectives are:

- To identify a suitable material model for the ACL.
- To create a joint-level multibody model of the human knee that is validated by comparing predicted joint kinematics and kinetics to the results of experimental tibiofemoral tests from the Open Knee(s) dataset.
- To use the model to assess the sensitivity of model outputs to variation in modelling parameters.
- To use the model to investigate joint kinematics and kinetics for an intact knee and to compare it to an ACL deficient knee.
- To use the model to determine the effect of ligament deficiency by comparing the changes in ligament force, cartilage contact force and meniscus contact force for intact and ACL deficient knees.

1.4 Scope

Experimental data from other research groups (Bennetts *et al.*, 2015; Bonner *et al.*, 2015; Colbrunn *et al.*, 2015; Erdemir *et al.*, 2015; Erdemir, 2016) will be

used as this study does not have the means to conduct its own experiments. An overview of the experimental protocol and methods will be provided and the reader will be referred to the relevant references in the text in case more information or clarification is required.

Chapter 2

Literature review

This chapter will provide the background information of the study. The chapter will start with a brief introduction to the human anatomy and biomechanics of the lower limb, with emphasis on the knee joint and its ligaments. Next, mechanisms of non-contact cruciate ligament injury will be discussed and finally, an overview of computational methods for modelling of the knee will be presented.

2.1 Anatomy and functions of the knee joint

2.1.1 Anatomy of the knee joint

The lower limb is connected to the upper body via the pelvic girdle. Shown in Figure 2.1, the lower limb is composed of four main bones (the femur, patella, tibia and fibula) and the foot (consisting of the tarsal bones, metatarsal bones and phalanges). Three main joints (the hip, knee and ankle) connect these structures: the hip connects the pelvis to the femur, the knee connects the femur to the tibia, fibula and patella and the ankle connects the tibia and fibula to the foot.

The knee is responsible, in conjunction with the hip and ankle for supporting the body's weight during a variety of activities, such as standing, walking and running (Martini *et al.*, 2012). The knee is structurally composed of two joints, enclosed in a synovial capsule, also known as an articular capsule (Figures 2.2 and 2.3). These two joints are the tibiofemoral joint, which facilitates contact between the tibia and the femur, and the patellofemoral joint, which facilitates interaction between the patellar surface and the femur. The patellofemoral joint also facilitates knee extension by increasing the mechanical advantage of the quadriceps. These surfaces for articular cartilage contact are shown in a parasagittal section of the knee joint in Figure 2.3. Prominent fat pads (Figure 2.3), which are also located in the articular capsule, provide padding around the joint and assist the bursae (Figure 2.3) in reducing friction

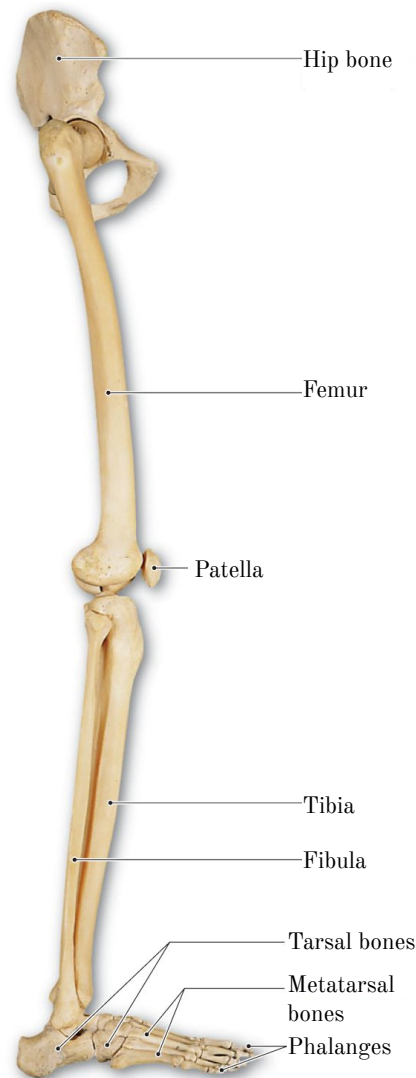


Figure 2.1: Lateral view of the right lower limb (Martini *et al.*, 2012)

between the patella and surrounding tissues.

A pair of fibrocartilaginous pads, the medial and lateral menisci, lie between the femoral and tibial surfaces (Figures 2.3 and 2.4). The menisci have different functions in the knee: they act as cushions between the femur and the tibia and conform to the shape of the articulating surfaces, guiding the femur as it changes position. Furthermore, the menisci increase the surface area of the tibiofemoral joint and provide stability to the knee (Figure 2.4).

There are seven major ligaments that connect and stabilize the knee joint. These ligaments are grouped as intra- and extracapsular ligaments. Shown in Figure 2.4, the intracapsular ligaments include the anterior cruciate ligament (ACL) and the posterior cruciate ligament (PCL).

The cruciate ligaments attach to the intercondylar area of the tibia and to

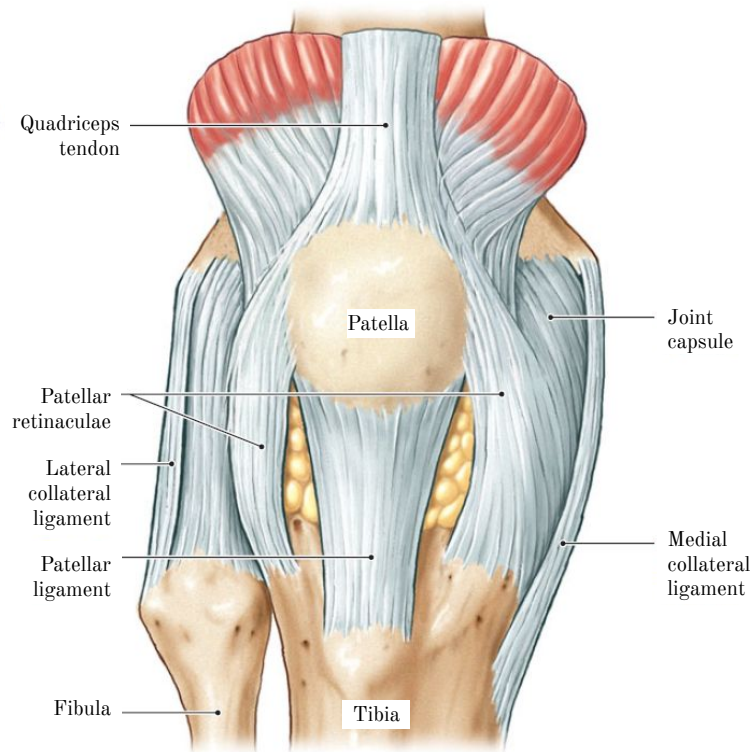


Figure 2.2: Anterior view of the extended right knee (Martini *et al.*, 2012)

the inner condylar surfaces of the femur. One the main functions of the cruciate ligaments are to ensure stability of the knee. The ACL achieves this by primarily restricting anterior tibial translation (Markolf *et al.*, 1976; Fukubayashi *et al.*, 1982). The ACL has a secondary function of restricting internal-external tibial rotation (Markolf *et al.*, 1976; Seering *et al.*, 1980; Markolf *et al.*, 1981; Shoemaker and Markolf, 1985). The PCL provides primary restraint to posterior tibial translation (Markolf *et al.*, 1976; Butler *et al.*, 1980) and it also acts as a secondary restraint to internal-external tibial rotation (Markolf *et al.*, 1976; Butler *et al.*, 1980; Grood *et al.*, 1988).

The extracapsular ligaments include the medial collateral ligament (MCL), the lateral collateral ligament (LCL) and the two superficial popliteal ligaments (Figures 2.4 and 2.5). These ligaments reinforce the lateral surfaces of the knee and assist in providing lateral stability against varus and valgus loading. The MCL provides primary restraint against valgus rotations (Markolf *et al.*, 1976; Seering *et al.*, 1980; Grood *et al.*, 1981), and provides secondary restraint to anterior tibial translation (Markolf *et al.*, 1976) and internal tibial rotation (Markolf *et al.*, 1976; Seering *et al.*, 1980; Shoemaker and Markolf, 1985). The LCL provides the primary restraint against varus rotations (Markolf *et al.*, 1976; Grood *et al.*, 1981; Gollehon *et al.*, 1987; Grood *et al.*, 1988), and provides a secondary restraint to anterior tibial translation (Markolf *et al.*, 1976; Grood *et al.*, 1981; Gollehon *et al.*, 1987; Grood *et al.*, 1988) and external tibial

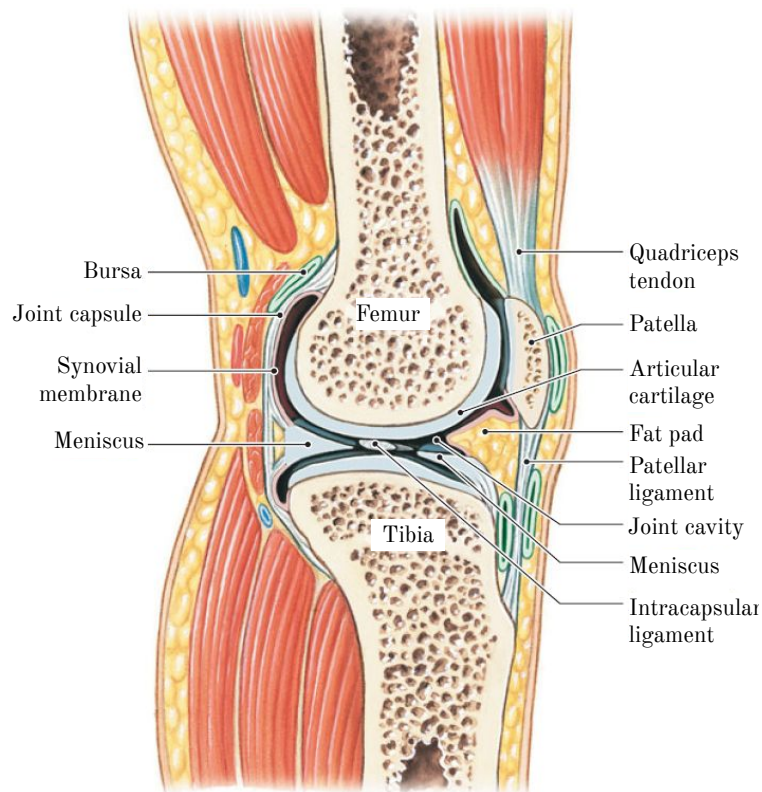


Figure 2.3: Parasagittal section through the extended right knee (Martini *et al.*, 2012)

rotation (Markolf *et al.*, 1976; Gollehon *et al.*, 1987; Grood *et al.*, 1988). The popliteal ligaments extend between the femur and the heads of the tibia and fibula, with the function of reinforcing the back of the knee joint (Nielsen and Helmig, 1986*a,b*). Finally, the patellar ligament (Figure 2.2) connects the anterior surface of the patella to the anterior surface of the tibia.

2.1.2 Biomechanics of the lower limb

The function of the knee joint is to permit the movement during locomotion and to allow for static stability (Machado *et al.*, 2010). A combination of five muscles contribute most significantly to human locomotion. These muscles are the gluteus maximus, gluteus medius, quadriceps, soleus, and gastrocnemius (Pandy and Andriacchi, 2010).

Figure 2.6 shows the six degrees of freedom of the tibiofemoral joint. The primary motions of the knee are flexion and extension in the sagittal plane. Flexion motion is the backward movement of the shin relative to the thigh and extension is in the opposite direction. Extension and flexion motions occur along an ‘floating’ axis that translates in the anterior-posterior directions. This is due to the curvature of the femoral condyles, which do not have a constant

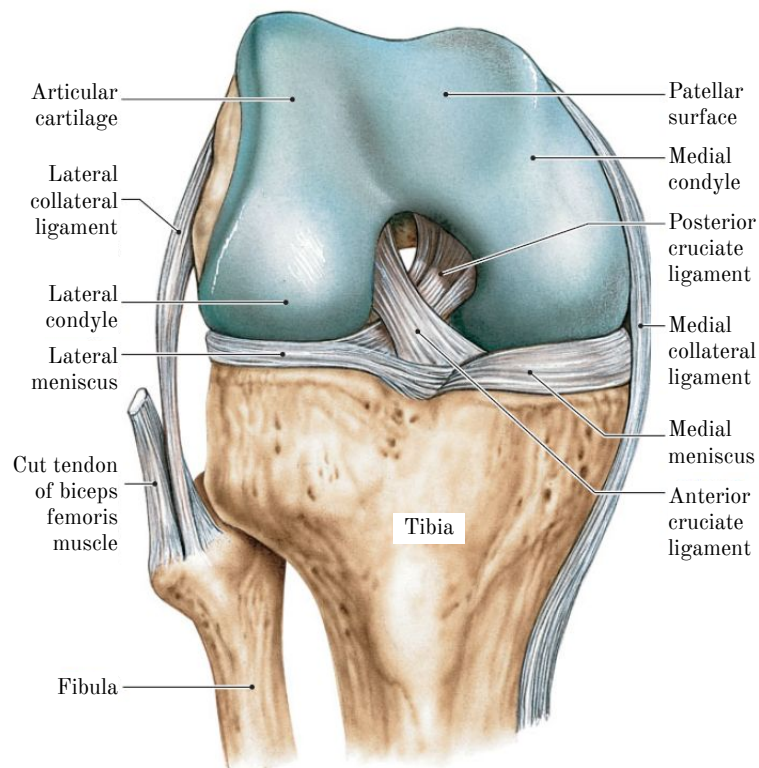


Figure 2.4: Anterior view of the right knee at full extension after removal of the joint capsule, patella and related ligaments (Martini *et al.*, 2012)

centre of rotation (Grood and Suntay, 1983; Freeman and Pinskerova, 2003; Machado *et al.*, 2010; Seth *et al.*, 2010). The other motions of the knee include axial rotation (internal-external rotation), varus-valgus rotation (also known as abduction and adduction), medial-lateral translation and superior-inferior translation (also known as distraction and compression). The patellofemoral joint (not included in Figure 2.6) adds an additional six degrees of freedom as the patella slides on the femoral condyles.

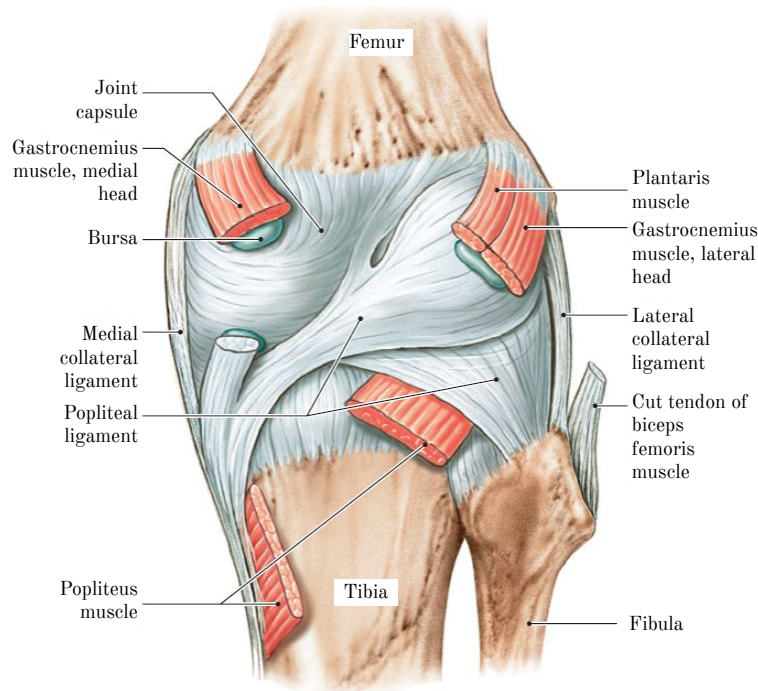


Figure 2.5: Posterior view of the extended right knee (Martini *et al.*, 2012)

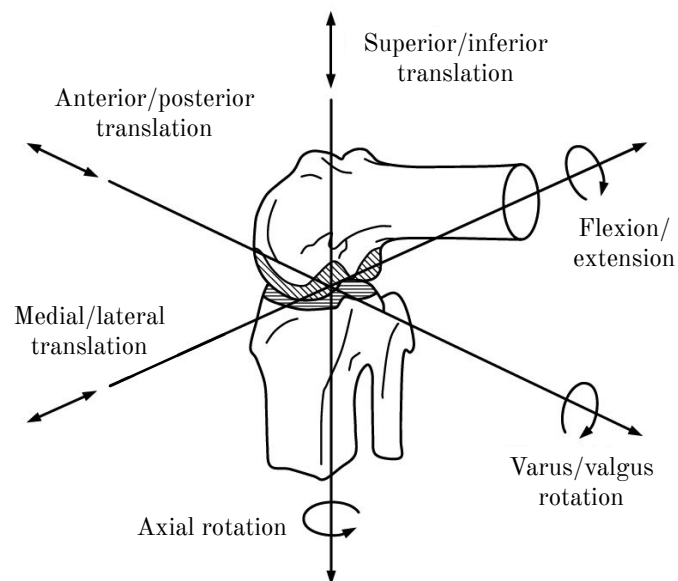


Figure 2.6: The six degrees of freedom of the knee (adapted from Machado *et al.* (2010))

2.1.3 Muscles, tendons and ligaments

Muscle tissue is specialized for contraction and can be divided into three categories, i.e. skeletal, cardiac and smooth muscle (Martini *et al.*, 2012). The

former will be discussed briefly. Skeletal muscles are responsible for producing movement and to maintain body position and posture. Skeletal muscles are composed out of long and slender muscle cells, also referred to as muscle fibres. Muscle fibres contain myofibrils. Inside the myofibrils are the actin and myosin filaments, which contract upon neural stimulation, providing the central neural system voluntary control. At the end of each muscle, the collagen fibres of the connective tissue surrounding the muscle converge to form a tendon. The function of a tendon is to fix the muscle to bone or skin.

Bones are connected to other bones via ligaments. Ligaments are tough, dense connective tissue that constrain the relative movement of bones. Ligaments consist of fibroblast cells and the extracellular matrix. Fibroblast cells produce collagen, reticular and elastic fibres, along with ground substance (consisting of proteins and polysaccharides) which constitutes to the extracellular matrix (Martini *et al.*, 2012; Marieswaran *et al.*, 2018). Collagen and elastic fibres make up most of the ligament and enables the ligament to withstand substantial loads.

2.1.4 Biomechanical properties of ligaments

The force-elongation properties of ligaments can be described by two regions, shown in Figure 2.7. These regions are the non-linear region (also known as the ‘toe-region’) and the linear region (Weiss and Gardiner, 2001; Kia *et al.*, 2016). Beyond the linear region, permanent damage occurs as collagen fibrils break, eventually leading to tear of the ligament.

2.2 Mechanisms of ACL injury

Non-contact ACL injuries often occur during sudden deceleration and acceleration motions, such as running or jumping. These motions introduce frontal loading on the knee and subject the ACL to anterior shear force. Injuries are especially likely while the weight bearing knee is at a shallow flexion angle, near full extension (Markolf *et al.*, 2004; Shimokochi and Shultz, 2008; Martini *et al.*, 2012). Excessive valgus combined with internal rotation results in increased ACL loading and it has been observed that internal rotation moments yield higher ACL forces than external rotation moments (Markolf *et al.*, 1995; Kanamori *et al.*, 2000). However, motions such as sidestep cutting observed during non-contact injury also include external rotation of the tibia, thus making it an important consideration for ACL injury (Markolf *et al.*, 2008; Guess and Stylianou, 2012; Guess and Razu, 2017). The application of excessive quadriceps contraction and reduced hamstrings co-contraction at or near full knee extension also results in higher loading of the ACL, further increased by the addition of an internal rotation moment applied to the tibia (Markolf *et al.*, 2004; Wetters *et al.*, 2015). Hence, mechanisms for non-contact ACL loading

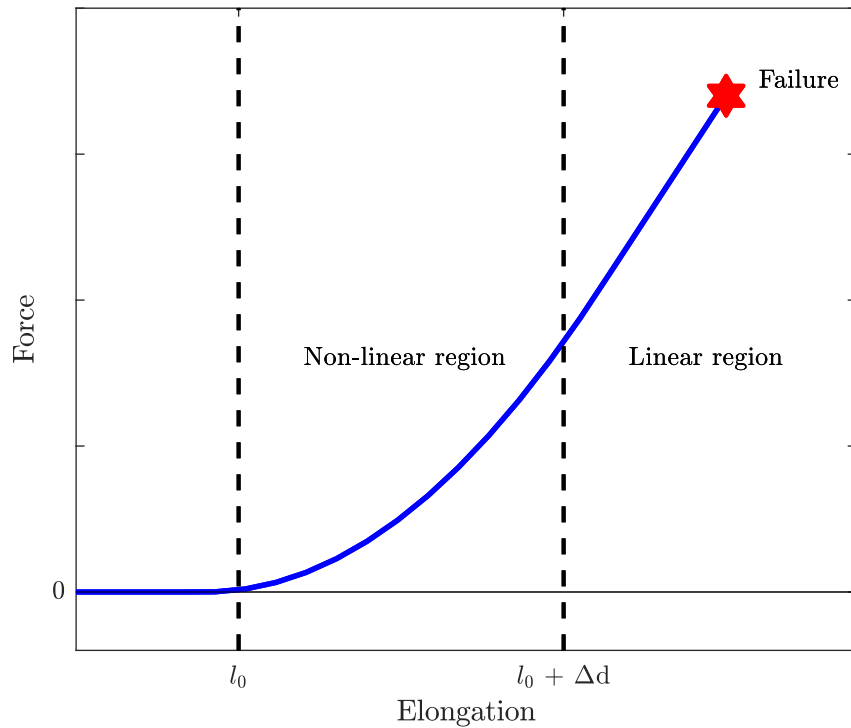


Figure 2.7: Force-elongation relationship for a ligamentous fibre. The slack length of the ligament is indicated by l_0 , and the change in ligament length is depicted by Δd .

are a combination of neuromuscular response and multiplanar motions of an extended knee, with combinations of valgus moments and rotation of the tibia being the main causes of ACL failure (Markolf *et al.*, 1995; Shimokochi and Shultz, 2008).

2.3 Computational techniques for modelling the knee joint

A variety of computational techniques are used to create models of the knee. These techniques can vary greatly in terms of complexity and computational expense. To use a model effectively, the benefits, capabilities and restrictions of the modelling method should be clearly understood. It is also important that the necessary assumptions and approximations are considered when deciding which modelling method is best suited to investigate the research question. This section will discuss techniques used to model the knee joint, with the focus on multibody modelling.

2.3.1 A brief overview of modelling techniques

Analytical models were one of the first methods introduced to model joints in the human body (Crowninshield *et al.*, 1976). An analytical model (Figure 2.8) determines the forces in the ligaments that are caused by joint translations and rotations. These translations and rotations are determined when considering the initial and displaced configurations of the joint. These models describe knee kinematics mostly through mathematical and geometric relationships. Crowninshield *et al.* (1976) developed one of the first analytical models of the knee that accounted for knee geometry, joint kinematics for flexion angles between 0° and 90° , and included the major knee ligaments. Their model did however make simplifications regarding the kinematic behaviour of the knee as the contribution of curved joint surfaces to the mechanical behaviour of the knee was ignored. Wismans *et al.* (1980) accounted for the curved joint surfaces by representing the surfaces as polynomials in space. To include the effect of articular contact on joint kinematics, simple contact points between the femur and tibia were included. This model did not include the menisci.

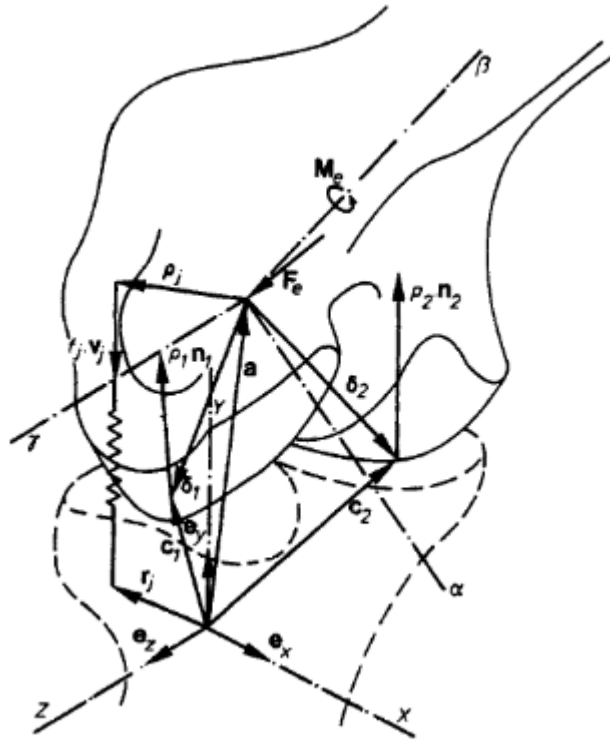


Figure 2.8: A schematic representation of an analytical model of the knee (Wismans *et al.*, 1980)

Including representations of contact interactions significantly increases the model complexity and number of equations of motion that need to be solved (Trad *et al.*, 2018). For such problems, higher level computational techniques

are required. These techniques refer to methods using computers to solve large problems iteratively that would otherwise be tedious or unsolvable using hand calculations. The two main computational techniques currently used to model the knee joint are based either on a finite element analysis or a multibody approach. A multibody approach (Figure 2.9) describes the kinematics between two interacting bodies and is generally used when complex interaction with the surrounding environment is investigated, for example, simulation of gait or jumping activities. Multibody models are often referred to as rigid body models, due to model parts being defined as non-deformable. Multibody modelling utilizes different techniques to solve for kinematics and the corresponding kinetics. These techniques are inverse kinematics, inverse dynamics, forward dynamics and static optimization.

Inverse kinematics is a mathematical process that uses kinematic equations to determine joint parameters, specifically joint angles, from experimental data. The inverse kinematics method computes the joint angles for a musculoskeletal model that best reproduce the motion of a specific subject, without knowledge of the forces and moments that produce the motion. For a set of recorded motion data, software such as OpenSim (Delp *et al.*, 2007) uses the inverse kinematics method to determine a best fit between experimental markers (used to record motion data) and markers in the model.

A method for estimating kinetics is through *inverse dynamics*. Inverse dynamics is the process of determining kinetic information (total joint reaction forces and total joint moments) from measured kinematic information (joint angles, positions, velocities and accelerations). Measured kinetic data such as

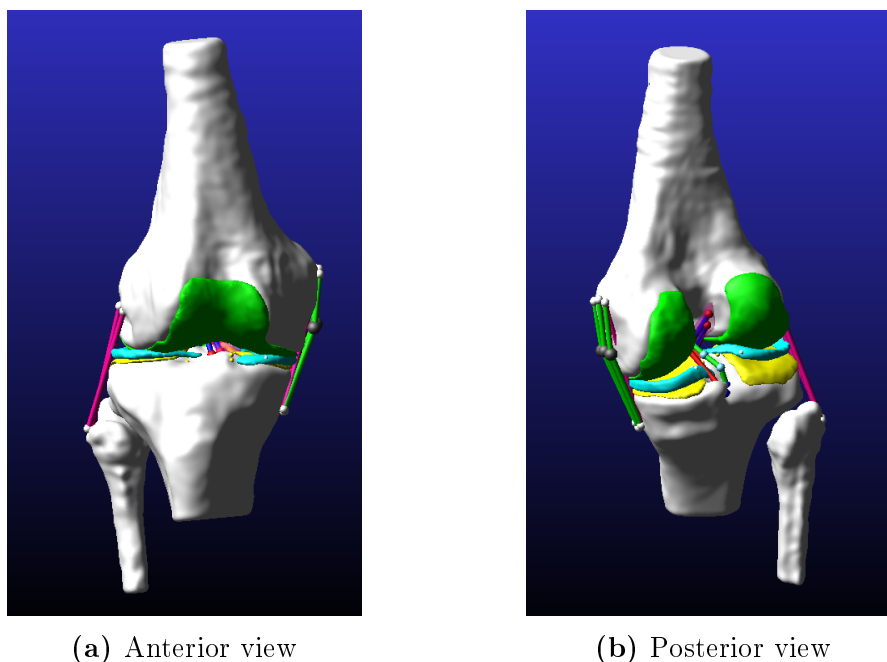


Figure 2.9: A multibody model of the knee developed in this study

ground reaction forces can also be included. To perform an inverse dynamics calculation, estimation of the mass and inertia is required. This is required to derive the equations of motion of the system. Using the joint angles determined from inverse kinematics, the ground reaction forces from experiments and the equations of motion for the system, the total joint forces and moments are solved iteratively. Muscle forces can also be included as model boundary conditions (Delp *et al.*, 2007; Schmitz and Piovesan, 2016a; Walter and Pandy, 2017).

The method of inverse dynamics does have its limitations as it relies on assumptions for mass distribution and joint friction that have not been confirmed for all cases. Joint friction due to a disease such as osteoarthritis will introduce an additional moment about the joint axes of rotation. Also, the non-uniform distribution of mass of a limb requires assumptions to be made regarding the inertia and center of mass, which will have an effect on the system's equations of motion. Furthermore, due to the complex geometry and interactions of the knee joint, the joint centre of rotation changes during rotation. This could lead to errors when estimating the joint center (Holden and Stanhope, 1998; Seth *et al.*, 2010). In many cases, especially when the patient is obese, the hip joint center of rotation is deep and cannot be accurately tracked by a marker. To mitigate this problem, anthropometry can be used to estimate the position. Anthropometric approximations and generalizations are also required for very skinny participants. Other sources of measurement error occur due to inaccuracies in co-alignment of force plate and motion tracking, specifically due to motion at the skin-bone interface (Holden and Stanhope, 1998).

A restriction of the use of inverse dynamics is that it can only determine the net forces and moments about joints. Thus, it is not able to determine the components of forces due to different muscles. However, a technique called *static optimization* mitigates this restriction. Static optimization is an extension to inverse dynamics that further resolves the net joint moments into individual muscle forces at each simulation time step. The muscle forces are resolved by minimizing the sum of squared muscle activations.

The final technique used in multibody modelling is *forward dynamics*. Forward dynamics works opposite to inverse dynamics – a mathematical model describes how coordinates and their velocities change due to applied forces and moments. Forward dynamics is used to better understand how muscles generate motion and for the prediction of performance if a muscle or joint is changed.

Many three-dimensional multibody knee models are dynamic with non-deformable contact representations (Bei and Fregly, 2004; Bloemker *et al.*, 2012; Guess and Stylianou, 2012; Guess *et al.*, 2015; Guess and Razu, 2017; Kia *et al.*, 2016; Harris *et al.*, 2016). Multibody contact modelling consists of two parts – determining the state of contact (i.e. whether the articulating surfaces are in contact, partially in contact or out of contact) and calculation of the

distance between two articulating surfaces. The former is the primary source of computational expense (Bei and Fregly, 2004; Lin *et al.*, 2010*a*; Thelen *et al.*, 2014; Eskinazi and Fregly, 2018). Despite the fact that computationally efficient multibody models that included deformable contact of cartilage and the menisci have been developed (Guess *et al.*, 2010, 2013), finite element models are usually used to model deformable contact.

Finite element (FE) analysis provides information about the current state of stress and strain at a current point in time, allowing for evaluation of the deformation of a part in a model. FE models (Figure 2.10) are typically used to provide information about localized structural deformations that need to be analysed in detail (Machado *et al.*, 2010).

FE models vary in complexity but are generally more computationally expensive than multibody models, especially for dynamic simulations and for complex contact evaluations. This resulting computational load often becomes prohibitive (Eskinazi and Fregly, 2015). Due to the tendency of FE analyses to be computationally expensive, dynamic simulations within a finite element workflow are typically avoided, although dynamic FE models have been developed (Baldwin *et al.*, 2012; Kiapour *et al.*, 2014).

For dynamic simulations involving deformable contact, FE analysis can be included in a multibody workflow as part of a co-simulation strategy. Many current multibody models use inverse and forward dynamics techniques to simulate the kinematics of gait or passive flexion. A problem with this approach is that tibiofemoral contact forces induce motions about the joint axes, which are not incorporated into the calculation of net forces and moments acting

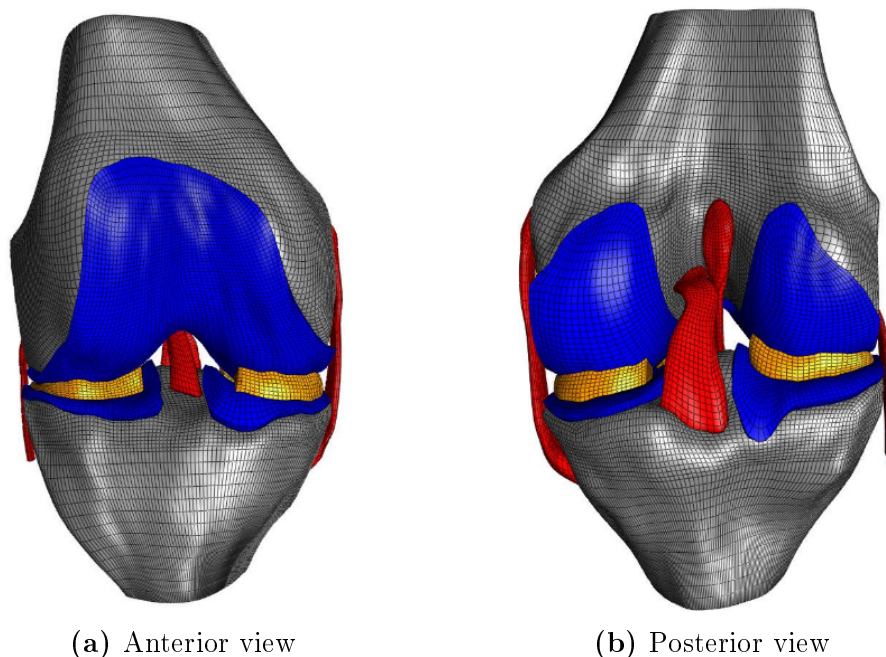


Figure 2.10: A finite element model of the knee (Erdemir, 2016)

on the joint (Thelen *et al.*, 2014). Co-simulation is a modelling technique that combines FE and multibody workflows and provides a method to mitigate the above-mentioned problem (Thelen *et al.*, 2014; Schmitz and Piovesan, 2016*a,b*). Co-simulation couples the modelling of joint kinematics and tissue mechanics involved in articular contact. It does however involve significant computational expense (Thelen *et al.*, 2014).

Past studies (Halloran *et al.*, 2009, 2010; Walter and Pandy, 2017) investigated including surrogate models in an effort to reduce the computational load during co-simulation. Surrogate models provide a more computationally efficient method of modelling and have shown to be very useful for contact modelling in musculoskeletal biomechanics (Lin *et al.*, 2010*a*; Eskinazi and Fregly, 2015). A surrogate model fits or interpolates input-output relationships from a computational model, such as a FE model. Surrogate models can incorporate different techniques to fit input-output relationships. Multiple linear regression and kriging-based methods are two commonly used surrogate modelling approaches. Eskinazi and Fregly (2015) showed that machine learning in the form of artificial neural networks can also be used in time-independent regression problems.

2.3.2 Boundary conditions

Computational models require boundary conditions to constrain the model and to avoid prediction of unrealistic kinetics or kinematics. Boundary and initial conditions used in computational models are acquired using various methods.

Mechanical simulators, also referred to as whole joint simulators, are often used for *in vitro* studies. These simulators, like the Kansas knee simulator (Halloran *et al.*, 2010), provide a controlled and repeatable loading environment for comparative evaluation of component designs or surgical alignment under dynamic conditions (Baldwin *et al.*, 2012). Other simulators used in published research include the Oxford knee rig (Zavatsky, 1997), the Stanmore (Godest *et al.*, 2002) and the Purdue (Halloran *et al.*, 2005) simulators. Along with providing boundary conditions, these simulators provide experimental data to validate computational models. A disadvantage of *in vitro* studies is that the use of a mechanical simulator to facilitate articulation of the joint restricts the level of movements for which testing data can be collected.

In vivo experiments are necessary to verify cadaver-based simulations. However, *in vivo* measurement is technically challenging (Hosseini *et al.*, 2015) and measurement devices should not damage tissue or alter ligament or joint function (Fleming and Beynon, 2004). Invasive techniques include the use of strain gauges and fibre optic sensors to measure forces in ligaments (Roriz *et al.*, 2014), or instrumented prosthesis to measure forces in articulating surfaces (Fregly *et al.*, 2012). Non-invasive methods include ultrasonography and magnetic resonance imaging. The values obtained for stresses and strains can

be used either to validate simulation results, or as boundary conditions in simulations.

Due to the complex structure and loading of internal soft tissues, *in vivo* measurements are difficult to obtain and cartilage contact pressures cannot be measured directly during ambulatory activities (Fleming and Beynnon, 2004; Guess *et al.*, 2013). However, joint contact forces can be measured *in vitro* using pressure films. These measurements are used to estimate the magnitude of tibiofemoral and patellofemoral contact force, as well as the center of pressure location during cadaver testing (Bei and Fregly, 2004; Guess *et al.*, 2013; Kiapour *et al.*, 2014; Walker *et al.*, 2015).

Several implantable sensors have been developed and used for *in vivo* measurement of force in ligaments and other soft tissues (Holden *et al.*, 1994; Platt *et al.*, 1994; Finni *et al.*, 1998; Fleming *et al.*, 1999; Bull *et al.*, 2005). These sensors work by being implanted between fibres in the ligament mid-substance. Fibres around the sensor subject it to a compressive load when a tensile force is applied to the ligament. The compressive load on the sensor is then used to estimate force in the ligament. Even though the forces measured are useful to compare with *in vitro* measurements, insertion of a sensor within a ligament changes the sensitivity of the ligament to loading (Holden *et al.*, 1995; Fleming and Beynnon, 2004).

For both *in vivo* and *in vitro* experiments, it is important to measure joint kinematics. Currently, optical motion tracking is a popular and reliable method of obtaining kinematic data for both *in vivo* and *in vitro* experiments (Boeth *et al.*, 2013; Guess *et al.*, 2015; Guess and Razu, 2017; Wouda *et al.*, 2018). The kinematic data can be used as a boundary condition to limit the range of motion (e.g. flexion-extension), to drive a simulation using the inverse dynamics method (Thelen *et al.*, 2014; Xu *et al.*, 2017) or to validate the computational model.

2.3.3 Modelling assumptions and approximations

The choice of modelling technique and the level of detail in the model is typically dictated by the available computational resources and the intended use of the model (Galbusera *et al.*, 2014), where more detail is added only to the region of interest.

Modelling parameters, initial conditions and boundary conditions are often subject to assumptions and approximations (Trad *et al.*, 2018). Assumptions and approximations are necessary to simplify the problem to a level that can be described satisfactorily by a model, and which can be solved using the available computational resources. Biological materials present a significant modelling challenge due to their highly non-linear anisotropic behaviour and complex geometry (Weiss and Gardiner, 2001). Additionally, joint constraints are often multiplanar and cannot be modelled with conventional joints such as hinges

or ball joints. Instead, models require a complex combination of conventional joints to include all of the required degrees of freedom (Seth *et al.*, 2010).

Material assumptions are mostly based on literature as many studies do not have the resources to conduct their own experiments (Piazza and Delp, 2001; Galbusera *et al.*, 2014). Biological materials are sensitive to the testing protocol and might differ from one specimen to another (Butler *et al.*, 1986; Woo *et al.*, 1999). Material properties of tissues may also differ between *in vivo* and *in vitro* measurements (Kluess *et al.*, 2009; Nasab *et al.*, 2016). Kikapour *et al.* (2014) showed that the choice of a constitutive model will have a significant effect on the predicted joint kinematics.

It is common for surgeons to use autografts (tissue from the same specimen), allografts (tissue from a donor) or synthetic grafts during ACL reconstruction surgery (Dargel *et al.*, 2007; Macaulay *et al.*, 2012; Cerulli *et al.*, 2013). Auto or allografts are often made from the hamstring tendon or the patellar tendon (Macaulay *et al.*, 2012; Cerulli *et al.*, 2013), which could result in a change in stiffness value of the reconstructed ACL. The length of the ACL might also change as a result of the graft being fixed in a different location than the original ligament.

Variation in ligament attachment site locations have been shown to have a significant effect on joint kinematics during cadaveric experiments (Grood *et al.*, 1989; Hefzy *et al.*, 1989). Hence, ligament insertion sites are typically determined by digitizing the point cloud around the site (Bei and Fregly, 2004; Bloemker *et al.*, 2012; Guess *et al.*, 2013; Harris *et al.*, 2016). If digitization is not possible, the accuracy of ligament attachment site approximation can be verified by cadaveric inspection (Markolf *et al.*, 2006, 2008; Baldwin *et al.*, 2009).

Furthermore, cartilage, ligament and meniscus geometries are subject to approximation due to tolerances of CT and MRI scanning equipment and segmentation techniques. Image segmentation entails partitioning of image layers into multiple segments, with the intention of isolating a region or structure of interest. Common segmentation techniques include using thresholding or edge detection methods. The geometries generated by segmentation will depend on the technique and the parameters used. This is an important consideration as variation in geometry, such as cartilage thickness, will influence the predicted contact stress and affect joint kinematics (Trad *et al.*, 2018).

Another simplification common in multibody models is to model ligaments as a one-dimensional spring, as opposed to a three-dimensional deformable body (Blankevoort and Huiskes, 1991; Blankevoort *et al.*, 1991; Guess *et al.*, 2010; Bloemker *et al.*, 2012; Guess *et al.*, 2013; Harris *et al.*, 2016; Kia *et al.*, 2016; Schmitz and Piovesan, 2016a; Guess and Razu, 2017). This is because the functional benefits of a complex three-dimensional ligament representation are often rejected in favour of the computational speed of a simpler representation. Similarly, including deformable contact increases model complexity and computational load as opposed to using rigid body contact methods (Lin

et al., 2010a). Hence, most multibody models rely on non-deformable contact, although previous computational studies have created models that are able to predict response similar to deformable contact using rigid body elements for articular contact (Guess *et al.*, 2013), and the menisci (Guess *et al.*, 2010; Kia *et al.*, 2016; Guess and Razu, 2017).

2.4 Current state of the art multibody models

New models are a product of the modelling techniques introduced and validated by its predecessors. Recently developed models have been focussed on the role of the menisci (Guess *et al.*, 2010, 2015; Guess and Razu, 2017) and the role of articular contact on the knee joint (Bei and Fregly, 2004; Lin *et al.*, 2010a; Guess *et al.*, 2013; Eskinazi and Fregly, 2015, 2018). Multibody models have also been used to study the effects of ligament deficient knees (Shelburne *et al.*, 2005; Guess and Stylianou, 2012; Ali *et al.*, 2016; Guess and Razu, 2017).

There are two main areas of state-of-the-art multibody model development, the first of which being aimed at improving model performance by reducing computational load. Strategies to reduce computational load include using surrogate models (Lin *et al.*, 2010a; Eskinazi and Fregly, 2018; Halloran *et al.*, 2009, 2010) and artificial neural networks (Eskinazi and Fregly, 2015). These techniques require the development of finite element models to provide solution sets for surrogate models and to train artificial neural networks.

The second area of development focusses on the representation of modelled knee structures to more accurately predict joint behaviour. One example of improving model representation is by adding ligament wrapping. Ligament wrapping was first suggested by Hefzy and Grood (1983) and was first implemented by Blankevoort and Huiskes (1991). The latter showed that the ligament-bone interaction on the medial side of the tibia redirected the ligament force to more effectively counterbalance valgus moments on the tibia (Blankevoort and Huiskes, 1991; Weiss and Gardiner, 2001). Since, ligament wrapping has been included in multiple multibody knee models (Guess *et al.*, 2010; Kia *et al.*, 2016; Guess and Razu, 2017).

Multibody models often use a mathematical expression to describe ligament behaviour, based on the Wismans *et al.* (1980) and Blankevoort and Huiskes (1991) formulation. This expression represents a force-strain relationship for elastic line elements to model ligament fibre bundles. A parameter representing the linear strain limit (based on Butler *et al.* (1986)) is used to represent the transition from non-linear to linear ligament response. This parameter is used to determine the reference length of the ligament, i.e. the length at which the ligament begins to resist applied loading.

Bloemker *et al.* (2012) noted the importance of defining ligament reference lengths correctly as it has a significant effect on the predicted ligament forces and knee kinematics. Additionally, assumed slack length could incorrectly

compensate for structures that were not modelled, such as the menisci or intra-capsular ligaments (Blankevoort *et al.*, 1991; Blankevoort and Huiskes, 1996; Smith *et al.*, 2017). Bloemker *et al.* adapted the ‘reference strain method’ (Blankevoort *et al.*, 1991), by replacing the generalized strain parameter with an experimentally measured reference length. This made the model more subject specific. Similarly, Kia *et al.* (2016) used a robotic manipulator in a novel strategy to estimate the slack length of ligaments. Their study combined experimental measurements with a subject specific multibody model of the knee to estimate ligament slack length. This was done to improve model accuracy when predicting cruciate ligament forces from full extension to deep flexion – a motion for which computational models are known to predict ligament force incorrectly (Yang *et al.*, 2010).

A major restriction of multibody modelling is that it cannot be used to simulate soft tissue deformation of cartilage or the menisci. This is because parts are modelled as rigid bodies. However, as briefly mentioned before, Guess *et al.* (2010, 2013) introduced a method of incorporating soft tissue deformation in a multibody modelling workflow by discretizing the soft tissue geometry and connecting the discrete elements via six-degree-of-freedom stiffness matrices. The stiffness matrices constrain the relative displacement and rotation of discretized elements. A design of experiments approach was used to optimize stiffness matrix parameters with the aim to minimize error between the multibody model and an identically loaded finite element model. The parameters were optimized at full extension of the knee. To model articular contact, a compliant contact model (`impact` model in MSC Adams) was used. Contact model parameters were also optimized by comparing predicted multibody kinematics to an identically loaded finite element model of the knee that simulated tibiofemoral contact. This technique of discretizing rigid geometries enables the multibody model to include representation of deformable contact between soft tissues, while retaining the computational benefits of using the multibody modelling workflow.

In this study, a multibody modelling workflow was used to develop the model as the aim of the study is to investigate the changes in kinematics and kinetics for an intact and ACL deficient knee. Considering the aim of this study, a multibody model is better suited and less computationally expensive for dynamic simulations than a comparable FE model. A multibody model can also be adapted relatively quickly, by adding or removing elements in the model. Finally, the multibody modelling workflow can be elaborated to include a finite element model of a structure of interest, such as the ACL, in a co-simulation workflow.

Chapter 3

Materials and methods

This chapter introduces the Open Knee(s) dataset from which the model was formulated, and discusses the development of the model in MSC Adams (Adams 2018.1, MSC Software Corporation). Furthermore, this chapter describes the application of model boundary conditions, the simulation of knee biomechanics and the evaluation of model sensitivity. This chapter concludes with how the model was validated.

3.1 Open Knee(s) project dataset

Specimen geometries from the Open Knee(s) project (Bennetts *et al.*, 2015; Bonner *et al.*, 2015; Colbrunn *et al.*, 2015; Erdemir *et al.*, 2015; Erdemir, 2016) were used to create the multibody model. The Open Knee project provides freely available testing and simulation data for collaborative *in silico* exploration of the human knee joint. The multibody model developed in this study includes the femur and tibia, along with their respective cartilage structures, the menisci, the anterior and posterior cruciate ligaments and the medial and lateral collateral ligaments. Specimen data used in the formulation of the computational model is given in Table 3.1.

Table 3.1: Specimen characteristics

Characteristic	Value
Specimen ID	OKS001
Gender	Male
Age	71
Race	Caucasian
Height	1.83 m
Weight	77.1 kg
BMI	23.1
Disease state of joint	Possibly osteoarthritic

Subject specific anatomical representations of the knee structures (ligaments, cartilage and bone) were created by segmentation¹ of the magnetic resonance images (MRI) of the specimen and the volumetric reconstruction of these structures (image acquisition scanning properties can be found in Appendix A). This was done in two stages: defining tissue boundaries as an image volume and creating a surface representation of the image volume in stereolithographic (STL) file format. The generated geometries are smoothed using Meshlab (Cignoni *et al.*, 2008).

Geometry smoothing was done in five steps²: (1) ‘Laplacian smoothing’ (smoothing steps set to 20), (2) ‘surface reconstruction’ (set voxel size to the same value as the MRI resolution, i.e. 0.35 mm to 0.7 mm), (3) ‘Taubin smoothing’ (suggested parameters $\lambda = 0.5$, $\mu = -0.5$), (4) ‘iso parametrization’ and ‘iso parametrization remeshing’ (use default sampling rate of 10) and finally, (5) repeated application of ‘Taubin smoothing’, with the same parameters as in step (3). After smoothing was completed, the geometries are checked if manifold and watertight.

Before imaging, registration markers were placed on the knee. These markers served as reference points to establish the position and orientation of the tibia and femur in the computational environment. Their positions were recorded using a digitizer to determine the anatomical bone coordinate systems required for applying kinematic boundary conditions in the computational model.

A six degree-of-freedom robot (Rotopod R2000, Parallel Robotic Systems Corp., Hampton, NH, USA) was used to apply loading conditions to the joint. To apply loading profiles, the robot was used in a real-time ‘force feedback’ control mode (Borotikar, 2009; Noble *et al.*, 2010). Force control is achieved by using a feedback control loop between the robot and the universal force sensor (load cell). Joint kinematics were determined for five degrees of freedom, as the flexion angle was prescribed for each experiment. The tibia was attached to the stationary robot frame through a six-axis load cell. For all experiments, the joint was mounted in an inverted position, with the tibia pointing upwards. The femur was attached to the robot and articulated relative to the tibia.

The tibiofemoral joint testing protocol was adapted from Borotikar (2009), and included joint testing at 0°, 30°, 60° and 90° flexion for three isolated degrees of freedom (internal-external rotation, varus-valgus rotation, anterior-posterior translation) and combined loading tests. Combined loading tests included simultaneous application of internal-external (IE) rotation moments (-5 Nm to +5 Nm in 1 Nm increments), varus-valgus (VV) rotation moments (-10 Nm to +10 Nm in 2.5 Nm increments) and anterior-posterior (AP) drawer forces (-100 N to +100 N in 10 N increments). The protocol for

¹<https://www.slicer.org>, 2019

²<https://simtk.org/plugins/moinmoin/openknee/Specifications/GeometryGeneration>, 2019

tibiofemoral joint testing did not include patellofemoral joint loading. Hence, the patellofemoral joint was omitted from the model. Joint kinematics were recorded with Optotrak sensors (NDI, Ontario, Canada) and robot position output.

Although tibiofemoral testing was done at 0°, 30°, 60° and 90° flexion, only data recorded at 0° and 30° was used. This is because ACL injuries typically occur near or at full extension. Clinical studies comparing intact (ACLi) and ACL deficient (ACLd) knees often only test at low flexion angles (< 30°) when subjecting specimens to combined loading (Woo *et al.*, 2002; Gabriel *et al.*, 2004). Additionally, studies that developed multibody models (Yang *et al.*, 2010; Kia *et al.*, 2016) have warned to be cautious of using the same model at both low and high flexion angles. Their suggestion is to have two separate models for testing at low and high flexion angles. One of the reasons is due to a combination of a simplified soft tissue constraint (as opposed to a complex material model used in FE models) and the way in which ligaments engage to resist applied loads. This causes ligament behaviour to be in disagreement with true behaviour (Harris *et al.*, 2016) as model kinematics and ligament insertion sites could be different from the specimen that it is based on. Hence, this study will only use experimental data to simulate knee biomechanics at 0° and 30° of knee flexion.

3.2 Computational model formulation

3.2.1 Model geometries

The STL files (Chapter 3.1) of the femur and tibia bones, femur and tibia cartilage, and menisci were converted to rigid parasolid geometries (Adams 2018.1, MSC Software Corporation) and assigned a density of $2.0 \times 10^3 \text{ kg/m}^3$, $1.0 \times 10^3 \text{ kg/m}^3$, and $1.1 \times 10^3 \text{ kg/m}^3$ for osseous, cartilage and menisci respectively (Guess and Razu, 2017).

3.2.2 Coordinate system

Rigid body geometries were created in the MRI coordinate system, i.e. the image coordinate system (ICS). To apply the forces and motions for inverse dynamics or forward dynamics simulations, the model components (osseous, ligaments, cartilage) had to be transformed from the ICS to the anatomical knee joint coordinate system (KJCS) as described by Grood and Suntay (1983). Transformation matrices were determined by acquiring the coordinates of landmarks on the femur and tibia using a digitizer. These transformation matrices were used to transform the coordinates of the registration markers from the ICS to their relative positions in the KJCS. The local bone coordinate

systems are shown in Figure 3.1. The femur coordinate system corresponds to the KJCS as described by Grood and Suntay (1983).

3.2.3 Ligaments

For dynamic analysis applications, such as the evaluation of joint kinematics, simplified ligament representations are effective and computationally inexpensive (Baldwin *et al.*, 2009). Single-component force elements were defined between the ligament insertion sites on the femur and the tibia. Ligament insertion sites were estimated based on MRI geometries as their locations were not recorded using a digitizer. The single-component force elements act in the line of sight between the two insertion sites. The force-displacement relationship for the ligaments are based on a combination of the Blankevoort and Huiskes (1991) formulation, and the method used by Bloemker *et al.* (2012) to determine ligament slack length. Ligament behaviour consists of both linear and non-linear response, depending on ligament strain. The force-displacement relationship is given by equation 3.1.

The stiffness values for the different ligaments and ligament bundles are based on values estimated by Blankevoort and Huiskes (1991), Guess *et al.* (2015) and Guess and Razu (2017) and are given in Table 3.2. The non-linear strain level parameter ϵ_l is assumed to be 0.03 for all ligaments (Butler *et al.*,

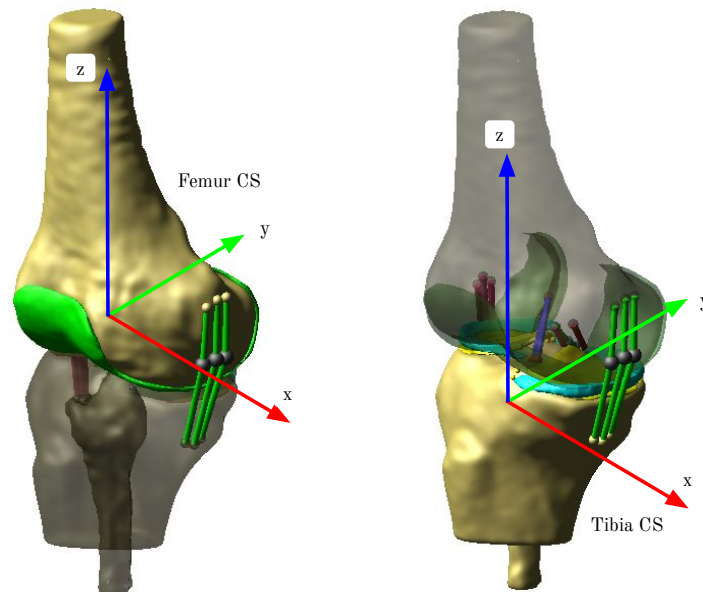


Figure 3.1: Model coordinate system (CS) in terms of the knee joint coordinate system. The figure shows the local coordinate system for the femur (left) and the tibia (right). The femur coordinate system corresponds to the KJCS as described by Grood and Suntay (1983). The direction of the arrows correspond to the medial (x), posterior (y) and superior (z) directions.

$$f(\epsilon) = \begin{cases} \frac{1}{4}k\frac{\epsilon^2}{\epsilon_l} & 0 \leq \epsilon \leq 2\epsilon_l \\ k(\epsilon - \epsilon_l) & \epsilon > 2\epsilon_l \\ 0 & \epsilon < 0 \end{cases} \quad (3.1)$$

with:

f	Ligament force	[N]
k	Ligament stiffness parameter	[N]
ϵ	Ligament strain	[mm/mm]
ϵ_l	Non-linear strain parameter	[-]

1986). Additionally, a damping term (damping coefficient of 0.5 Ns/mm) was included in the single-component force elements to help improve model stability (Guess *et al.*, 2010).

As noted by Bloemker *et al.* (2012), the ligament force is very sensitive to the length at which force in the ligament reduces to zero. This is referred to as the ligament ‘zero-load length’ (ZLL). Ligament ZLL is estimated from a kinematic envelope of motion test. This test estimates the full range of motion while applying minimal force to the joint. The procedure for determining ligament ZLL will be discussed in more detail in Chapter 3.3.3. The ZLL is used to determine ligament strain, given by equation 3.2. The strain calculated in equation 3.2 is then used to determine ligament force in equation 3.1.

$$\epsilon = \frac{l - l_0}{l} \quad (3.2)$$

with:

ϵ	Ligament strain	[mm/mm]
l	Ligament length	[mm]
l_0	Ligament zero-load length	[mm]

The model included two ligament bundles for the ACL (Blankevoort *et al.*, 1991; Duthon *et al.*, 2006; Guess *et al.*, 2010; Amis, 2012; Bloemker *et al.*, 2012; Guess *et al.*, 2015; Guess and Razu, 2017) and the PCL (Blankevoort *et al.*, 1991; Race and Amis, 1994; Guess *et al.*, 2010; Amis, 2012; Bloemker *et al.*, 2012; Guess and Razu, 2017) and three ligament bundles for the MCL and the LCL (Blankevoort *et al.*, 1991; Park *et al.*, 2005; Harris *et al.*, 2016; Kia *et al.*, 2016).

The most common method of ligament representation in multibody models is the use of spring-damper elements acting in the line-of-sight of ligament insertion sites. By contrast, ligaments are modelled as deformable structures

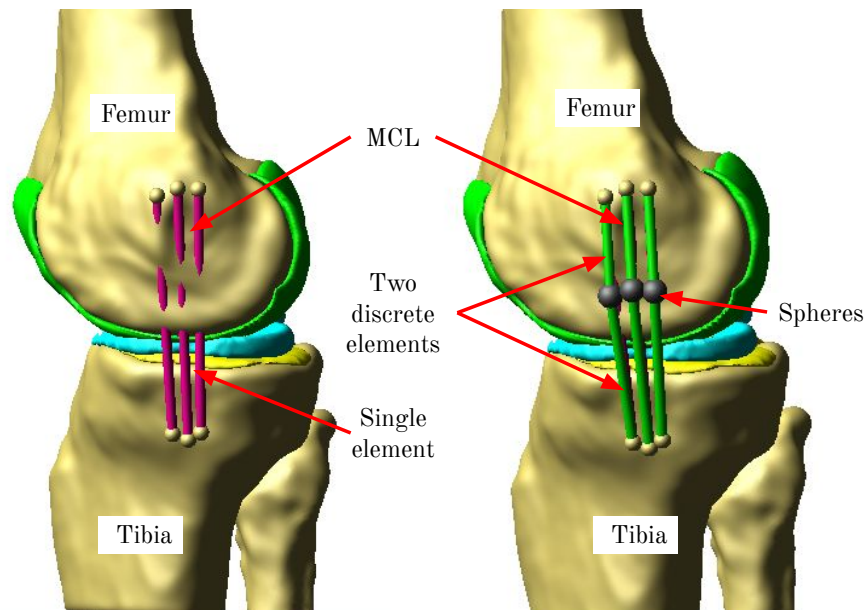


Figure 3.2: MCL bundles with single discrete elements (left) and two discrete elements per bundle (right). As a result of the ligament bundles acting in the line-of-sight of insertion locations, the bundles in the left-hand side of the figure penetrate the femur geometry. Modelling ligament bundles with two or more discrete elements (right-hand side), connected via spheres enables representation of ligament wrapping in the model.

in finite element models of the knee, which enables them to wrap around the bone and have a physiologically accurate representation. Wrapping the ligament around a bony edge of the tibia will redirect some of the force from the femur and influence equilibrium equations (Blankevoort and Huiskes, 1991). By modelling ligaments as point-to-point spring-damper elements, some of the physiological accuracy is lost, and joint mechanics are altered. To allow additional degrees of freedom and to improve physiological accuracy of ligament representation in the model, a technique similar to Kia *et al.* (2016) and Guess and Razu (2017) was employed to include wrapping of the MCL.

Inclusion of ligament wrapping involves dividing the ligament into two or more discrete elements, which have the same mechanical properties as the original single ligament element. The elements are connected via a sphere and are free to rotate. Spheres are modelled as rigid bodies with the same density as the femur and tibia. Contact is defined between the sphere and the osseous, which enables the ligament to wrap around the bone and translate on the bone geometries. Figure 3.2 shows the differences between a model with and without ligament wrapping of the MCL. The figure also shows the difference between a single and a multi-element ligament bundle.

To determine whether modelling ligaments with additional degrees of freedom improves the accuracy of model predicted joint kinematics and kinetics,

three separate simulations of 30° anterior-posterior tibial drawer were conducted. The results of simulations were compared to the experimentally measured kinematics and kinetics. The process of evaluating the influence ligament wrapping will be discussed in more detail in Chapter 3.3.2.

Lastly, the menisci were attached to the tibia by means of the meniscal horn attachments. These attachments were also modelled as single-component force elements (Guess *et al.*, 2015; Guess and Razu, 2017; Guess *et al.*, 2018). The movement of the menisci were not constrained in any other way. The parameters used to define ligaments in the model are summarized in Table 3.2.

Table 3.2: Ligament parameters used in the model. The ligament bundle suffix ‘a’, ‘p’, ‘i’ and ‘s’ refer to the relative anatomic position of each ligament bundle, i.e. anterior, posterior, inferior or superior. Note that the unit of ligament stiffness, k is in Newton, as given in equation 3.1.

Ligament	Ligament bundle	k [N]	ZLL [mm]	Reference
Anterior cruciate ligament	ACL _a	6200	28.95	Guess <i>et al.</i> (2015)
	ACL _p	3400	21.37	
Posterior cruciate ligament	PCL _a	12 500	42.13	Guess <i>et al.</i> (2015)
	PCL _p	1500	40.43	
Medial collateral ligament	MCL _a	2700	58.06	Blankevoort <i>et al.</i> (1991)
	MCL _i	2700	60.56	
	MCL _p	2700	58.57	
Lateral collateral ligament	LCL _a	2000	52.63	Blankevoort <i>et al.</i> (1991)
	LCL _p	2000	52.48	
	LCL _s	2000	55.83	
Meniscus horn attachments	Lateral anterior	2800	12.16	Guess and Razu (2017)
	Lateral posterior	1300	10.64	
	Medial anterior	2350	14.49	
	Medial posterior	1500	10.61	

3.2.4 Contacts

Contacts were defined between the menisci, the femoral cartilage and the tibial cartilage. Contact mechanics were modelled by a compliant contact (impact function in Adams), described by equation 3.3. The algorithm also allows for specification of the effective distance over which contact damping is applied. Damping is zero at zero penetration and maximum at a penetration depth of d_{max} .

$$F_c = k\delta_{int}^{exp} + C\dot{\delta}_{int} \quad (3.3)$$

with:

F_c	Compliant contact force between two solid bodies	[N]
k	Compliant contact stiffness coefficient	[N/mm]
δ_{int}	Overlap of interfacing bodies	[mm]
exp	Elastic coefficient	[-]
C	Damping coefficient	[Ns/mm]
$\dot{\delta}_{int}$	Rate of overlap of interfacing bodies	[mm/s]

Contact was modelled as frictionless. This assumption is based on the articulating cartilage surfaces having a very low friction coefficient (0.002 – 0.01) (Caligaris and Ateshian, 2008; Oungoulian *et al.*, 2016). The range of coefficient value is dependent on the loading rate of the joint and the amount of interstitial fluid exchange across joint surfaces (Ateshian, 2009; Halloran *et al.*, 2012). Incorporating variation in friction as a function of the amount of interstitial fluid adds substantial complexity to the model. To the author's best knowledge, only one recent multibody study included the effects of friction in the contact model (Guess *et al.*, 2013) when simulating a walking cycle. The study found that including friction was only significant for medial-lateral translation, valgus rotation and internal rotation, but not significant for anterior-posterior translation, superior-inferior translation, flexion-extension, or contact pressure. However, it is important to note that the menisci were omitted from the model. The menisci play an important role in the redistribution of forces in the knee and including the menisci could have changed the significance of including friction.

Stiffness and damping parameters are often manipulated during model validation to match experimental estimates, hence the large variation of parameters used in validated multibody knee models. Many studies spend considerable time and computational resources to optimize the contact parameters for their model. For the current representation of the model, contact parameters are based on parameter values used by Guess and Razu (2017) for a similar study that also simulated ACL deficiency. The contact parameters used for

modelling cartilage-to-cartilage contact and cartilage-to-meniscus contact are provided in Table 3.3.

Table 3.3: Compliant contact parameters for cartilage-to-cartilage contact and cartilage-to-meniscus contact. The subscript ‘c’ refers to cartilage-to-cartilage contact and the subscript ‘m’ refers to cartilage-to-meniscus contact.

Parameter	Value	Unit	Reference
k_c	300	[N/mm]	Guess <i>et al.</i> (2010); Guess and Razu (2017)
C_c	5	[Ns/mm]	
exp_c	1.5	[-]	
d_{max_c}	0.01	[mm]	
k_m	20	[N/mm]	Guess <i>et al.</i> (2010); Guess and Razu (2017)
C_m	0.1	[Ns/mm]	
exp_m	2	[-]	
d_{max_m}	0.01	[mm]	

3.2.5 Boundary conditions

A forward dynamics approach was implemented, in which forces applied by the robot were used as input boundary conditions for the model. No additional kinematic constraints were applied in order to note any change in kinematics when simulating ACL deficiency. Model outputs are joint kinematics, joint kinetics, ligament forces and contact forces. Model inputs and outputs are shown schematically in Figure 3.3. Details of applied loading conditions are discussed in Chapter 3.3.

Experimental data was processed using a five-point moving average filter function³ in MATLAB (Matlab R2018a, The MathWorks, Inc., Natick, MA, USA). This is equivalent to low-pass filtering, but does not require specifying a cut-off frequency. Additionally, this filtering method enables resistance to outliers as it uses a locally weighted regression for data-points within the five-point span. Test data was filtered to reduce the effects of any sudden accelerations of parts in the model due to experimental noise and irregularities in the recorded signal, which improved model stability. A sample of the unfiltered and filtered experimental data is shown in Figure 3.4.

³<https://www.mathworks.com/help/curvefit/smoothing-data.html>, 2019

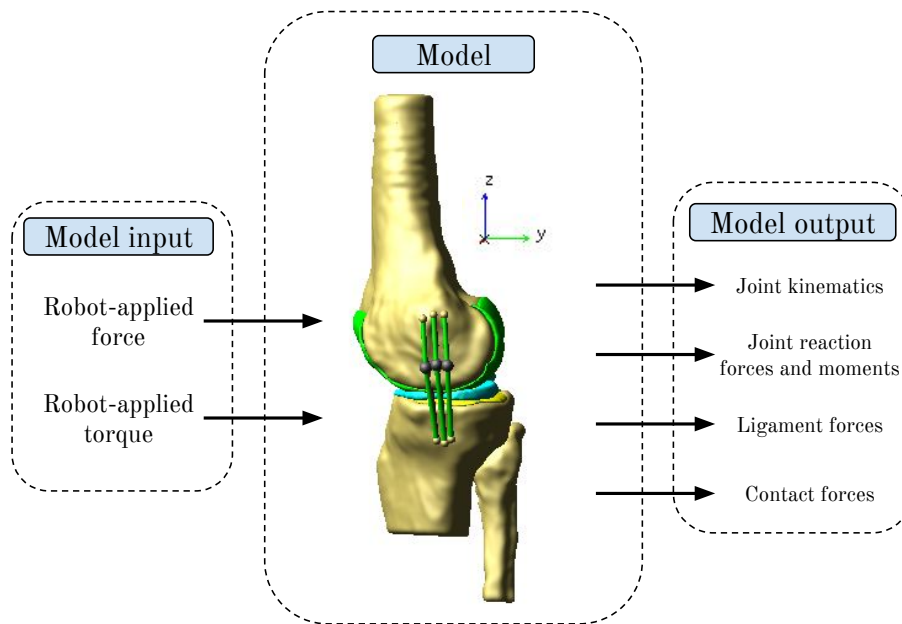


Figure 3.3: Schematic representation of model input and output boundary conditions.

3.2.6 Solver parameters

A dynamic rigid body solver (Adams 2018.1, MSC Software Corporation) was used to solve for the equations of motion at each timestep. The GSTIFF and WSTIFF integrators are two backward difference formula (BDF) integrators in MSC Adams which work well for solving numerically ‘stiff’ problems. Stiff integrators are used when ordinary differential equations (ODEs) of the system of equations of motion have widely separated eigenvalues (large ratio between highest overdamped eigenvalue and the lowest underdamped eigenvalue), causing it to be numerically unstable. BDF integrators are also known as ‘predictor-corrector’ type of numerical integrators. These integrators solve the ODEs iteratively in two phases. Integrators perform the initial ‘prediction’ step, based on the historical results (or initial conditions in case of the initial timestep). Predictions seldom satisfy the equations of motion, but constitute a good initial guess for the solution. Refining the solution is done in the next step, ‘correction’. The correction step refines the initial approximation by using the predicted value and iterative scheme, such as the Newton-Raphson method, to determine the solution. This is repeated until convergence criteria are met (error residual is less than the specified integration error parameter). Typically, corrector failures occur when the Newton-Raphson iterations do not converge to a solution. The GSTIFF integrator uses Taylor’s series

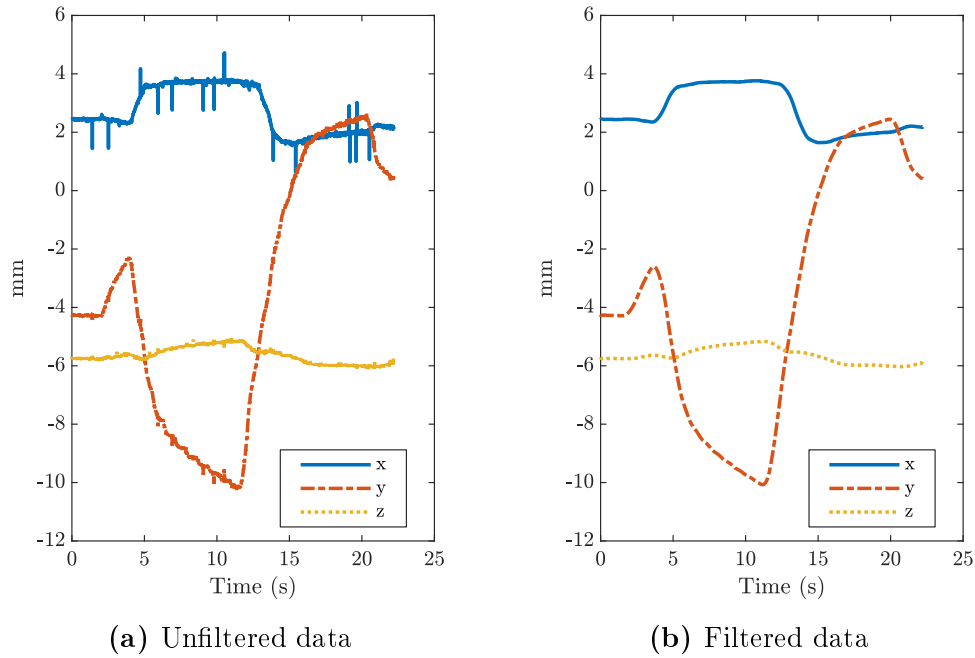


Figure 3.4: A sample of experimental kinematic data filtering. The data refers to medial-lateral translation (x), anterior-posterior translation (y) and superior-inferior translation (z) for anterior drawer testing.

expansion to predict the initial value of the solution, whereas WSTIFF uses Newton's divided difference interpolation method. Although both the GSTIFF and WSTIFF integrators were capable of solving the system ODEs, the GSTIFF integrator was used.

Integrator formulation controls how the corrector is applied, and is specific to the type of integrator. The Index 3 (I3) corrector is the default for BDF integrators, and requires the solver to monitor integration errors in displacement when solving the equations of motion. The alternative corrector formulation for the GSTIFF and WSTIFF integrators is the Stabilized Index 2 (SI2) formulation. For the SI2 formulation, the solver also monitors the velocity errors. This formulation is better suited to deal with simulations involving abrupt changes and high frequencies, which are common for contact modelling. This improves the robustness of solutions and decreases corrector failures due to ill-conditioning of the Jacobian. Hence, the SI2 corrector is better suited for the current simulations than the I3 formulation. The corrector in a stiff integrator ensures that all solutions predicted by the solver satisfy the system equations of motion. The 'original' and 'modified' correctors differ in terms of convergence criteria. The original corrector was used, as it has stricter criteria than the modified corrector.

The maximum step size was set to the same value as the integrator step size. Although restricting the maximum step size increases simulation time, it will prevent the integrator from stepping over important events such as

contact and prevent integration failures that result from too large step sizes. The minimum step size was not specified as the default setting is equal to 1.0×10^{-6} times the maximum step size. The initial step size was chosen to be smaller than the minimum step size to improve solver stability for the initial time step.

The integration error parameter specifies the relative and absolute local error tolerance that the integrator must satisfy at each step. If the integration error is not satisfied at each step, the solution does not converge, and the solver aborts the simulation. The default integration error parameter is 0.001. Integration failures typically occur when the specified step size is too large, resulting in local truncation error becoming larger than the error specified.

The adaptivity parameter is used to ‘loosen’ corrector tolerance when the step size gets small to prevent corrector failures. This parameter was not changed, with the default setting being ‘off’.

The interpolation parameter specifies that the integrator does not have to control step size to hit an output point. Therefore, if the integrator passes an output point, an intermediate solution can be calculated, which can be then refined by interpolating to the desired output point. This setting was used with the default interpolation parameters. Interpolation helps improve solver stability. The solver parameters used and are summarized in Table 3.4.

Table 3.4: Solver parameters

Parameter	Value
Step size [s]	1.0×10^{-3}
Start at equilibrium	No
Integrator	GSTIFF
Formulation	SI2
Corrector	Original
Error	1.0×10^{-3}
Hmax (maximum step size) [s]	1.0×10^{-3}
Hmin (minimum step size) [s]	Default
Hinit (initial step size) [s]	1.0×10^{-5}
Adaptivity	Default
Interpolate	On
Kmax (maximum integration order)	6
Maximum iterations	5
Fixed iterations	Off

3.3 Using the model to simulate ACL biomechanics

Ligament deficiency was simulated by ‘deactivating’ the bundles of the ACL, which was equivalent to transection of the ligament fibres to predict the effects on joint kinematics and kinetics. By subjecting the ACL deficient (ACLd) knee to the same loading conditions as the intact (ACLi) knee, changes in joint loading and joint motions can be observed and quantified.

3.3.1 Experimental tibiofemoral testing

A schematic comparing elements in the experiment to the corresponding elements in the model is shown in Figure 3.5. As shown in the figure, the femur was fixed to the articulating arm of the robot and the tibia was mounted to a load cell, which was fixed to the robot frame.

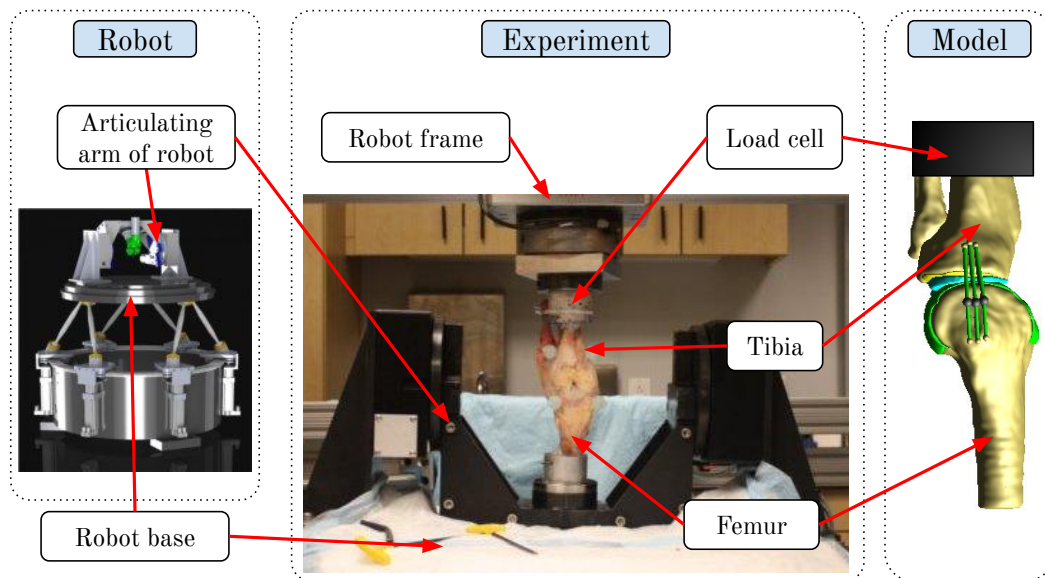


Figure 3.5: Schematic comparison between the robot, experiment and the model.

3.3.2 30° Anterior-posterior drawer testing

The 30° anterior-posterior drawer tests are primarily used to test ACL biomechanics, as anterior tibial force at a flexion angle of 30° has the most direct loading of the ACL (Markolf *et al.*, 1995, 2008). The secondary purpose was to serve as a reproducibility test to ensure that there was no injury or damage

to any of the structures in the joint. The 30° AP drawer tests were repeated three times during the experiment and are referred to as Trials 1, 2 and 3.

The experimental protocol⁴ consisted of using the robot to test knee mechanics at 0°, 30°, 60° and 90° flexion. Before adjusting the robot for testing at a 0° flexion angle, the first of the three 30° AP drawer trials (Trial 1) was performed. After Trial 1 was completed, the robot was set to the position corresponding to 0° knee flexion and the isolated loading (discussed in Chapter 3.3.3) and combined loading experiments (discussed in Chapter 3.3.4) were performed. The robot was adjusted to 30° flexion, and the isolated and combined loading experiments were repeated, followed by the second AP drawer test (Trial 2). Next, isolated and combined loading experiments were performed at 60° and at 90° flexion. After the final experiment at 90°, the flexion angle was adjusted back to 30° and the third and final AP drawer test (Trial 3) was performed. The desired loading profile of the 30° AP drawer tests is shown in Figure 3.6.

Anterior-posterior translation and internal-external tibial rotation are two parameters used to assess knee stability (Markolf *et al.*, 1981, 2008; Sakane *et al.*, 1999; Abulhasan *et al.*, 2016; Harris *et al.*, 2016; Noyes *et al.*, 2017). Experimental data from the 30° AP drawer tests were used as model boundary conditions to evaluate the change in AP translation and IE rotation for the intact and ACL deficient knees. Additionally, the three separate tests could be used to quantify small changes in joint laxity that may occur from repetitive loading.

Experimental data of the three AP drawer trials was also used to evaluate the influence of ligament wrapping on the root mean square (RMS) error of model outputs. For each of the simulated trials, ligament wrapping of the MCL was enabled and the simulation time and RMS errors were recorded. Simulations were then repeated, but with wrapping of the MCL disabled (i.e. the ligament acts in the line-of-sight between the femur and tibia insertion sites). The RMS errors for simulations that included ligament wrapping were then compared to the RMS errors of simulations that did not include wrapping.

3.3.3 Isolated loading testing

Isolated loading testing helps determine the kinematic range of motion of the knee joint, and can be used to evaluate the effect of isolated degree-of-freedom loading on joint mechanics. These experiments test joint kinematics for three individual degrees of freedom, i.e. internal-external rotation, varus-valgus rotation and anterior-posterior translation.

Data from the isolated loading tests were used to estimate the zero-load lengths (ZLL) of ligaments. This was done by measuring the maximum line-

⁴<https://simtk.org/plugins/moinmoin/openknee/Specifications/Experimentation-JointMechanics>, 2019

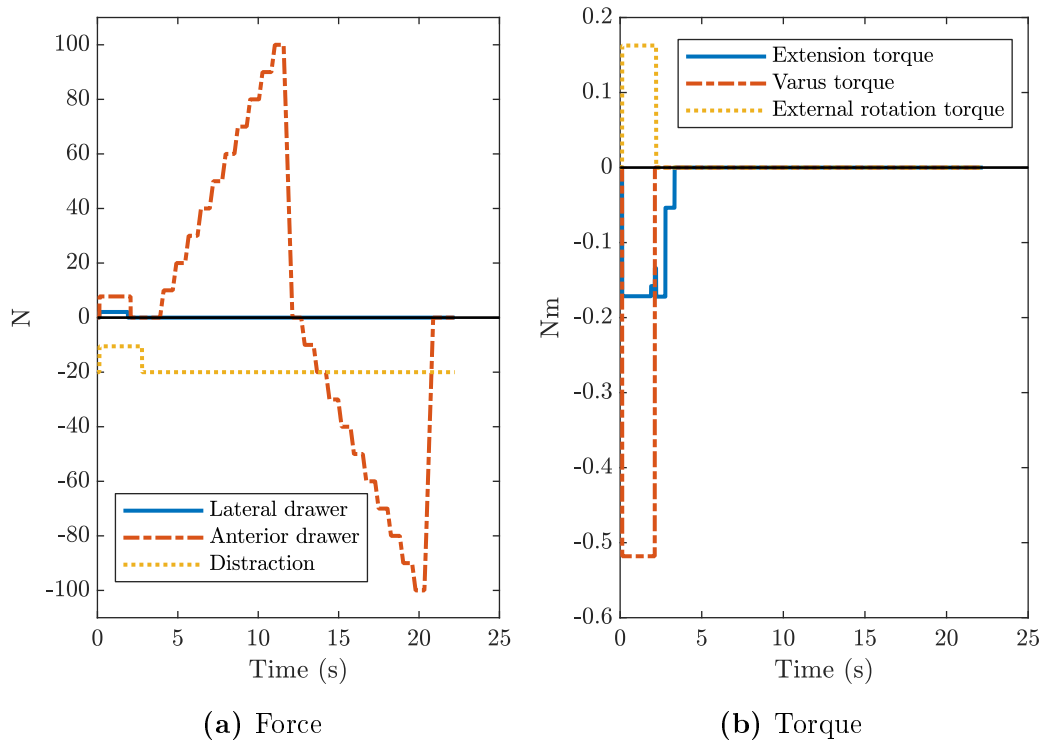


Figure 3.6: Desired loading profile for 30° anterior-posterior tibial drawer testing

of-sight length of each ligament during simulation. Based on the approach of Bloemker *et al.* (2012), the ZLL was estimated as a percentage value of the maximum ligament length. This percentage value was adjusted iteratively during model validation (Chapter 3.5) to match measured and predicted joint kinematics. The loading profile is shown in Figure 3.7.

3.3.4 Combined loading testing

Combined loading tests apply multi-degree-of-freedom loads to the joint that could be encountered in dynamic activities such as squatting, jumping or running. Simultaneous application of joint loads allows for comparison to clinical studies that also tested combinations of loading conditions (Markolf *et al.*, 1995, 2008; Sakane *et al.*, 1999; Kanamori *et al.*, 2000; Woo *et al.*, 2002; Gabriel *et al.*, 2004). Combined loading experiments tested simultaneous application of AP drawer force, VV torque and IE torque. The loading profile is shown in Figure 3.8.

3.3.5 Points of interest

Isolated anterior tibial loading, internal or external tibial torque and valgus torque are known to result in greater force in the ACL, especially when applied

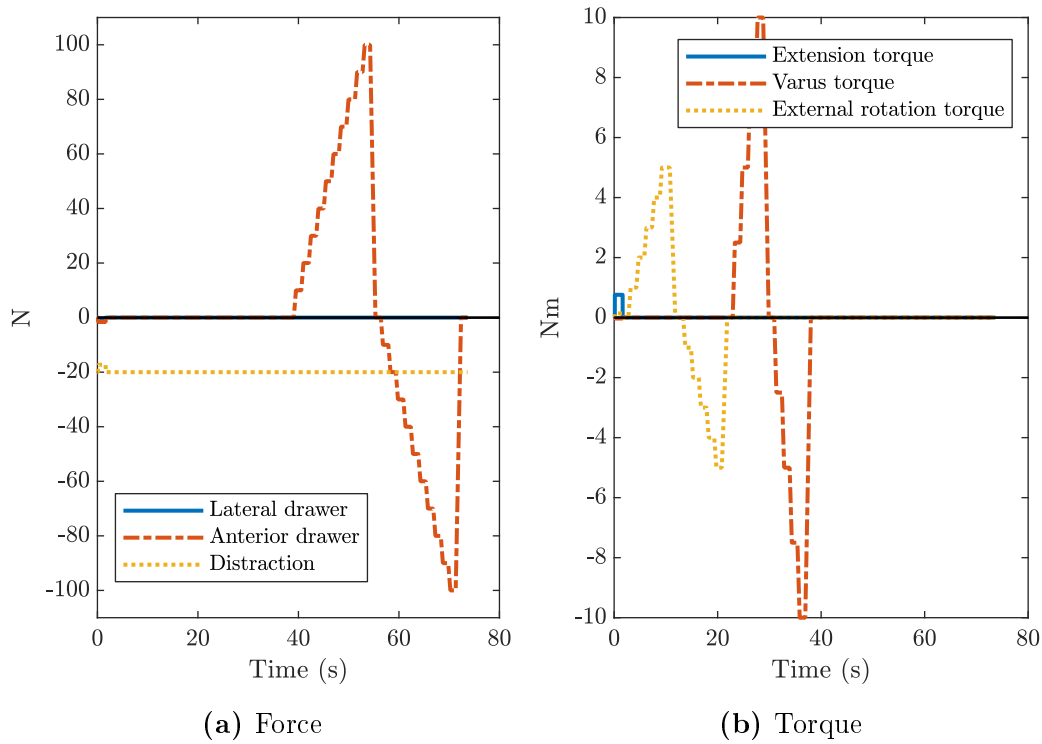


Figure 3.7: Desired loading profile for isolated loading testing

simultaneously (Markolf *et al.*, 1995). To compare ligament forces and joint contact kinetics for various flexion angles and load combinations, points of interest (POIs) were defined for isolated and combined loading tests. These POIs are similar to loading conditions that have been evaluated in other clinical studies (Markolf *et al.*, 1995, 2008; Sakane *et al.*, 1999; Kanamori *et al.*, 2000; Woo *et al.*, 2002; Gabriel *et al.*, 2004). The POIs and their corresponding applied loading conditions are given in Table 3.5.

3.4 Parametric study

In a model, there exist many parameter dependencies and some parameters are more sensitive to changes than others. A parametric study was done investigate the sensitivity of model outputs to changing ligament stiffness, ligament zero-load length and tibiofemoral contact stiffness.

Ligament stiffness values were varied in steps from +30 % to -30 % of the reference values in Table 3.2, according to variance in literature (Butler *et al.*, 1986; Blankevoort *et al.*, 1991) and the values used to model ligaments in multibody studies (Guess *et al.*, 2010, 2015; Guess and Razu, 2017). Ligament zero-load length was varied in steps from +20 % to -20 % of the reference values in Table 3.2, according to Bloemker *et al.* (2012) and Kia *et al.* (2016).

The values of compliant contact modelling parameters used in published

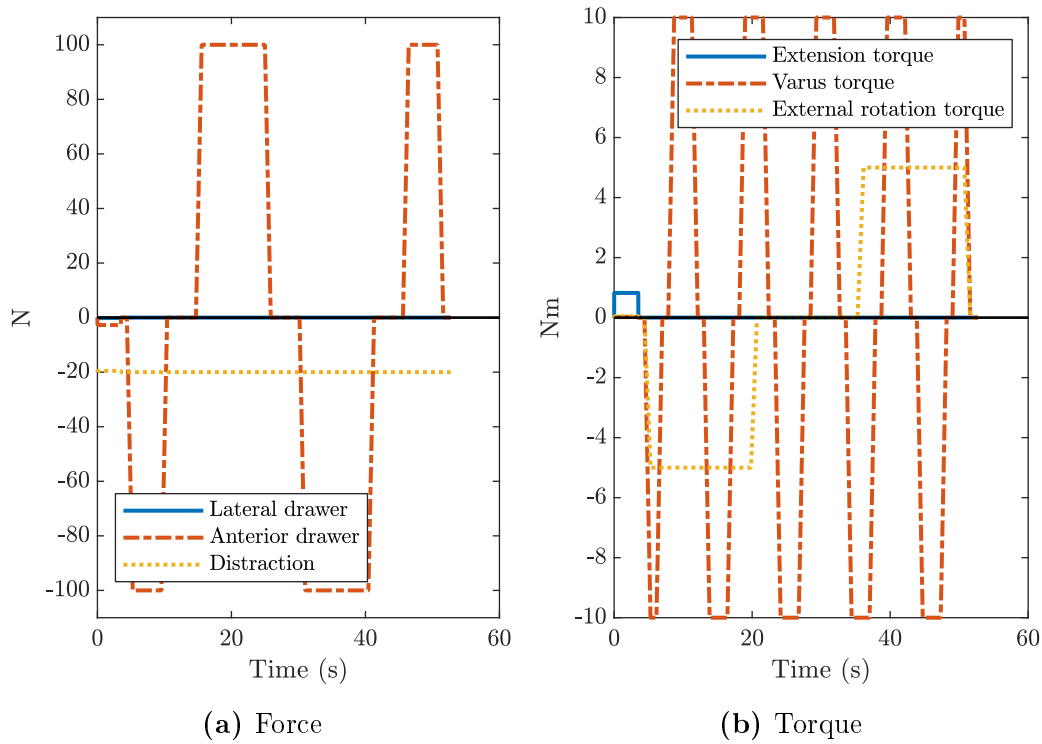


Figure 3.8: Desired loading profile for combined loading testing

Table 3.5: Points of interest for isolated and combined degree of freedom loading tests. Timesteps for isolated loading POIs refer to Figure 3.7 and timesteps for combined loading POIs refer to Figure 3.8.

Point of interest	Loading condition	Timestep [s]
Isolated loading POI 1	10 Nm varus torque	36.7
Isolated loading POI 2	100 N anterior tibial force	54.0
Isolated loading POI 3	10 Nm valgus torque	28.5
Combined loading POI 1	100 N anterior tibial force	16.4
	10 Nm valgus torque	
	5 Nm internal rotation torque	
Combined loading POI 2	100 N anterior tibial force	46.6
	10 Nm valgus torque	
	5 Nm external rotation torque	

multibody studies vary considerably as each model is optimized for its given set of boundary conditions. By comparing a range of cartilage stiffness values used, the effect on model predicted results can be investigated. Tibiofemoral contact stiffness was varied in steps from +50 % to -50 % of the value in Table 3.3, according to differences in stiffness parameters used in multibody

models (Guess *et al.*, 2010, 2013).

The range of variation and the corresponding minimum and maximum values of the parameters are shown in Table 3.6. Only one parameter was changed at a time. All results were normalized relative to a 0 % change in the input parameter value. Variation of meniscal horn attachment stiffness was not included in the parametric study.

Table 3.6: Parameters in sensitivity analysis

Parameter	Lower	Upper	Reference
Ligament stiffness [N]	-30 %	+30 %	Butler <i>et al.</i> (1986); Blankevoort and Huiskes (1991); Guess <i>et al.</i> (2010, 2015); Guess and Razu (2017)
ACL _a	4340	8060	
ACL _p	2380	4420	
PCL _a	8750	16250	
PCL _p	1050	1950	
MCL _a	1925	3575	
MCL _i	1925	3575	
MCL _p	1925	3575	
LCL _i	1400	2600	
LCL _p	1400	2600	
LCL _s	1400	2600	
Zero-load length [mm]	-20 %	+20 %	Bloemker <i>et al.</i> (2012); Kia <i>et al.</i> (2016)
ACL _a	23.163	34.745	
ACL _p	17.097	25.645	
PCL _a	33.705	50.557	
PCL _p	32.346	48.518	
MCL _a	46.448	69.672	
MCL _i	48.444	72.666	
MCL _p	46.855	70.283	
LCL _i	42.102	63.154	
LCL _p	41.986	62.978	
LCL _s	44.666	67.000	
Contact stiffness [N/mm]	-50 %	+50 %	Guess <i>et al.</i> (2010, 2013)
k_c	150	450	

3.5 Model validation

The computational model was validated in two parts. Model predicted joint kinematics were compared to experimental measurements, and model predicted joint kinetics were compared to forces and moments measured by the load cell mounted on the robot frame. Load cell force error thus refers to the difference in the experimentally measured load cell force and the model predicted reaction force at the tibia fixation point. All kinematics are determined relative to the position and orientation of the KJCS.

For both the kinematics and kinetics, a root mean square (RMS) error was calculated using the formula in equation 3.4. The model predicted variable is denoted by \hat{y} and the corresponding variable measured during experiments is denoted by y . The number of samples recorded during the experiment is represented by N . Based on the magnitude of the RMS errors the model could be validated. A schematic representation of model validation is shown in Figure 3.9.

$$RMS\ error = \sqrt{\frac{\sum_{n=1}^N (\hat{y}_n - y_n)^2}{N}} \quad (3.4)$$

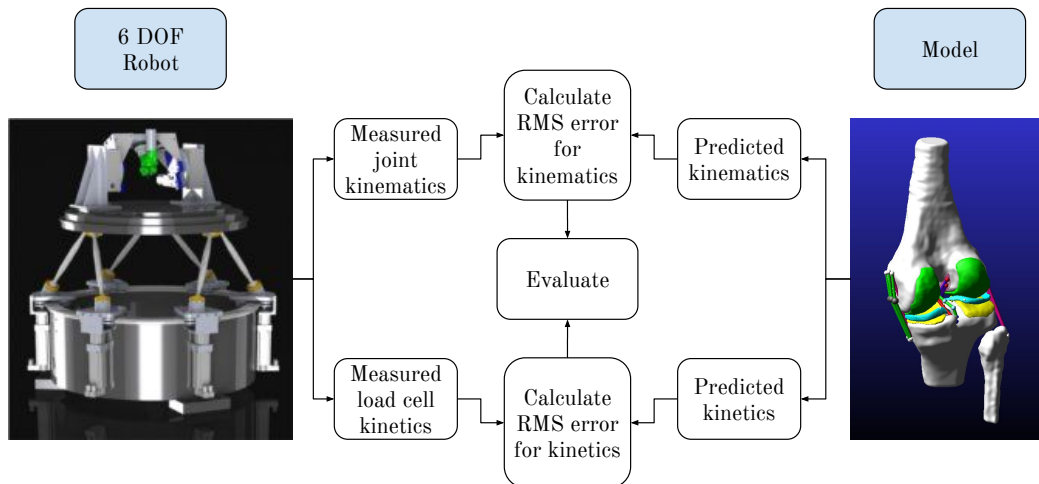


Figure 3.9: Schematic representation of model validation

Chapter 4

Results

A summary of the root mean square (RMS) errors of model predicted results will be given and the results of simulations with and without ligament wrapping will be compared. Furthermore, results of joint kinematics, ligament forces and joint contact forces will be given for intact and ACL deficient knees at various angles of flexion. Finally, the sensitivity of model outputs to changes in modelling parameters will be presented. The results presented here will be discussed in Chapter 5.

4.1 Model validation

The model is validated by comparing model outputs to experimental measurements of joint kinematics and joint kinetics. Table 4.1 summarizes the RMS errors and standard deviations of predicted kinematics and kinetics for the ACL intact (ACL_i) simulations. The RMS errors in the table represent the average of each type of experimental test as a magnitude error between experimentally measured and model predicted output. Errors for individual simulations are given in Appendix C.

As shown in Table 4.1, the magnitude of load cell force RMS errors were maximum in the z-direction for all simulations (24.1 N for 30° AP drawer, 20.1 N for isolated loading and 23.3 N for combined loading). Load cell moment errors were greatest about the y-axis for isolated loading and combined loading simulations (2.8 Nm and 5.6 Nm respectively) and largest about the x-axis for 30° AP drawer simulations (1.9 Nm). Position errors were greatest in the x-direction for isolated loading and combined loading simulations (2.9 mm and 4.4 mm respectively), and greatest in the z-direction for 30° AP drawer (2.5 mm). Orientation errors were largest about the z-axis for isolated loading (3.2°) and combined loading (6.5°) simulations, and greatest about the y-axis for 30° AP drawer simulations (2.6°).

Table 4.1: RMS errors of simulations

Measured parameter	30° AP drawer		Isolated loading		Combined loading	
	RMSe	σ	RMSe	σ	RMSe	σ
Load cell force						
X [N]	9.8	0.73	8.8	0.52	12.6	0.02
Y [N]	4.7	0.12	3.7	0.51	9.8	2.45
Z [N]	24.1	4.08	20.9	4.41	23.3	4.64
Load cell moment						
X [Nm]	1.9	0.46	2.1	0.21	4.7	0.92
Y [Nm]	1.4	0.41	2.8	0.17	5.6	0.65
Z [Nm]	1.0	0.27	2.1	0.24	4.4	0.39
KJCS position						
X [mm]	1.5	0.04	2.9	0.93	4.4	0.5
Y [mm]	1.1	0.07	2.0	0.38	4.2	0.17
Z [mm]	2.5	0.07	1.8	0.82	3.2	0.4
KJCS orientation						
X [°]	1.6	0.12	2.8	1.6	5.3	2.59
Y [°]	2.6	0.18	3.1	0.35	5.8	0.29
Z [°]	1.8	0.28	3.2	0.63	6.5	0.77

KJCS, knee joint coordinate system; AP, anterior-posterior; RMSe, root mean square error magnitude; σ , standard deviation.

4.2 Ligament wrapping

The CPU time required for simulations with, and without ligament wrapping is shown in Table 4.2. Simulations that included ligament wrapping had considerably longer CPU times than simulations without ligament wrapping. Simulation time for trials with ligament wrapping were 18.8 hours for Trial 1 (T1), 9.4 hours for Trial 2 (T2) and 10.9 hours for Trial 3 (T3). For trials that did not include ligament wrapping, the simulation times were 0.5 hours, 1.1 hours and 1.0 hours for T1, T2 and T3 respectively. The longest CPU time required was 18.8 hours for T1, with ligament wrapping enabled. Conversely, the shortest CPU time required was 0.5 hours for T1, with ligament wrapping disabled.

The RMS errors for KJCS position, KJCS orientation, load cell force and load cell moments are shown in Figure 4.1 for trials with and without ligament wrapping. As shown in Figure 4.1(a), the RMS errors for KJCS position is greater for T2 and T3 when ligament wrapping is enabled (1.78 mm and 1.8 mm) than when ligament wrapping is disabled (1.75 mm and 1.73 mm).

Table 4.2: CPU time of simulating 30° AP drawer with and without ligament wrapping enabled. Trials 1, 2 and 3, with wrapping enabled, are indicated by ‘1 wrap’, ‘2 wrap’ and ‘3 wrap’. Trials 1, 2 and 3, with wrapping disabled, are indicated by ‘1 no wrap’, ‘2 no wrap’ and ‘3 no wrap’.

Trial	CPU time [hours]
1 no wrap	0.5
1 wrap	18.8
2 no wrap	1.1
2 wrap	9.4
3 no wrap	1.0
3 wrap	10.9

However, enabling ligament wrapping provided a slight reduction in RMS error in T1 (1.65 mm for wrapping compared to 1.66 mm without wrapping).

RMS errors for KJCS orientation, shown in Figure 4.1(b), were larger when wrapping was enabled (2.64°, 2.59° and 2.59° for T1, T2 and T3 respectively) compared to simulations with wrapping disabled (1.96°, 2.11° and 1.97° for T1, T2 and T3 respectively). The largest orientation error was for T1 with wrapping enabled (2.64°).

RMS errors for load cell force, shown in Figure 4.1(c), were greater for simulations that included ligament wrapping (23.62 N, 124.07 N and 62.49 N for T1, T2 and T3 respectively) than for simulations that did not include wrapping (13.25 N for T1, 13.94 N for T2 and 11.37 N for T3). The largest load cell force error was 124.07 N for T2, with wrapping enabled. The smallest error was 11.37 N for T3, with wrapping disabled.

Finally, as shown in Figure 4.1(d), RMS error for load cell moments were larger when wrapping was enabled (3.25 Nm, 15.84 Nm and 9.21 Nm for T1, T2 and T3 respectively) compared to simulations without wrapping (1.42 Nm, 1.80 Nm and 1.09 Nm for T1, T2 and T3 respectively). T2 with wrapping enabled had the largest error (15.84 Nm) and T3 with wrapping disabled had the smallest error (1.09 Nm).

4.3 Knee kinematics

The results of model predicted joint kinematics for 30° AP drawer testing, isolated loading and combined loading simulations are presented in this section. Results for both ACLi and ACLd knees are also presented.

4.3.1 30° AP drawer testing

Figure 4.2 shows joint position of the ACLi and ACLd knee as a function of time. As a reference, the experimental position data is also shown on the graph

as a bold line.

Transient response can be observed for the initial second in Figure 4.2. The transient response is due to the model achieving steady state at the set flexion angle. Comparing ACLi and ACLd knees in Figure 4.2, a large deviation can be observed for anterior-posterior and superior-inferior position from 7 to 12 seconds. Maximum anterior displacement occurs at 11 seconds, which corresponds to the maximum anterior force applied to the knee.

The deviation between the data and trial results for the medial-lateral and superior-inferior positions in Figure 4.2 correspond to the RMS errors for x- and z-position reported in Table 4.1. The large medial and superior displacement (at 12 seconds) for ACLd knees is due to anterior dislocation of

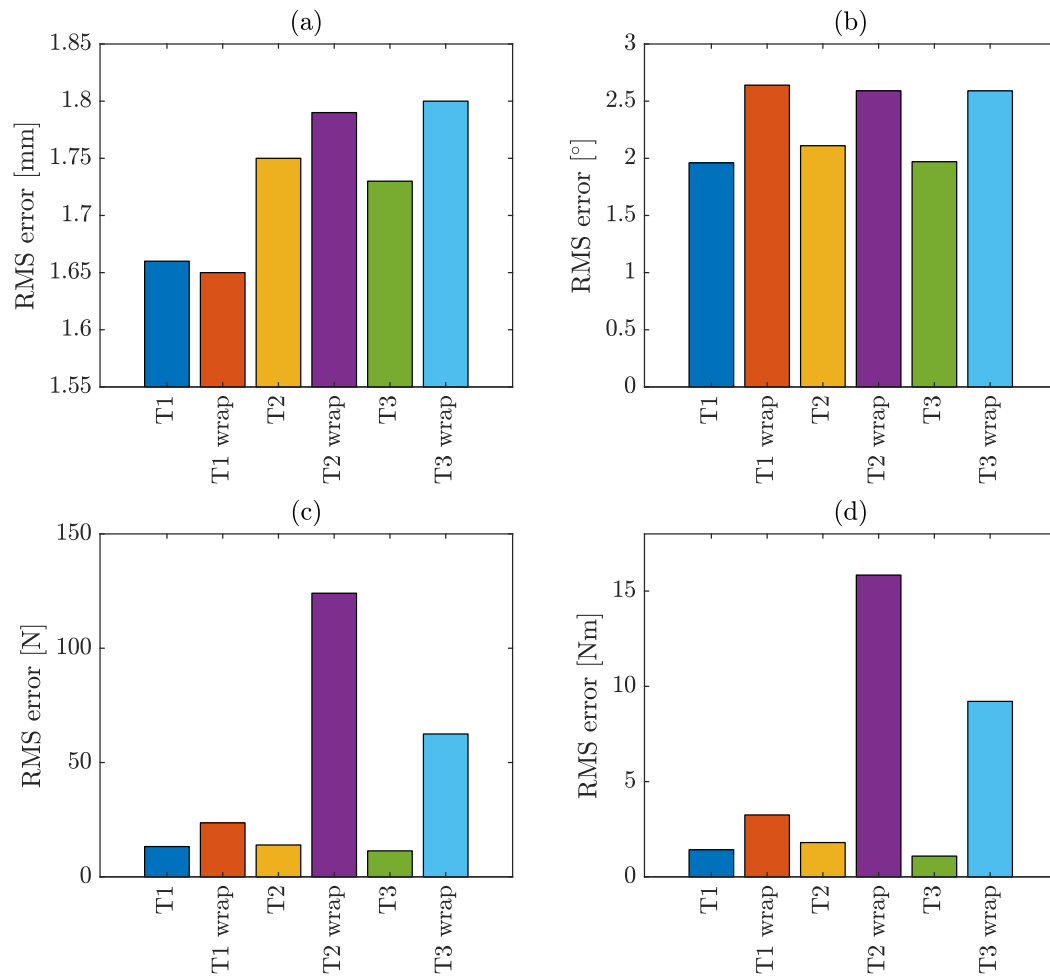


Figure 4.1: RMS errors of (a) KJCS position, (b) KJCS orientation, (c) load cell force and (d) load cell moments for simulation of 30° AP drawer with and without ligament wrapping activated. T1, T2 and T3 are trials that did not include ligament wrapping. T1 wrap, T2 wrap and T3 wrap are trials that included ligament wrapping.

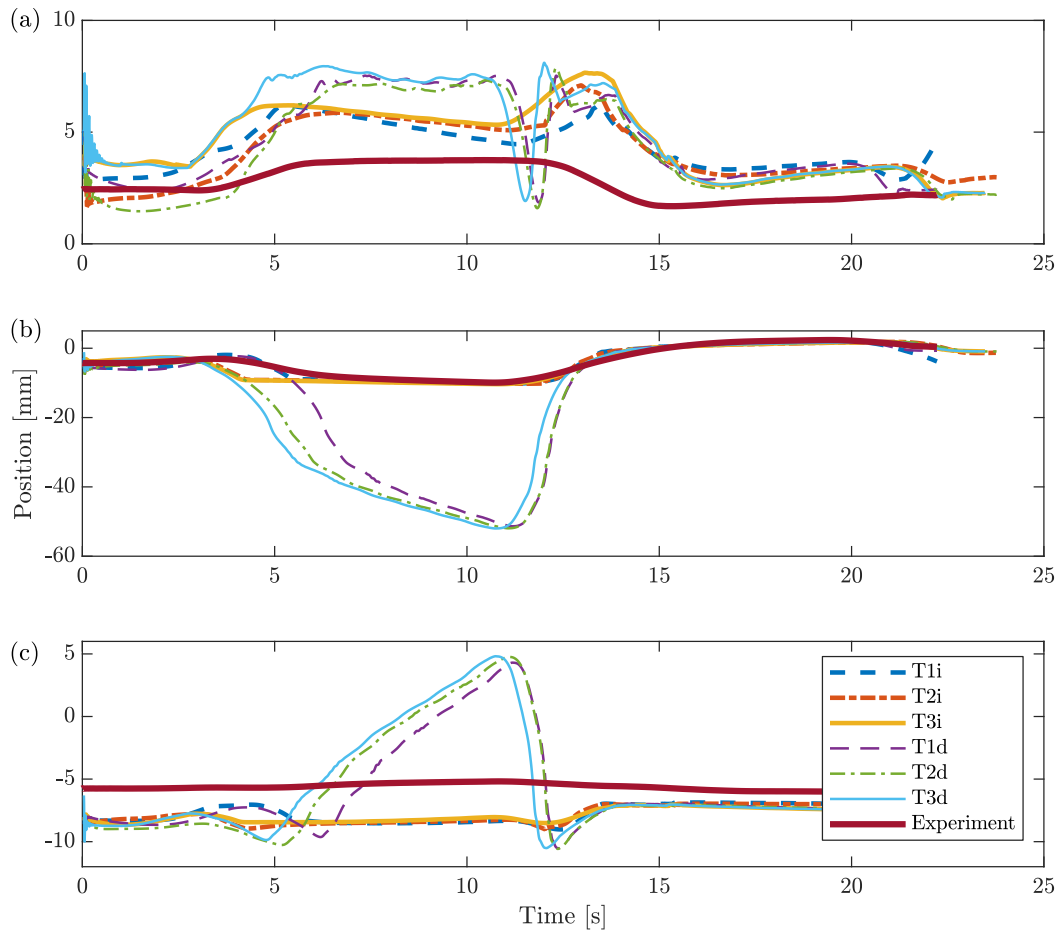


Figure 4.2: Joint position of ACLi and ACLd knees for 30° AP drawer test data. T1, T2 and T3 refers to Trial 1, 2 or 3, and ‘i’ or ‘d’ refers to the ACL ‘intact’ or ACL ‘deficient’ knee. All translations are in terms of the KJCS. Note that the scale is different for each plot. (a) Medial-lateral translation (+: medial); (b) anterior-posterior translation (+: posterior); (c) superior-inferior translation (+: superior).

the knee. The increase in superior displacement is as a result of the femur being in contact with and translating over the posterior edge of the menisci.

Figure 4.3 depicts joint orientation of the ACLi and ACLd knee as a function of time. For reference, experimental data is also included in the graph as a bold line.

A large difference (approximately 5°) between model predicted flexion angle and experimental data can be observed. The difference occurs during the timesteps (5 to 12 seconds), which corresponds to the timesteps when the anterior tibial load is applied. The error occurs due to the large moment caused by the applied load about the flexion axis. There are relatively large (4°) differences between experimental and model predicted valgus angles at

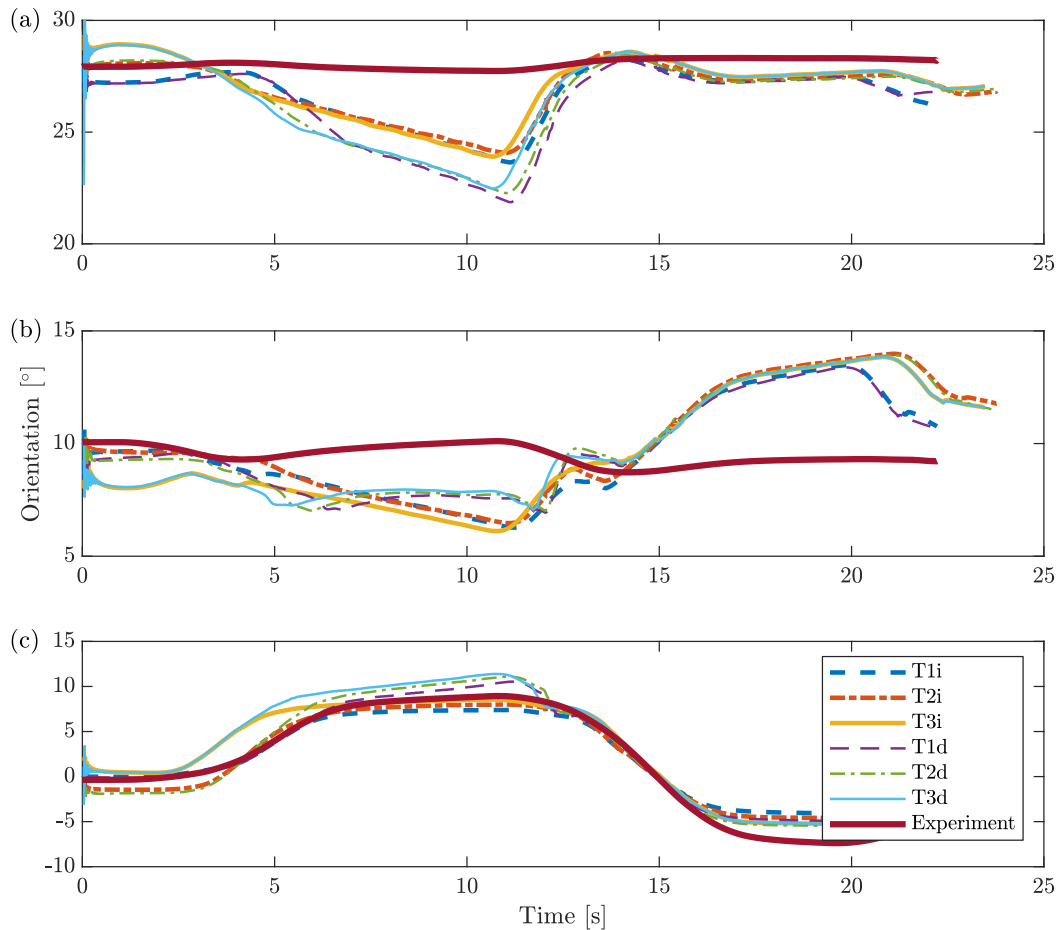


Figure 4.3: Joint orientation of ACLi and ACLd knees for 30° AP drawer test data. T1, T2 and T3 refers to Trial 1, 2 or 3, and ‘i’ or ‘d’ refers to the ACL ‘intact’ or ACL ‘deficient’ knee. All rotations are in terms of the KJCS. Note that the scale is different for each plot. (a) Flexion-extension (+: flexion); (b) varus-valgus (+: valgus); (c) internal-external tibial rotation (+: internal).

12 seconds and at 20 seconds. The large valgus error is a result of medial-lateral displacement error (Figure 4.2). At 12 seconds, the applied tibial loading changes from a 100 N anterior to a 100 N posterior tibial load. This causes the valgus angle to increase to approximately 4° more than the experimentally measured angle at 20 seconds. The change in the direction of the applied tibial force also results in a change in the internal rotation angle of the tibia. The orientation of the tibia changes from approximately 8° internal rotation (3 to 14 seconds) to 6° external rotation (15 to 20 seconds).

4.3.2 Kinematic range of motion

To compare the stability parameters at different flexion angles, the kinematic range of motion for AP translation and IE rotation is determined for the 30° AP

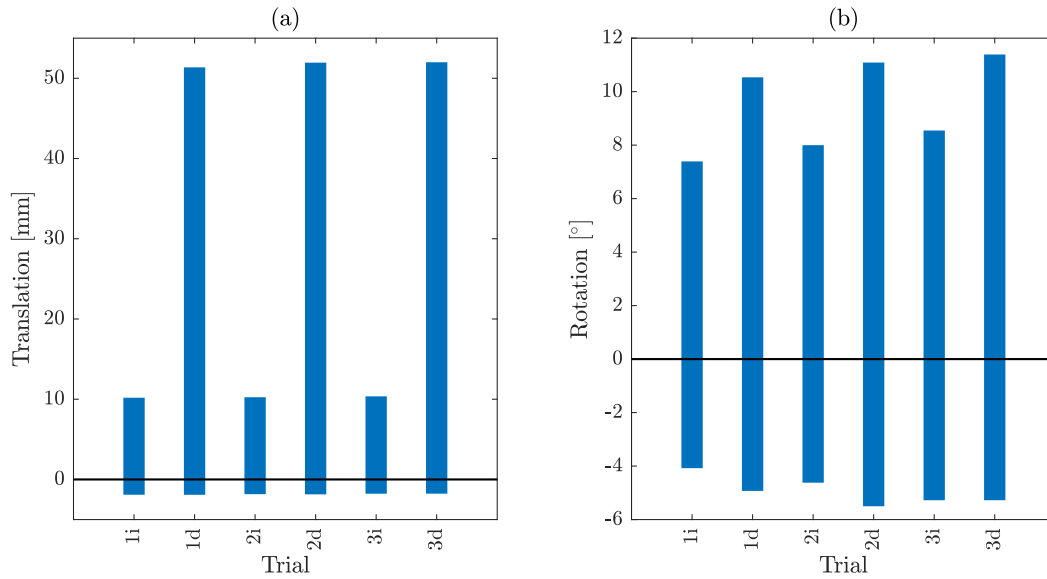


Figure 4.4: Comparison of the kinematic range of motion for ACLi and ACLd knees for 30° AP drawer simulation. Axis labels ‘1i’, ‘2i’ and ‘3i’ refer to Trials 1, 2 and 3 for ACLi knees. Likewise, ‘1d’, ‘2d’ and ‘3d’ refer to trials for ACLd knees. (a) Anterior-posterior translation (+: tibia moves anteriorly with reference to the femur); (b) internal-external tibial rotation (+: internal tibial rotation).

drawer, isolated loading and combined loading experiments. Figure 4.4 compares the change in the kinematic range of motion for the intact and ligament deficient knee when subjected to the loading conditions of the 30° AP drawer tests. Positive displacement refers to the tibia moving anteriorly with reference to the femur. Positive orientation corresponds to internal rotation of the tibia.

Figure 4.4(a) shows a substantial difference for all trials comparing AP translation for the intact and ACL deficient knees. The average range of AP translation is 12.1 mm (standard deviation, $\sigma = 0.03$ mm) and 53.6 mm ($\sigma = 0.29$ mm) for the ACLi and ACLd trials respectively. The average posterior translation is 1.83 mm for both ACLi and ACLd trials, confirming that posterior translation is not affected by ACL deficiency.

Figure 4.4(b) compares the IE rotational range of motion. The average range of IE rotation for ACLi knees is 12.6° ($\sigma = 1.2^\circ$) and 16.2° ($\sigma = 0.7^\circ$) for ACLd trials. An increase in internal rotation for ACLd knees confirms that the ACL contributes to restricting internal rotation in the knee.

Figure 4.5 compares the range of motion for (a) AP translation and (b) IE rotation at 0° and 30° flexion for both isolated loading and combined loading simulations. The AP range of motion was determined by calculating the difference between the maximum anterior translation and the maximum posterior translation during the simulation. A similar calculation was done to determine

the IE rotational range of motion.

For isolated loading simulations, the model predicted AP translation decreased slightly (1.8 mm) from 0° to 30° flexion for the ACLi knee. Model predicted AP translation for the ACLd knee increased from 0° to 30° flexion by 7.3 mm. Model predicted IE rotation increased by 7.5° and 7.6° from 0° to 30° flexion for both the ACLi and ACLd cases respectively.

For the combined loading simulations, the AP translation decreased from from 0° to 30° flexion for both the ACLi and ACLd knee for combined loading by 2.7 mm and 3.9 mm respectively. Model predicted IE rotation increased by 9.4° and 15.3° for both the ACLi and ACLd knees respectively from 0° to 30° flexion.

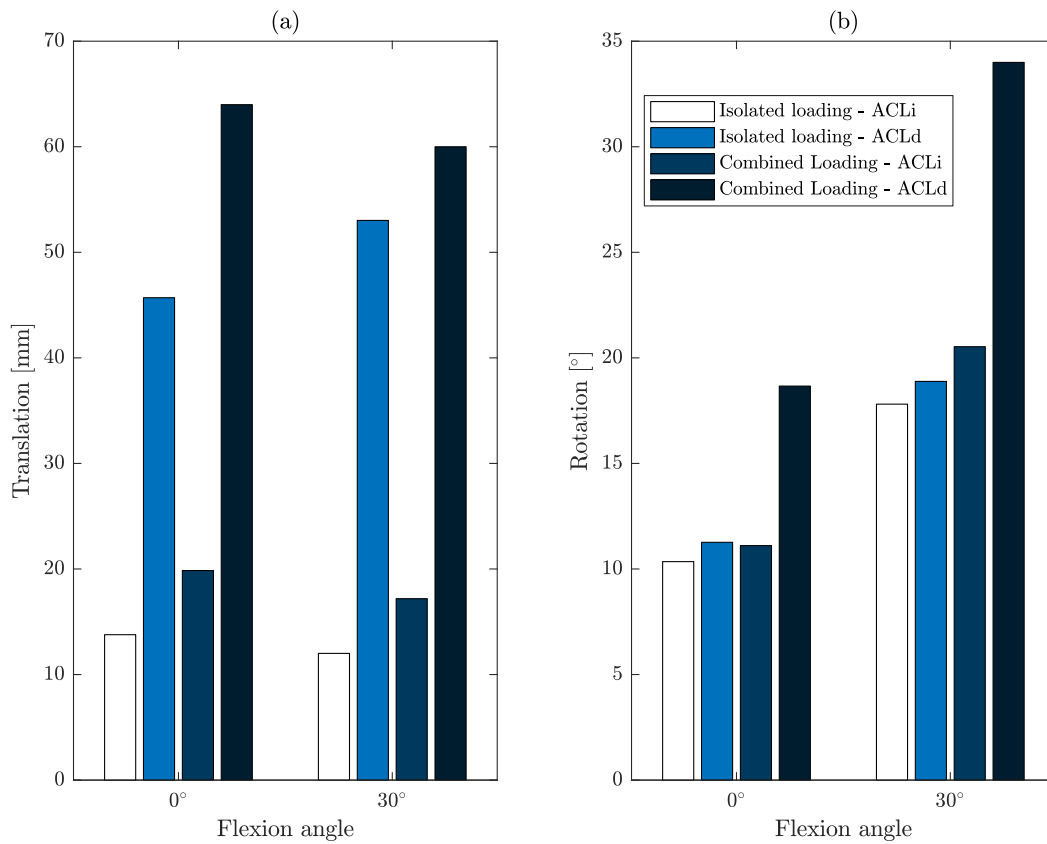


Figure 4.5: Comparison of the kinematic range of motion at different flexion angles for ACLi and ACLd knees for isolated loading and combined loading simulations. (a) Anterior-posterior translation (+: tibia moves anteriorly with reference to the femur); (b) internal-external tibial rotation (+: internal tibial rotation).

4.4 Ligament forces

Ligament forces are predicted for both the intact and ACL deficient knees. Changes in ligament forces due to ACL deficiency are determined at points of interest for isolated loading and combined loading tests.

4.4.1 30° AP drawer testing

Figure 4.6 depicts the total ligament forces in the intact and ACL deficient knees for Trial 1. The other 30° AP drawer tests, Trial 2 and 3, have very similar ligament forces and are not shown in this section. For simulations of ACL deficiency, the ACL was deactivated in the model and the resulting ACL force is thus zero.

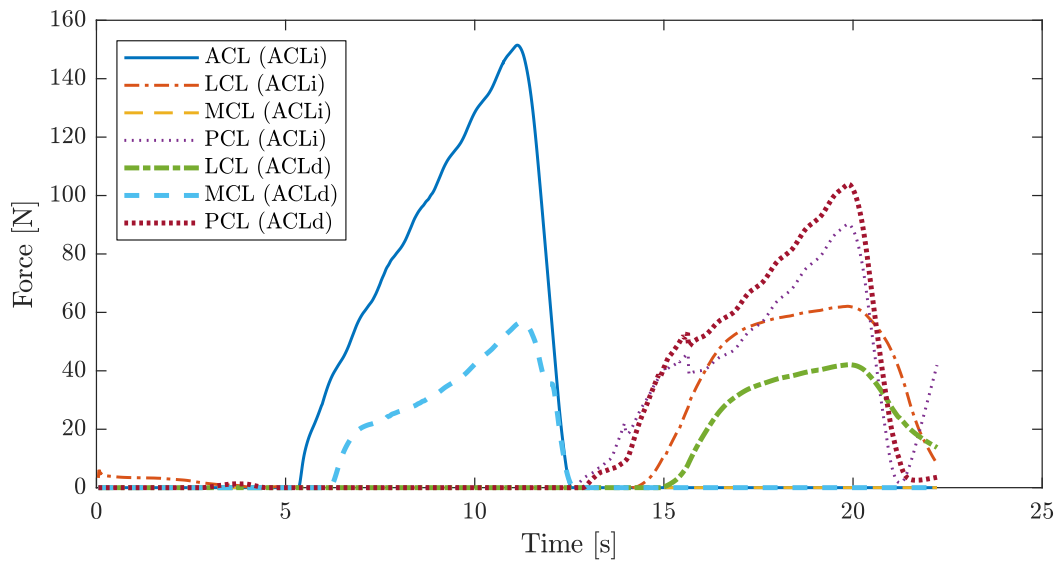


Figure 4.6: Ligament forces for ACLi and ACLd knees during 30° AP drawer simulation.

The maximum predicted loading of the ACL is 151 N and occurs at 12 seconds, corresponding to the timestep where the maximum anterior tibial loading is applied. Peak PCL loading (90 N) occurs at 20 seconds, which is when the maximum posterior tibial loading is applied. The force in the MCL is less than 5 N for the duration of the ACLi simulation and the LCL force is a maximum of 62 N at 20 seconds.

For the ACLd case, the MCL loading increases to 56 N at 12 seconds. When the posterior tibial force is applied, a slight change is observed for the PCL (increase of 13 N) and the LCL (decrease of 10 N).

4.4.2 Isolated loading testing at points of interest

Ligament forces at POIs, as described in Chapter 3.3.5, are shown in Figure 4.7. POIs for isolated loading experiments are for isolated degree of freedom applied loads. The bars in the chart depict the change in ligament force from 0° to 30° flexion. Changes in ACL forces are not shown in Figure 4.7 as its purpose is to compare the changes in ligament forces between flexion angles for an intact and ACLd knee.

Figure 4.7 shows that the model predicted LCL force at POI 1 decreases by 9.5 N and 11.9 N for the ACLi and ACLd cases respectively. At POI 2, model predicted force in the MCL remains unchanged for the ACLi case and increases by 38 N for the ACLd case. At POI 3, the MCL force remains unchanged for the ACLi case and decreases by approximately 3 N from 0° to 30° for the ACLd knee.

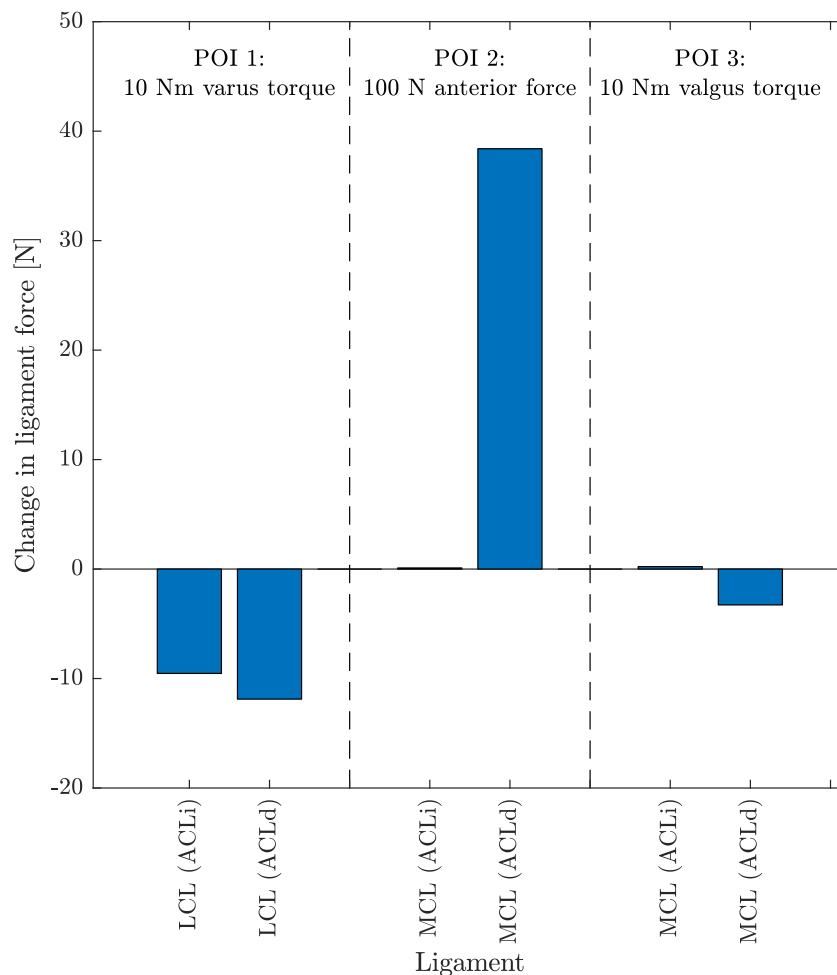


Figure 4.7: Change in ligament forces from 0° to 30° flexion for ACLi and ACLd knees at POIs for isolated loading testing.

4.4.3 Combined loading testing at points of interest

Changes in ligament forces at two points of interest, as described in Chapter 3.3.5, are shown in Figure 4.8. Changes in ACL forces are not shown in Figure 4.8.

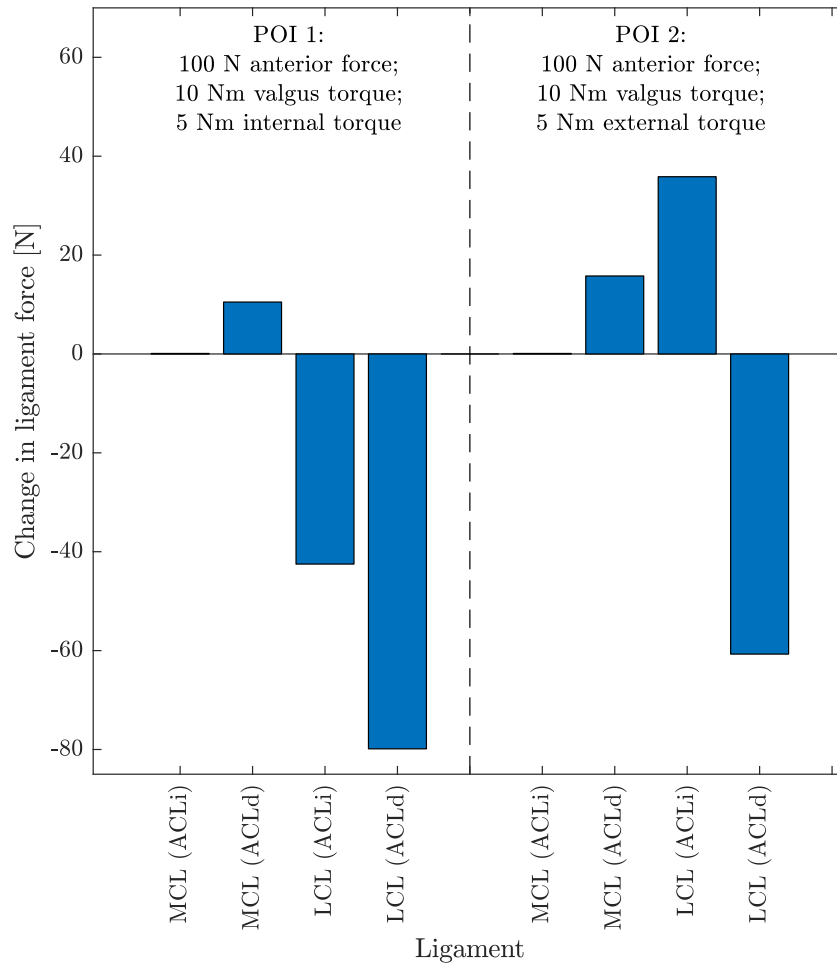


Figure 4.8: Change in ligament forces from 0° to 30° flexion for ACLi and ACLd knees at POIs for combined loading testing.

The force in the MCL remains unchanged for the ACLi case at both POI 1 and POI 2. For the ACL deficient case, the force in the MCL increases by 10.5 N and 15.7 N from 0° to 30° flexion at POI 1 and POI 2 respectively. LCL force decreases with flexion angle for both the intact (42.5 N) and ACLd (79.0 N) case at POI 1. LCL force increases for the ACLi case (35.9 N) and decreases for the ACLd case (60.7 N) at POI 2. At both POIs, the force in the LCL reduces for the ACLd knee as flexion angle increases from 0° to 30° . A decrease in LCL force for the ACLd knee was also observed at the POIs in Figure 4.7.

4.5 Contact forces

Contact forces were estimated at points of interest for isolated loading and combined loading tests. For both these tests, the change in contact forces from 0° to 30° flexion are determined for ACLi and ACLd knees. No contact between the femur and tibia osseous was observed, hence femur and tibia refer to the respective cartilage structures.

4.5.1 Isolated loading testing at points of interest

The model predicted change in contact forces at POIs is shown in Figure 4.9. Model predicted contact forces in Figure 4.9 include both ACLi and ACLd knees.

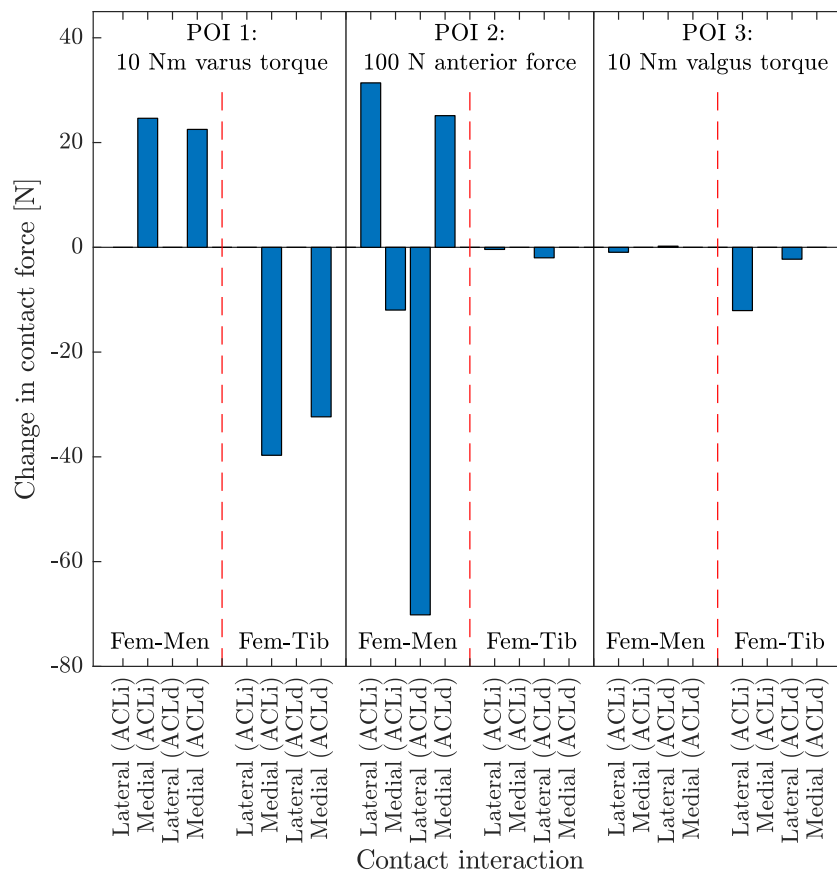


Figure 4.9: Change in contact forces from 0° to 30° flexion for ACLi and ACLd knees at POIs for isolated loading testing. Contact interactions are between the femoral cartilage and the menisci ('Fem-Men') and the femoral and tibial cartilage ('Fem-Tib').

At POI 1, for 10 Nm varus torque, medial meniscofemoral (MF) contact force increases from 0° to 30° flexion for both the ACLi (24.6 N) and ACLd (22.5 N) case. Medial tibiofemoral (TF) contact reduces for both the ACLi (39.7 N) and ACLd (32.4 N) cases from 0° to 30° flexion. Due to the varus torque, the lateral side of the femur is out of contact with the meniscus and the tibial cartilage. Hence, the lateral contact forces are zero.

For the anterior tibial loading applied at POI 2, lateral MF contact force increases by 31.4 N for the ACLi case and decreases by 70 N for the ACLd case. Conversely, medial MF contact decreases by 12 N and increases by 25.1 N for the ACLi and ACLd cases respectively. Lateral TF contact forces reduce by less than 2 N for the ACLi and ACLd cases. Medial TF contact forces do not change for either ACLi or ACLd case.

At POI 3, lateral MF contact changes by less than 1 N from 0° to 30° flexion for both ACLi and ACLd cases. Lateral TF contact reduces by 12.1 N and 2.3 N for the ACLi and ACLd cases respectively. Medial contact forces are zero due to the applied valgus loading, causing the femur to be out of contact with the medial meniscus and the tibia.

4.5.2 Combined loading testing at points of interest

Model predicted change in contact forces at combined loading POIs is shown in Figure 4.10, and includes both the ACLi and ACLd knees.

Contact forces in the intact knee between the femur and the menisci increase from 0° to 30° at POI 1. Lateral MF contact force increases by 15.6 N and medial contact force by 15.4 N. For the ACLd case, MF contact force decreased by 53.5 N and 4.6 N for the lateral and medial sides respectively. Lateral TF contact force increased from 0° to 30° (6.3 N), while the medial force decreased (75.7 N). TF contact force in the ACLd knee did not change with flexion for the lateral or the medial side.

At POI 2, both the lateral and medial MF contact force increased from 0° to 30° flexion for the intact knee by 2.6 N and 36.2 N respectively. Conversely, both decrease for the ACLd case (51 N for the lateral and 8.6 N for the medial side). Medial TF contact increased with flexion angle for both the ACLi (17.2 N) and ACLd (40.7 N) cases. Lateral TF contact increased from 0° to 30° flexion for the intact knee by 27.1 N but remained unchanged for the ACLd case.

4.6 Loading of the menisci in the ACL deficient knee

Figure 4.11 shows the model predicted contact force between the femoral cartilage and the medial and lateral menisci. These results are of Trial 3 of the

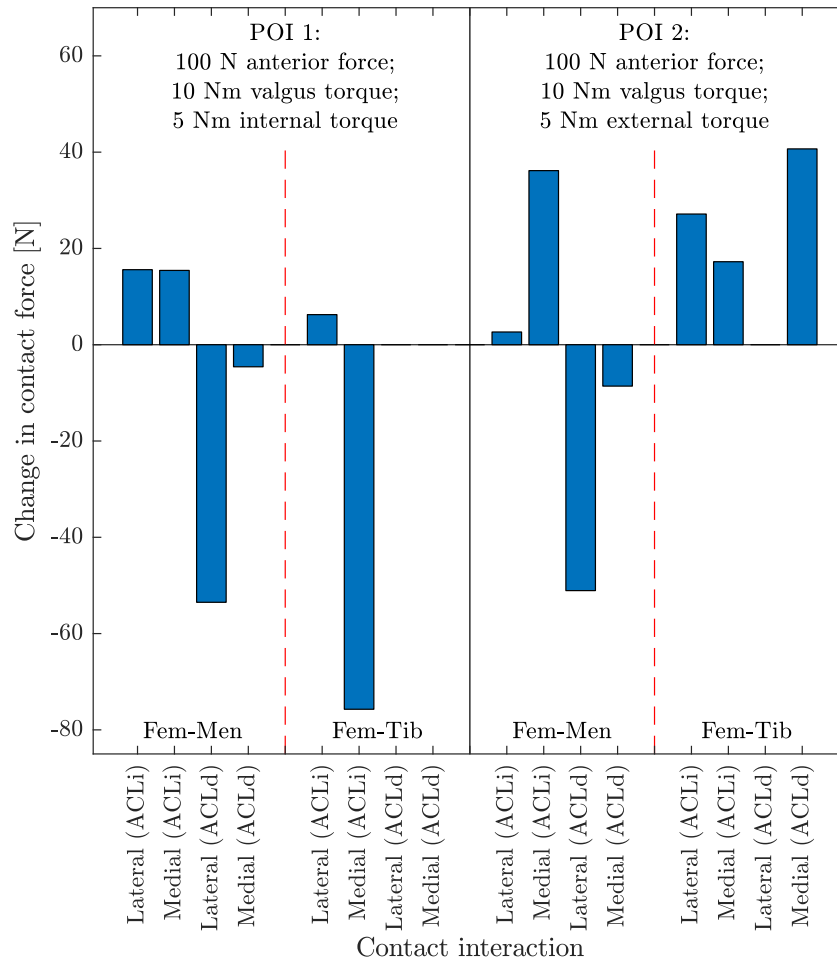


Figure 4.10: Change in contact forces from 0° to 30° flexion for ACLi and ACLd knees at POIs for combined loading testing. Contact interactions are between the femoral cartilage and the menisci ('Fem-Men') and the femoral and tibial cartilage ('Fem-Tib').

30° AP drawer tests and show the results of both the ACLi and ACLd simulations.

Lateral meniscal contact force increases gradually to a maximum of 30.6 N at 10 seconds, corresponding to the timestep of maximum anterior tibial loading. The increase in lateral contact force is due to the increase in internal tibial rotation angle (Figure 4.3). Medial meniscus loading remains low for the duration of the simulation of the ACLi knee, with a maximum contact force of 10 N at the initial timestep.

Predicted contact forces change considerably for the ACLd simulation. At approximately 3.5 seconds, the lateral contact force increases more for the ACL deficient knee than for the intact knee. As the anterior tibial translation increases due to the increase in applied anterior tibial load, so does contact with the medial meniscus. A reduction in lateral contact force is concurrent

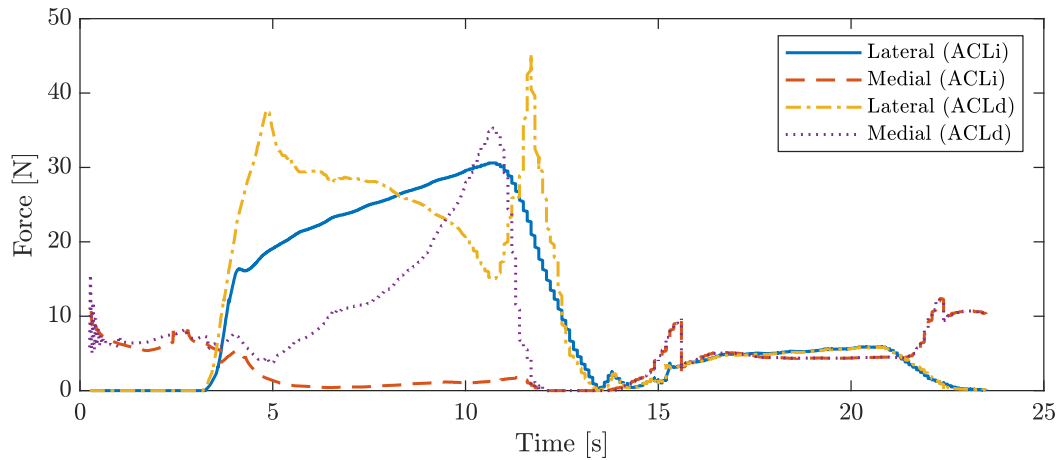


Figure 4.11: Meniscomfemoral contact forces for 30° AP drawer Trial 3. The figure shows the contact force for both ACLi and ACLd simulation.

with the increase in the medial contact force, until approximately 10 seconds, when the maximum medial contact force is predicted (35.3 N). This is followed by a sudden increase in lateral contact force and a maximum predicted force at 12 seconds, just after the applied tibial load has been removed. No difference in predicted contact forces is observed for the second half of the trial (time > 14 s), when posterior tibial loading is applied.

4.7 Parametric study

The sensitivity of model outputs (predicted joint kinematics and reaction forces) to changes in input parameters were evaluated. Changes in ligament stiffness (Table 3.6) had very little effect on the change in predicted kinematics and kinetics. Changes in output parameters were all less than 5 % for a -30 % to +30 % change in ACL stiffness. The greatest change was seen for average position error, which increased by 5 % when ACL stiffness was reduced by 30 %. For changes in LCL stiffness, the greatest change in output parameters were observed for a 30 % reduction in LCL stiffness, where the load cell force and moment errors increased by 10 %. Position and orientation errors changed by less than 2 %. Changes in output parameters were negligibly small for changes in PCL and MCL stiffness (< 1 % for predicted kinematics and kinetics). The resulting changes in model outputs for varying ligament stiffness are included in Appendix D.

Figure 4.12 shows the changes in model outputs compared to changes in tibiofemoral cartilage-to-cartilage contact stiffness. The figure also shows that the average orientation error is not very sensitive to changes in contact stiffness, as it does not change by more than 2 %. Change in position error is also low, with a maximum increase of 5 % at -40 % change in contact stiffness.

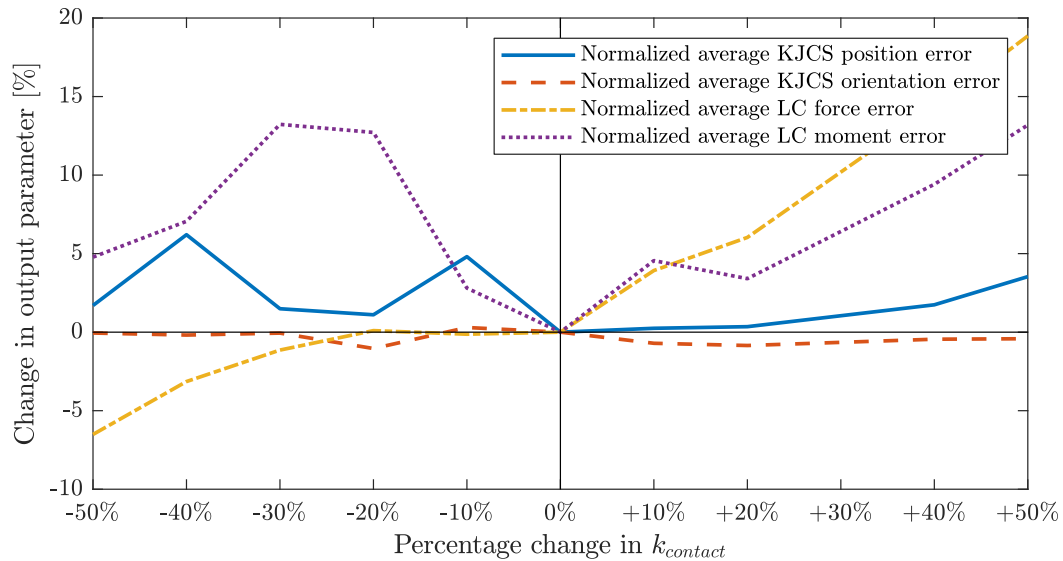


Figure 4.12: Percentage change of output parameters relative to changes in tibiofemoral contact stiffness.

The change in average load cell force error correlates with change in contact stiffness as it decreases with a decrease in contact stiffness and increases with an increase in contact stiffness. The average load cell moment error increases, for both an increase and a reduction in contact stiffness.

The greatest changes in output parameters were observed when changing the ligament zero-load lengths (ZLL). Figure 4.13 shows the change in output parameters as a result of changes in the ACL ZLL. Average position error, orientation error and load cell force error all increase as ACL ZLL is increased. Load cell moment error has a quadratic relationship to changes in ACL ZLL, with a minimum error (-1.5%) for a 4% reduction in ACL ZLL.

Figure 4.14 shows the change in output parameters as a result of changes in the MCL ZLL. Average orientation error, load cell force error and load cell moment error all decrease as MCL ZLL is increased from -20% to 0% . The average position error increases from -20% to -8% before it also decreases as ZLL is increased. From approximately a 4% increase in MCL ZLL, the output parameters remain unchanged by changes in MCL ZLL.

The results of changes in the ligament zero-load lengths for the PCL and LCL are included in Appendix D, along with the results for changing ligament stiffness.

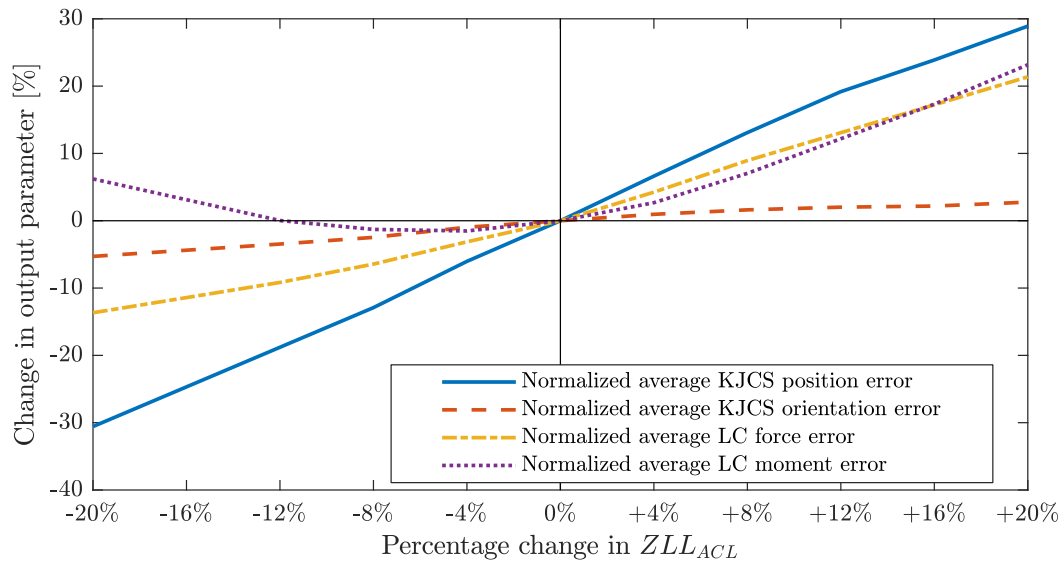


Figure 4.13: Percentage change of output parameters relative to changes in ACL zero-load length.

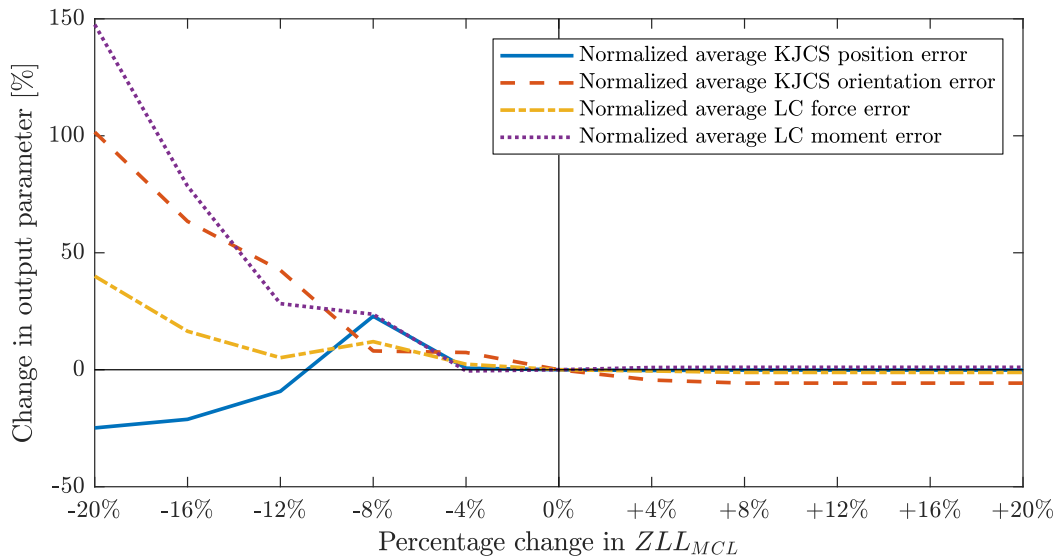


Figure 4.14: Percentage change of output parameters relative to changes in MCL zero-load length.

Chapter 5

Discussion

The aim of this study was to develop a multibody model of the human knee joint that includes the anterior and posterior cruciate ligaments, the medial and lateral collateral ligaments, the femoral and tibial cartilage, as well as the medial and lateral menisci. The model was used to investigate the mechanics of the ACL and the effect of ACL deficiency on joint kinematics, joint kinetics and the surrounding knee ligaments and cartilage. This chapter will discuss model validation, the ligament wrapping technique, the kinematic and kinetic results of simulations and the results of the parametric study.

5.1 Model validation

Although the model errors in position and orientation (Table 4.1) were comparable to RMS values reported by previous *in silico* studies (Guess *et al.*, 2010; Bloemker *et al.*, 2012; Kia *et al.*, 2016), the model accuracy needs to be improved. RMS error magnitudes were large compared to the range of kinematics reported in Chapter 4.3.

Medio-lateral and inferior-superior force and position errors (Table 4.1) were the result of morphological mismatches caused by imaging and segmentation errors. Morphological studies (Faber *et al.*, 2001; Draper *et al.*, 2006; Eckstein *et al.*, 2006) have shown tibial and femoral cartilage thickness to vary between 1.3 to 1.5 mm and 2 to 2.5 mm respectively. The resolution of the MRI used to create 3D cartilage geometries was 0.7 mm (Table B.1). This means that the cartilage thickness of the digitized geometry can be as thick as 3.2 mm or as thin as 0.6 mm. This range corresponds to the magnitude of RMS errors for the KJCS position seen in Table 4.1. Additionally, this variable thickness will also influence the medial-lateral translation as the femur is in contact with the tibial intercondylar eminence. This contact causes error in the KJCS position and force experienced in the medial and superior directions. The force in the medial direction causes an additional moment about the axis of valgus-varus rotation, which increases the valgus orientation error,

also seen in Table 4.1. Thus, it is important to note that model predicted kinetics are very sensitive to changes in kinematics. Small position errors result in additional contact and ligament forces acting on the joint.

The average KJCS orientation error is greater than position error. Because all the tests were conducted at a fixed flexion angle, the relative flexion angle between the femur and tibia remains near constant for the duration of the experiments. However, due to the application of peak AP drawer loads, the flexion angle changes by approximately 5° , which results in a large error for knee flexion.

The model developed in this study is a first attempt to gain insight into ACL biomechanics by comparing an intact to an ACL deficient knee. The next step in model development would be improve model accuracy by reducing RMS error between experimental measurements and model outputs. This will be done by optimization of modelling parameters and the locations of ligament insertion sites.

5.2 Ligament wrapping

Recently developed multibody models (Kia *et al.*, 2016; Guess and Razu, 2017) included ligament wrapping in their multibody models, with satisfactory results. However, the findings of this study suggests otherwise, as including ligament wrapping markedly increased simulation time and error in the model.

The MCL was modelled with three superficial ligament bundles, similar to Hosseini *et al.* (2015) and Guess and Razu (2017). However, both these groups also added additional deep bundles (three and two respectively) as shown in Figure 5.1 (a) and (b). Insertion sites of ligament bundles were estimated from the MRI geometries as data of their exact locations is not available in the dataset. Hence, attachment sites are approximated, and therefore not subject specific. The tibial insertion site in the current model (Figure 5.1 (c)) is more superior (closer to the tibial plateau) compared to the models of Hosseini *et al.* (2015) and Guess and Razu (2017). This means that the MCL is shorter and the wrapping angle is smaller compared to the other models. As ligament force is dependent on the combination of ligament ZLL and its position relative to the flexion axis of the tibiofemoral joint, unrealistic ligament force predictions could occur in the model.

Another reason for the increased RMS error is due to modelling artefacts that arise when simulating ligament wrapping. The method used to model ligament wrapping required dividing the ligament in two or more spring-damper elements, connected to each other via a sphere, shown in Figure 5.1 (b) and (c). The smooth sphere is in contact with the uneven bone surface. Although the contact was frictionless and non-deformable, irregular contact forces are introduced as the sphere translates on the bone surface. Additionally, due to the low mass of the spheres and the relatively high stiffness of the spring-damper

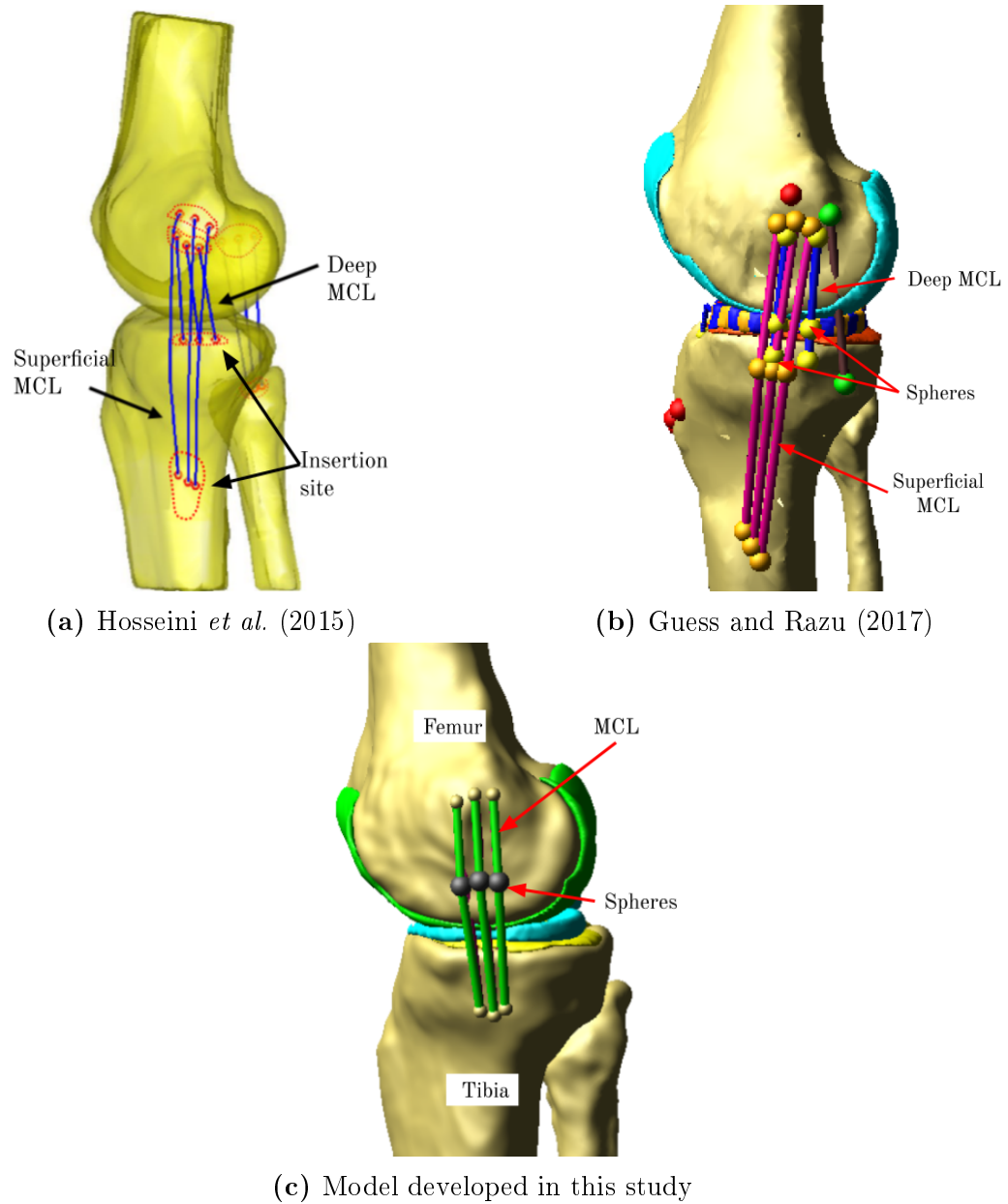


Figure 5.1: Medial view of the knee models showing wrapping of the MCL

elements, high frequency oscillations of the spheres occur. These oscillations and irregular contact forces cause sudden changes in the joint reaction forces and are known to cause solver errors (Eskinazi and Fregly, 2018).

Previous studies (Sakane *et al.*, 1999; Hosseini *et al.*, 2015) have determined that the role of the MCL only becomes significant when the knee is flexed above 60°. Other studies (Blankevoort and Huiskes, 1991; Gabriel *et al.*, 2004; Yang *et al.*, 2010) have also reported that the benefits of wrapping only become apparent at higher flexion angles as the overall behaviour of ligaments change due to the relative orientation of the ligaments insertion sites on the femur and tibia.

Despite the larger errors predicted by the model when ligament wrapping is included, the ligament wrapping technique cannot be disregarded as a method to improve physiological accuracy. An increase in computational load (and simulation time) is a result of increasing model complexity, and should be dealt with at solver level. A possible solution would be to investigate using large-scale optimizations to deal with the increased computational load.

Inclusion of ligament wrapping it is not critical for comparing ACL intact and ACL deficient knees and omission of wrapping will not affect the objectives of this study. Additionally, as higher flexion angles are not of interest in this study, CPU times were substantially longer and increased model error, wrapping of the MCL bundles was not included in further simulations.

5.3 Knee kinematics

5.3.1 30° AP drawer testing

Overall, kinematics for the intact knee correspond well to the experimental data and the increase in anterior translation (Figure 4.2), as well as internal rotation (Figure 4.3) in ACL deficient knee kinematics are consistent with what is reported in literature (Shoemaker and Markolf, 1985; Sakane *et al.*, 1999; Gabriel *et al.*, 2004; Amis, 2012; Boeth *et al.*, 2013). Furthermore, no difference between kinematics of ACLi and ACLd knees were observed when a posterior tibial load was applied.

The increase in superior translation (Figure 4.2) is due to the lateral meniscus being ‘wedged’ between the femur and the tibial plateau as a result of increased anterior translation in the ACLd knee. A similar explanation for the translation was given was given by Guess and Stylianou (2012). The superior translation would have been less if the menisci were modelled as deformable bodies, as opposed to rigid bodies.

A large valgus error was shown in Figure 4.3. This occurs when the femur is in contact with the tibial eminence, causing a medial force to be introduced. The medial force produces an additional valgus moment, which results in the large valgus error observed in Figure 4.3.

5.3.2 Kinematic range of motion: 30° AP drawer testing

Predicted values for AP translation of the intact knee correspond well to experimental values reported by Sakane *et al.* (1999), Gabriel *et al.* (2004), Markolf *et al.* (2008) and Harris *et al.* (2016), who applied similar AP loading at 30° flexion. However, the model predicted greater AP translation for the ACLd knee than what was reported by these studies. This is might be due to the MCL bundles being too lax in the current representation of the model, as the MCL is one of the primary restraints to anterior translation of the tibia in the ACLd knee (Sakane *et al.*, 1999). Furthermore, anterior dislocation of the joint occurred at maximum anterior load and resulted in additional anterior translation.

Fewer studies reported changes in internal rotation for purely anterior-posterior applied loads, compared to internal rotation resulting from isolated internal-external torques or from combined valgus-varus and internal-external torque. Model predicted internal rotation for the intact knee corresponds well to the experimental results reported by Gabriel *et al.* (2004). Harris *et al.* (2016) reported an increase of 3.6° in the range of internal-external rotation for ACLd knees, which is the same as the mean increase in internal-external rotation predicted by the model. However, the mean values for internal-external range of motion for ACLi and ACLd reported by Harris *et al.* (2016) were significantly greater than the model predicted values (40.9° and 44.5°, compared to 12.6° and 16.2°).

5.3.3 Kinematic range of motion: isolated and combined loading testing

Referring to Figure 4.5, for isolated loading testing, model predicted AP translation decreased slightly (1.8 mm) from 0° to 30° flexion for the ACLi knee and 100 N of anterior tibial force. Conversely, experimental results of studies (Sakane *et al.*, 1999; Gabriel *et al.*, 2004; Markolf *et al.*, 2008; Harris *et al.*, 2016) reported a mean increase in AP translation for the intact knee ranging from 1.4 mm to 4.5 mm. Model predicted AP translation for the ACLd knee increased from 0° to 30° flexion, which corresponds to the results of the above-mentioned clinical studies.

For isolated loading testing, model predicted IE rotation increased from 0° to 30° flexion for both the ACLi and ACLd cases for 5 Nm internal torque (an increase of 7.5° and 7.6° were predicted for the ACLi and ACLd cases respectively). These trends were also reported by clinical studies that measured internal rotation at similar loads. Markolf *et al.* (2008) reported a 13.2° for both the ACLi and ACLd cases, whereas Harris *et al.* (2016) reported 13.1° and 11.5° for the ACLi and ACLd cases respectively. Kanamori *et al.* (2000) reported an increase of 7.6° and 5.9° for the ACLi and ACLd cases respectively for an isolated internal tibial torque of 10 Nm.

For the combined loading tests, AP translation decreased from 0° to 30° flexion for both the ACLi and ACLd knee for combined loading by 2.7 mm and 3.9 mm respectively. This does not agree with the results of two clinical studies, who applied combined internal rotation and valgus torque at 15° and 30° flexion angles (Woo *et al.*, 2002; Gabriel *et al.*, 2004). Woo *et al.* (2002) applied a combined load of 10 Nm internal rotation and 10 Nm valgus torque at 15° and 30° flexion and reported an increase in AP translation of 2 mm for the intact knee and a 0.5 mm increase for the ACLd knee. Gabriel *et al.* (2004) applied a combination of 10 Nm valgus torque and 5 Nm internal torque at 15° and 30° flexion and also reported a 2 mm increase in AP translation for an intact knee (a ligament deficient knee was not subjected to combined loading tests). The differences can be attributed to the additional 100 N anterior tibial force applied to the knee that was not applied in either of the two studies mentioned above.

For the combined loading tests, model predicted IE rotation increased for both the ACLi and ACLd knees from 0° to 30° flexion by 9.4° and 15.3° respectively. This corresponds to the results of Gabriel *et al.* (2004), who reported an increase of 6.5° for the intact knee from 15° to 30° flexion. The same loading conditions were not applied by other studies, but the observed trends of individual loading conditions or other variants thereof are consistent with model predictions.

5.4 Ligament forces

5.4.1 30° AP drawer testing

The greatest difference between ligament forces in the intact and ACL deficient knee was seen for the MCL. This is because the MCL is the primary restraint against anterior tibial translation and internal tibial rotation for an ACL deficient knee, which corresponds to observations made by past studies (Butler *et al.*, 1980; Sakane *et al.*, 1999; Shelburne *et al.*, 2005).

The peak model predicted ACL force is 151 N (Figure 4.6). This is greater than the ligament forces measured experimentally by other studies, who reported ACL forces between 90 N and 115 N at 30° flexion angle for 100 N anterior tibial load (Markolf *et al.*, 1995, 2004, 2008; Sakane *et al.*, 1999; Woo *et al.*, 2002; Gabriel *et al.*, 2004). The maximum model predicted PCL force for the ACLi knee was 90 N. This was also greater than the force ranging between 45 N and 55 N that has been reported by other studies (Markolf *et al.*, 2004, 2006; Nasab *et al.*, 2016) for similar loading conditions. Differences in predicted ligament force could be due to the increase in valgus and external rotation angle of the knee (Figure 4.3) resulting from ACL deficiency. The reasons for differences in ligament forces will be discussed in more detail in Section 5.4.4.

5.4.2 Isolated loading points of interest

Model predicted ACL force (not shown in Figure 4.7) increases by 29.3 N from 0° to 30° flexion angle when a 100 N anterior load is applied (POI 2). This corresponds to observations by Woo *et al.* (2002) and Harris *et al.* (2016), who reported a mean increase of 17 N and 40 N respectively. Conversely, Markolf *et al.* (2008) reported a decrease of 40 N. Other studies reported no significant difference in the ACL force between 0° and 30°, although they reported that the maximum ACL force occurred around 15° flexion (Sakane *et al.*, 1999; Kanamori *et al.*, 2000; Woo *et al.*, 2002; Gabriel *et al.*, 2004). For varus rotation (POI 1) predicted ACL force decreased by 4.2 N and for valgus rotation (POI 3) ACL force decreases by 4.3 N. This agrees with trends observed by Markolf *et al.* (1995) and Woo *et al.* (2002).

The decrease in LCL force at POI 1 corresponds with a reduction in LCL ligament length from 0° to 30° flexion, as the valgus angle increases with flexion (Hosseini *et al.*, 2015). Conversely, observations by Harris *et al.* (2016) indicated a slight increase in the LCL force from 0° to 30° flexion. However, Harris *et al.* (2016) included measurement of force in the popliteofibular ligament (PFL), which assists the LCL in distributing loads in the posterolateral corner of the knee. From 0° to 30° flexion, a reduction in the PFL loading was reported. The PFL was not included in this model.

At POI 2, MCL force remains unchanged for the intact knee as flexion angle increases from 0° to 30°. This agrees with Harris *et al.* (2016), who also reported a decrease in MCL force. Sakane *et al.* (1999) reported a 3.2 N increase in MCL force from 0° to 30° flexion. For the ACLd case, MCL force increases with flexion angle. The reason for increase in MCL force, as discussed before, is because the MCL is the primary restraint to anterior tibial loading. Valgus and external tibial rotation angles increase along with increasing the flexion angle from 0° to 30°, causing an additional increase in MCL force.

At POI 3, MCL force remains unchanged from 0° to 30° flexion for the ACLi case, but decreases slightly for the ACLd case. This corresponds with Harris *et al.* (2016), who also reported a decrease in MCL force.

5.4.3 Combined loading points of interest

The force in the ACL due to combined loading was higher at POI 1 (34 % at 0° and 22 % at 30°) and POI 2 (17 % at 0° and 20 % at 30°) than the forces resulting from isolated anterior tibial loading. This corresponds with the observations of Markolf *et al.* (1995) that internal rotation, combined with anterior tibial load and valgus torque (POI 1) produces the highest load in the ACL. However, the predicted ACL force due to the combination of anterior tibial loading, valgus torque and external tibial torque was more than the force measured by Markolf *et al.* (1995).

Force in the MCL increases from 0° to 30° flexion at both POIs for the ACL deficient case. An increase in MCL force due to ACL deficiency corresponds to observations by other studies (Sakane *et al.*, 1999; Shelburne *et al.*, 2005). The increase in MCL force is also more for external tibial rotation (POI 2) than for internal tibial rotation (POI 1), which corresponds to Harris *et al.* (2016).

Similar to the discussion in the previous section, LCL force decreases with flexion angle for both the intact and ACLd case at POI 1 and the ACLd case at POI 2. This is as a result of the reduction in ligament length due to valgus torque and anterior tibial loading applied to the knee. Conversely, the LCL force increases for the ACLi case at POI 2. This is unexpected as the combination of valgus and external rotation would cause a reduction in LCL length and thus a reduction in LCL force. This result could be explained by Markolf *et al.* (1995), who noted that the force in a ligament subject to a state of combined loading is not simply the sum of individually applied loads.

At both POIs, the force in the LCL reduces for the ACLd knee as flexion angle increases from 0° to 30° . This is because the MCL resists most of the applied anterior loading in the absence of the ACL (Sakane *et al.*, 1999; Shelburne *et al.*, 2005).

5.4.4 Reasons for differences between model predicted and experimental ligament forces

There are a few instances where model predicted ligament forces differ from experimental results of past studies. Ligament forces are predicted based on changes in joint kinematics. The model was dynamically driven and no kinematic constraints were applied to the joint. Ligament parameters were adjusted to match predicted model kinematics to experimental measurements of joint motion. Good correlation between model predicted and experimentally measured kinematics were set as the criterium for model validation.

Ligament stiffness parameters used in computational models are based on tensile tests (Wismans *et al.*, 1980; Butler *et al.*, 1986; Blankevoort *et al.*, 1991; Race and Amis, 1994) and are not specific to the specimen (Blankevoort *et al.*, 1991; Bloemker *et al.*, 2012; Guess and Stylianou, 2012; Galbusera *et al.*, 2014). Stiffness, as well as the zero-load length determine the force-elongation relationship of the ligament (Blankevoort and Huiskes, 1991; Bloemker *et al.*, 2012; Kia *et al.*, 2016). For a given load, reducing the stiffness or the zero-load length will reduce ligament force but increase ligament elongation. In the current representation of the model, good agreement between experimentally measured and model predicted kinematics are obtained, but some ligaments such as the ACL and PCL are too stiff (Figure 4.6). This results in higher forces than what was measured in clinical experiments. Reducing the ligament stiffness or increasing the zero-load length will decrease the ligament force to

better match forces reported by other studies. However, these benefits will be at the cost of greater error between model predicted and experimentally measured kinematics due to an increase in joint laxity.

Another reason for the difference in ligament forces is the relative uncertainty of the location of ligament insertion sites, especially when insertion sites are estimated from MRI-based geometries. It has been shown that varying attachment site locations by as little as 2 mm has a significant effect on joint kinematics (Grood *et al.*, 1989; Hefzy *et al.*, 1989; Baldwin *et al.*, 2009). Small differences in insertion site will influence when ligaments engage (resist applied load) and disengage (become slack) in response to applied loading, resulting in ligament response that is in disagreement with real behaviour (Harris *et al.*, 2016). Additionally, *in situ* ligament forces are affected by capsular ligaments, such as the medial and lateral posterior capsular ligaments and the popliteal ligaments (Nielsen and Helmig, 1986b; Shelburne *et al.*, 2005; Baldwin *et al.*, 2009; Harris *et al.*, 2016), which were not included in the model. While these factors will influence the ligament forces predicted in the model, it is not the main cause of the difference between predicted and measured ligament forces.

Along with differences in test specimens, specimen preparation and experimental setup, the main reason for differences between model predicted and experimentally measured ligament forces is the oversimplified representation of the soft tissue constraint in the computational model. Ligaments are modelled as one-dimensional line elements with a non-linear force-elongation relationship (Blankevoort and Huiskes, 1991). Ligament bundles are modelled by including multiple line elements to represent the ligament anatomy. The number of line elements used to model a ligament bundle will affect joint kinetics as well as predicted ligament force (Baldwin *et al.*, 2009).

In contrast, a real ligament is three-dimensional and has anisotropic material properties (Weiss and Gardiner, 2001; Galbusera *et al.*, 2014; Kiapour *et al.*, 2014). Line elements are not capable of predicting the behaviour associated with strain-rate and deformation in the same way as a three-dimensional finite element model with a complex material law (Galbusera *et al.*, 2014; Trad *et al.*, 2018). Although simplified soft tissue constraint can predict satisfactory results when evaluating joint mechanics (Weiss and Gardiner, 2001; Galbusera *et al.*, 2014), prediction of ligament force is insufficient. This motivates the use of a finite element model of ligaments together with a joint-level multibody model in a co-simulation workflow.

5.5 Contact forces

Tibiofemoral contact forces can be measured *in vitro* by using pressure films (Bei and Fregly, 2004; Guess *et al.*, 2013; Kiapour *et al.*, 2014; Walker *et al.*, 2015) and *in vivo* by using instrumented prostheses (Fregly *et al.*, 2012). These measurements are used in conjunction with model predictions to describe con-

tact interactions in the knee. In this section, model predicted contact forces are discussed in terms of the joint kinematics and ligament kinetics predicted by the model.

5.5.1 Isolated loading points of interest

At POI 2, the effect of ACL deficiency is shown by how contact forces change between the intact and ACLd case (Figure 4.9). Lateral meniscomfemoral contact force increases from 0° to 30° flexion for the ACLi case, but decreases for the ACLd case. Conversely, medial meniscomfemoral contact decreases for the ACLi case and increases for the ACLd case. The reason for the change in contact force could be due to the increased anterior translation and internal rotation of the tibia, which results from ACL deficiency. Changes in tibiofemoral contact forces are very small for both the medial and lateral sides.

At POI 1 of isolated loading testing, medial meniscomfemoral contact force increases from 0° to 30° flexion for both the ACLi and ACLd cases, while medial tibiofemoral contact reduces. This is because the meniscus ensures that the femur is kept in position on the tibial plateau as the flexion angle increases, resulting in an increase in femur-to-meniscus contact. The menisci also contribute to distribution of loads within the knee (Guess *et al.*, 2010; Bloemker *et al.*, 2012), resulting in a reduction of tibiofemoral contact force.

The same is true when a valgus torque is applied at POI 3, although the change in lateral contact force is not as much as the change in medial contact force at POI 1. Due to the varus moment on the knee at POI 1, the lateral side of the femur is out of contact with the meniscus and the tibial cartilage. Hence, the contact force is zero. Likewise, medial contact forces are zero for a valgus load, applied at POI 3, as the medial side of the femur is out of contact.

5.5.2 Combined loading points of interest

Meniscomfemoral contact forces in the intact knee increased from 0° to 30° at POI 1 (Figure 4.10). The increase in meniscomfemoral contact force from 0° to 30° flexion angle is the result of the menisci distributing the applied load as the knee flexion angle increases (Guess *et al.*, 2010; Bloemker *et al.*, 2012). For the ACLd case, femur-to-meniscus contact reduced on both the medial and lateral sides. Valgus rotation reduces meniscomfemoral contact on the medial side, and lateral contact is reduced by the internal rotation of the tibia due to the applied internal rotation torque. Lateral contact reduced more than the medial contact due to a portion of the applied internal tibial rotation being resisted by the medial side of the knee. Overall, the meniscomfemoral contact forces in the ACLd knee reduced from 0° to 30° for both the lateral and medial menisci.

For the intact knee at POI 1, lateral tibiofemoral contact force increased from 0° to 30° flexion angle, while the medial force decreased. Lateral tibio-

femoral force increased due to the applied valgus torque. Medial tibiofemoral force reduced as the valgus angle of the knee increased and the medial condyle of the femur exerted less force on the tibial cartilage. For the ACLd case, no change in tibiofemoral contact force is observed with the change in flexion angle from 0° to 30° flexion. This is likely due to the increased anterior translation of the tibia, which caused a larger portion of the contact force to be distributed between the femur and the menisci (Guess *et al.*, 2010). Because no axial loading was applied to the knee, the tibiofemoral forces are small compared to other studies (Guess and Stylianos, 2012; Guess *et al.*, 2013; Guess and Razu, 2017) that included axial loading in their models. The absence of axial loading conditions could also be a reason why tibiofemoral contact forces did not change with flexion angle.

Both the lateral and medial meniscofemoral contact force increased from 0° to 30° flexion for the intact knee at POI 2. The medial meniscofemoral force increased more than at POI 1 due to external tibial rotation, which resulted in greater femur-to-meniscus contact at the posterior edge of the medial meniscus as the flexion angle increased. The increase in medial meniscofemoral force also caused a reduction in the lateral meniscofemoral contact force as forces are redistributed in the knee (Guess *et al.*, 2010). The change in meniscofemoral force for the ACLd case is not as apparent as for the intact knee. Medial meniscofemoral force in the ACLd knee reduces slightly more than at POI 1. The difference is more likely the result of the change in loading condition than the result of ACL deficiency.

Tibiofemoral contact force in the intact knee increased with flexion angle for both the medial and lateral sides at POI 2. The increase on the lateral side is due to the applied valgus torque, and the increase on the medial side could be due to the contact between the femur and the medial side of the tibial eminence. Contact with the tibial eminence results from the external rotation of the tibia in response to the applied external tibial torque. No change in lateral tibiofemoral contact force is seen for the ACLd case at POI 2, similar to the ACLd case at POI 1. Conversely, medial tibiofemoral force increases at POI 2 for the ACLd case. The increase is likely due to the same reason as for the ACLi case at POI 2.

5.5.3 Comparing contact forces with literature

Previously developed multibody studies have predicted contact forces for walking (Bei and Fregly, 2004; Guess *et al.*, 2010, 2013, 2015; Lin *et al.*, 2010*b*), squatting (Guess and Stylianos, 2012) and passive flexion with applied loading simulations (Guess and Razu, 2017). Some of these models also simulated ACL deficiency (Guess and Stylianos, 2012; Guess and Razu, 2017). The model most similar to the one developed in this study (Guess and Razu, 2017) determined contact forces at flexion angles between 0° and 90° for different applied loads, including a 100 N anterior tibial force and a 5 Nm external

tibial torque. However, their model also included a 300 N compressive force to represent the weight of the specimen. The dataset used to develop the model in this study did not include compressive loads. The addition of a compressive load will affect the predicted tibiofemoral contact forces and influence the distribution of joint forces between the menisci and the joint cartilage structures. Ligament forces will also change as an additional force will act along the axis of the femur. The addition of a compressive force in the model is not possible as the model will not be validated for this loading condition.

Thus, due to the differences in applied joint loading, comparison between model predicted contact forces and the above-mentioned studies is not viable. Additionally, predicted contact forces are highly dependent on model parameters. These parameters are often optimized for a specific model and not necessarily applicable to all specimens (Guess *et al.*, 2010, 2013; Guess and Razu, 2017). Hence, it is more important to evaluate trends in the predicted forces resulting from joint kinematics, rather than the magnitude of predicted contact force.

5.6 Loading of the menisci in the ACL deficient knee

An increase in contact force was observed for both the lateral and the medial meniscus for the ACL deficient knee compared to contact forces in the intact knee (Figure 4.11). The contact force in the lateral meniscus is much greater than the medial side for the ACLi knee due to the internal rotation of the tibia that occurs during anterior tibial loading. At approximately 3.5 seconds, a difference between the predicted lateral contact force for the ACLi and ACLd cases can be seen where the lateral contact force for the ACLd knee increases more than that of the ACLi knee. At this point, the lateral meniscus is ‘wedged’ between the tibial cartilage and the femur. This corresponds to an observation by Guess and Stylianou (2012).

The medial contact force increases noticeably for the ACL deficient knee compared to the intact knee. This corresponds to observations by Papageorgiou *et al.* (2001), who reported a 200 % increase in medial meniscus forces after transection of the ACL. A medial contact force with similar magnitude has also been reported in a computational study by Guess and Razu (2017), as well as a clinical study by Walker *et al.* (2015). Maximum medial contact force occurs near the timestep (10 seconds) where the joint dislocates due to the maximum anterior tibial loading. When the anterior tibial load is removed, the tibia returns to the unloaded position. As the tibia translates posteriorly, the femur impacts the lateral meniscus, resulting in a sudden increase in the predicted lateral contact force, visible at approximately 12 seconds. This motion corresponds to what is hypothesized to be the cause of meniscal ramp

lesions (Chahla *et al.*, 2016; Stephen *et al.*, 2016).

Meniscal ramp lesions is an injury that commonly coincides with ACL tears (Bollen, 2010; Chahla *et al.*, 2016; Stephen *et al.*, 2016). Ramp lesions result in an increase in tibiofemoral contact force (Arno *et al.*, 2015), further reduce resistance to anterior-posterior translation and compromise rotational stability of the knee (Walker *et al.*, 2015; Stephen *et al.*, 2016). For ACL injuries, lateral meniscal tears occur more often than medial tears (Butler *et al.*, 1980; Bollen, 2010; Chahla *et al.*, 2016), however, in the case of chronic ACL deficiency, medial meniscal tears are more common (Butler *et al.*, 1980; Smith and Barrett, 2001; Chahla *et al.*, 2016). This is likely due to the how the menisci are attached to the tibial plateau, with the medial meniscus being less mobile in comparison with the lateral side. A lack in mobility causes the medial side to be more susceptible to injury (Vedi *et al.*, 1999; Chahla *et al.*, 2016).

The rapid increase in predicted lateral meniscus force in Figure 4.11 supports the observation that lateral ramp lesions commonly coincide with the same event that results in ACL injury. Contact force in the medial meniscus is markedly higher for the ACLd knee than for the intact knee, however, the increase in medial force occurs more gradually than in the case of the lateral meniscus. This is in agreement with the observation that medial meniscus injury is more common for knees with chronic ACL deficiency.

5.7 Parametric study

Model outputs are the most sensitive to changes in the ligament zero-load lengths, which corresponds to the observations of previous studies (Bertozzi *et al.*, 2007; Bloemker *et al.*, 2012; Kia *et al.*, 2016). Model outputs were the least sensitive to variation in ligament stiffness, which is also in agreement with past studies (Wismans *et al.*, 1980; Bertozzi *et al.*, 2007).

When evaluating model sensitivity to changes in zero-load length, model outputs did not change when MCL ZLL was increased beyond the reference (0 % change) length. This is because the ligament became slack after increasing the ZLL beyond the length corresponding to the 0 % value. Hence, increasing the ligament length did not influence joint kinematics or kinetics as the MCL will not resist any applied loads.

Orientation and position outputs were not very sensitive to changes in cartilage-to-cartilage contact stiffness as it changed by less than 5 % for the total range of contact stiffness values evaluated. Force and moment errors both increased with increase in contact stiffness. Force errors decreased as contact stiffness was decreased, but moment errors increased. Parameter values for contact stiffness were used from Guess *et al.* (2010), who optimized contact parameters for their model. Even though contact parameters were not opti-

mized for this model, the parameters determined by Guess *et al.* serve as a good initial estimate, as both the model predicted position error, as well as the moment errors were at a minimum for the values specified by Guess *et al.* (i.e. at a 0 % change in contact stiffness).

It is important to note that the results of the parametric study are specific to this model. However, the trends predicted by the sensitivity analysis provides valuable insight to which modelling parameters will likely affect model outputs. Results can also be used as a first step in a design of experiments approach to optimize model parameters. Optimized model parameters could help to reduce the RMS error between model predicted and experimentally measured kinematics and kinetics.

5.8 Model limitations

The study has the following limitations. In the current model, only the four major knee ligaments (ACL, PCL, MCL and LCL) were modelled. The effect of capsular ligaments, such as those in the posterolateral corner (PLC) and the posteromedial corner (PMC) was not investigated. Past studies (Nielsen and Helmig, 1986*b*; Shelburne *et al.*, 2005; Baldwin *et al.*, 2009; Harris *et al.*, 2016) have noted that capsular ligaments act as secondary restraints to anterior tibial translation and internal rotation for ACL deficient knees, which would influence model predicted kinematics. Because the MCL is the primary restraint to anterior tibial translation and internal tibial rotation (Butler *et al.*, 1980; Sakane *et al.*, 1999; Shelburne *et al.*, 2005), the omission of the PLC and the PMC will not have an adverse effect on model predictions.

Previous studies have shown that the location of ligament insertion site could affect predicted kinematics (Grood *et al.*, 1989; Hefzy *et al.*, 1989; Baldwin *et al.*, 2009). A limitation of the dataset was that the exact positions of ligament insertion sites were not recorded during the experiments. Nevertheless, ligament insertion sites could be estimated from MRI based geometries. This enabled the model to predict joint translations and rotations that corresponded well to experimentally measured kinematics.

Modelled ligament properties were not subject specific as generalized ligament stiffness parameters (Butler *et al.*, 1986; Blankevoort *et al.*, 1991; Guess and Razu, 2017) were used. Similarly, material properties for cartilage structures and the menisci were based on the estimations of other studies (Guess *et al.*, 2010; Guess and Razu, 2017). Although subject specific parameters could affect subject specific joint biomechanics, the results from the parametric study showed that the model is not sensitive to changes in ligament stiffness and that the parameters used for contact stiffness were sufficient for prediction of joint kinematics and kinetics.

An inherent limitation of multibody models is that parts are modelled as rigid bodies. Tibiofemoral cartilage and the menisci deform when joint load-

ing is applied, which could have an influence on predicted kinematics. Some studies have included representation of soft tissue deformation in a multibody workflow using surrogate models (Halloran *et al.*, 2010; Lin *et al.*, 2010b; Eskinazi and Fregly, 2015, 2018), or by dividing rigid geometries into smaller discrete elements with constraints on their relative movement (Guess *et al.*, 2010, 2013). Although including deformable contact might be beneficial in terms of physiological accuracy, many multibody models still make use of rigid body representation of the menisci and tibiofemoral cartilage (Guess and Stylianou, 2012; Bloemker *et al.*, 2012; Guess *et al.*, 2015; Harris *et al.*, 2016; Kia *et al.*, 2016; Guess and Razu, 2017) as the compliant contact used allows for satisfactory and computationally efficient prediction of joint biomechanics.

Finally, it is important to note that experimental data from *in vitro* tests were used in the model. While this does not affect model validity or the outcomes of this study, it does limit the interpretation of the clinical relevance of the results. This is because joint loading was applied *in vitro* by a robot, which will not necessarily represent the exact *in vivo* kinematics of the knee (Woo *et al.*, 1999).

Chapter 6

Conclusion

This study developed a joint-level model of the knee using a multibody modelling approach. The multibody model was used to evaluate joint kinematics and kinetics for an intact and ACL deficient knee by using experimental data from the Open Knee(s) project. The model was validated for experimental tibiofemoral joint testing and predicted the changes in joint biomechanics for an intact and ACL deficient knee. For the ACL deficient knee, the model predicted that MCL force increases by 56 N at 30° flexion for a 100 N tibial drawer load compared to the intact knee. Anterior-posterior laxity and internal-external tibial rotation increased due to ACL deficiency by 343 % and 28 % respectively when a 100 N tibial drawer load was applied. The increase in laxity of the ACL deficient knee also resulted in an increase in meniscofemoral contact force at 30° flexion of 33.9 N and 14.7 N at 30° flexion on the medial and lateral sides respectively. The model was most sensitive to changes in the ligament zero-load length (> 30 % change in output for 20 % change of zero-load length) and least sensitive to changes in ligament stiffness (< 10 % change in output for a 30 % change in ligament stiffness). The model confirmed previous findings of the mechanism of meniscal ramp lesions that was described in literature, and predicted force magnitudes similar to what was measured experimentally and predicted by other models.

6.1 Objectives

The study achieved its objectives by identifying a suitable material model for the ACL and developing a joint-level multibody model that was validated against experimental data of tibiofemoral tests. The model was used to perform a sensitivity analysis of parameters used in multibody models, the results of which can be used when developing future models. The model was used to determine joint kinematics, joint kinetics and ligament forces for an intact knee, that was compared to an ACL deficient knee. Finally, the effect of ACL deficiency on the tibiofemoral and meniscofemoral contact forces was deter-

mined by using the model to compare the change in predicted forces of an intact and ACL deficient knee.

6.2 Future work

As briefly discussed in Chapter 5, the current workflow can be elaborated to include one or more finite element models of knee ligaments. Finite element models of the knee ligaments can be combined with the joint-level multibody model in a co-simulation workflow. Finite element models of ligaments will allow for the estimation of the stress state in a ligament and provide a better representation of ligament kinetics than the current one-dimensional ligament representation used in the model.

Although co-simulation has computational benefits compared to a dynamic finite element workflow, the computational expense will be significantly more (Thelen *et al.*, 2014) than for the current multibody model with simplified contact and ligament representations. Computational expense could be reduced by including surrogate models of the ligaments. Surrogate models would make predictions of ligament response based on the results of finite element simulations. A co-simulation workflow could also include a finite element representation of the menisci. This would be useful to have in conjunction with a model of an ACL deficient knee, to further investigate meniscus forces and mechanisms of concurrent injury.

Future uses of the model developed in this study could be to adapt it for use with kinematic boundary conditions. These kinematic boundary conditions could include simulation of walking or jumping activities. This would require using an inverse dynamics approach as opposed to the forward dynamics approach currently used.

For the development of future models, the results of this study has shown to take care when determining the ligament zero-load lengths as it had the greatest influence on model outputs of all parameters evaluated. It is recommended to record the ligament insertion locations using a digitizer probe in case the study conducts its own experiments, and to follow an approach similar to Bloemker *et al.* (2012) and Kia *et al.* (2016) when estimating ligament zero-load length experimentally. This study has also shown that the modelling parameters of ligament stiffness and compliant contact stiffness determined by previous multibody studies are a good starting point for model development.

Finally, future work could include cadaver testing of an intact knee and the same knee with a transected ACL to simulate an ACL tear. Experimental data can then be used to validate models for both an intact and ACL deficient knee.

Appendices

Appendix A

MRI settings

The scan settings for general purpose MRI are given in Table A.1, cartilage imaging in Table A.2 and finally connective tissue imaging in Table A.3.

Table A.1: General purpose MRI scan settings

Sequence	3D T1-weighted without fat suppression - isotropic voxel size
Plane	Sagittal
FS	None
Matrix (phase)	316
Matrix (freq.)	480
No. of slices	320
FOV (mm)	158 x 240
Slice thickness/gap (mm/mm)	0.5/0.0
Flip angle (deg.)	25
TE/TR (ms/ms)	6.01/20
Bandwidth (Hz/pixel)	210
Chemical shift (pixels)	N/A
No. excitations averaged	1
ETL	1
Phase encode axis	Anterior-posterior
Distance factor (%)	N/A
Phase oversampling	0
Slice oversampling	0
Phase resolution	0.5
Phase partial Fourier (8/8 = 1)	OFF
Readout partial Fourier (8/8 = 1)	OFF
Slice partial Fourier (8/8 = 1)	7/8
X-resolution (mm)	0.5
Y-resolution (mm)	0.52
Scan Time (min)	21:18

Table A.2: Cartilage MRI scan settings

Sequence	3D T1-weighted with fat suppression - anisotropic voxel size
Plane	Sagittal
FS	Fat saturation
Matrix (phase)	448
Matrix (freq.)	512
No. of slices	224
FOV (mm)	157 x 180
Slice thickness/gap (mm/mm)	0.7/0.0
Flip angle (deg.)	25
TE/TR (ms/ms)	5.34/29
Bandwidth (Hz/pixel)	210
Chemical shift (pixels)	N/A
No. excitations averaged	1
ETL	1
Phase encode axis	Anterior-posterior
Distance factor (%)	N/A
Phase oversampling	0
Slice oversampling	0
Phase resolution	0.35
Phase partial Fourier (8/8 = 1)	6/8
Readout partial Fourier (8/8 = 1)	OFF
Slice partial Fourier (8/8 = 1)	6/8
X-resolution (mm)	0.35
Y-resolution (mm)	0.35
Scan Time (min)	27:18

Table A.3: Connective tissue MRI scan settings

Sequence	MESE type - axial plane / sagittal plane / coronal plane
Plane	Sagittal
FS	None
Matrix (phase)	432
Matrix (freq.)	512
No. of slices	50
FOV (mm)	151 x 180
Slice thickness/gap (mm/mm)	1.4/1.4
Flip angle (deg.)	90/150
TE/TR (ms/ms)	9.7/10000
Bandwidth (Hz/pixel)	222
Chemical shift (pixels)	N/A
No. excitations averaged	1
ETL	14
Phase encode axis	Anterior-posterior
Distance factor (%)	100%
Phase oversampling	0
Slice oversampling	0
Phase resolution	0.35
Phase partial Fourier (8/8 = 1)	OFF
Readout partial Fourier (8/8 = 1)	OFF
Slice partial Fourier (8/8 = 1)	OFF
X-resolution (mm)	0.35
Y-resolution (mm)	0.39
Scan Time (min)	04:52

Appendix B

Estimation of experimental uncertainty

Experimental uncertainty was determined and compared to RMS errors of simulations as part of model validation in Section 5.1. Estimated accuracy for position is 0.95 mm to 1.90 mm, 1° for orientation, 0.5 N to 1 N for load cell force and 0.05 Nm to 0.5 Nm for load cell moments. The tolerances of transducers and data acquisition devices are given in Table B.1. References for transducer tolerances can be found in the experimental infrastructure specifications on the Open Knee project site¹.

¹[https://simtk.org/plugins/moinmoin/openknee/Infrastructure/Experimentation Mechanics](https://simtk.org/plugins/moinmoin/openknee/Infrastructure/ExperimentationMechanics), last accessed 31 July 2019

Table B.1: Tolerances of experimental measurement devices

Measurement	Lower bound	Upper bound
Position		
Robot position [m]	5.00E-05	3.00E-04
Optotrak Sensor [m]	-	1.00E-04
Digitizer [m]	-	1.00E-04
MRI voxel size [m]	3.50E-04	7.00E-04
Segmentation (based on MRI) [m]	3.50E-04	7.00E-04
Total positional tolerance [m]	0.00095	0.0019
Orientation		
Optotrak sensor angles [°]	0.5	1
Load cell		
Load cell force [N]	0.5	1
Load cell moments [Nm]	0.05	0.05

Appendix C

RMS errors

This Appendix includes the RMS errors for all simulations. The averages of each type of simulation is given in Table 4.1. The tables below show the RMS errors for individual simulations.

Table C.1: RMS errors of individual 30° AP drawer simulations

Model output	Trial 1	Trial 2	Trial 2	Average	σ
Load cell force					
Fx [N]	8.9	10.2	10.1	9.8	0.7
Fy [N]	4.7	4.8	4.5	4.7	0.1
Fz [N]	26.2	26.8	19.4	24.1	4.1
Load cell moment					
Mx [Nm]	2	2.2	1.4	1.9	0.5
My [Nm]	1.2	1.9	1.2	1.4	0.4
Mz [Nm]	1.1	1.3	0.7	1	0.3
KJCS position					
x [mm]	1.5	1.5	1.5	1.5	<0.0
y [mm]	1.1	1.2	1.1	1.1	0.1
z [mm]	2.4	2.5	2.6	2.5	0.1
KJCS orientation					
x [°]	1.8	1.5	1.6	1.6	0.1
y [°]	2.4	2.7	2.8	2.6	0.2
z [°]	1.7	2.1	1.6	1.8	0.3

Table C.2: RMS errors of individual isolated loading simulations

Model output	0°	30°	Average	σ
Load cell force				
Fx [N]	9.2	8.4	8.8	0.5
Fy [N]	4.1	3.4	3.7	0.5
Fz [N]	24	17.8	20.9	4.4
Load cell moment				
Mx [Nm]	2.2	1.9	2.1	0.2
My [Nm]	2.7	2.9	2.8	0.2
Mz [Nm]	2	2.3	2.1	0.2
KJCS position				
x [mm]	3.5	2.2	2.9	0.9
y [mm]	2.3	1.8	2	0.4
z [mm]	1.2	2.4	1.8	0.8
KJCS orientation				
x [°]	3.9	1.6	2.8	1.6
y [°]	2.8	3.3	3.1	0.3
z [°]	2.8	3.7	3.2	0.6

Table C.3: RMS errors of individual combined loading simulations

Model output	0°	30°	Average	σ
Load cell force				
Fx [N]	12.6	12.6	12.6	0.02
Fy [N]	8.1	11.5	9.8	2.45
Fz [N]	26.6	20	23.3	4.64
Load cell moment				
Mx [Nm]	5.4	4.1	4.7	0.92
My [Nm]	5.1	6.1	5.6	0.65
Mz [Nm]	4.1	4.7	4.4	0.39
KJCS position				
x [mm]	4	4.7	4.4	0.5
y [mm]	4.1	4.4	4.2	0.17
z [mm]	2.9	3.5	3.2	0.4
KJCS orientation				
x [°]	7.1	3.5	5.3	2.59
y [°]	5.6	6	5.8	0.29
z [°]	5.9	7	6.5	0.77

Appendix D

Parametric study

This section includes the results of the parametric study that is not included in the main body of the document.

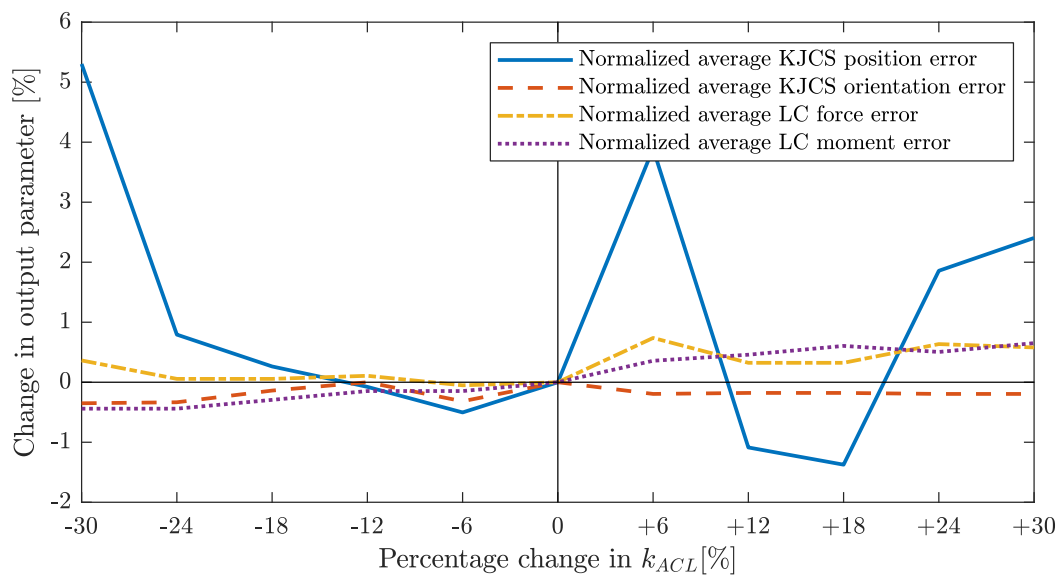


Figure D.1: Percentage change of output parameters relative to changes in ACL stiffness.

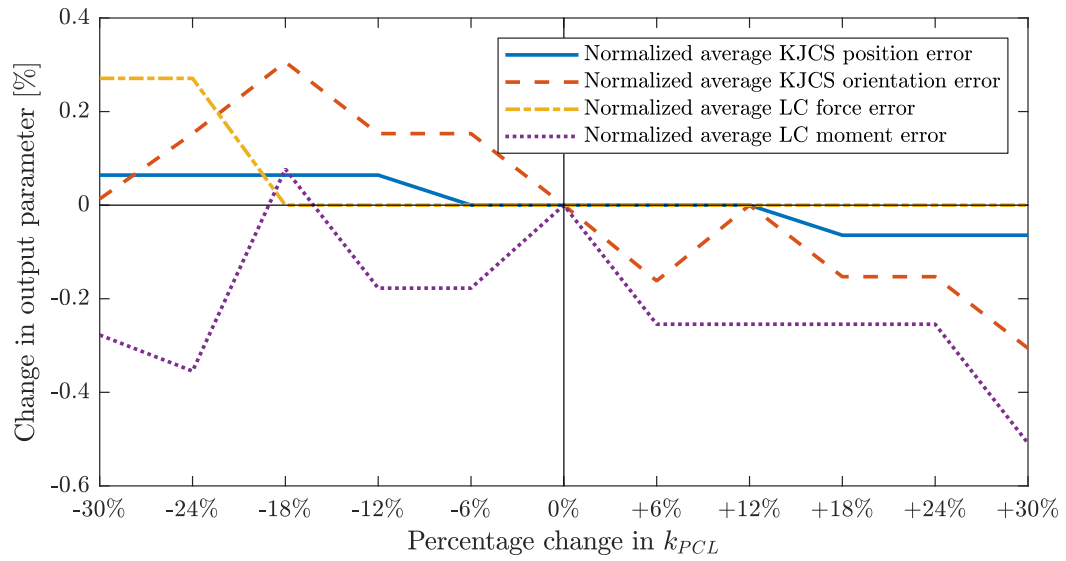


Figure D.2: Percentage change of output parameters relative to changes in PCL stiffness.

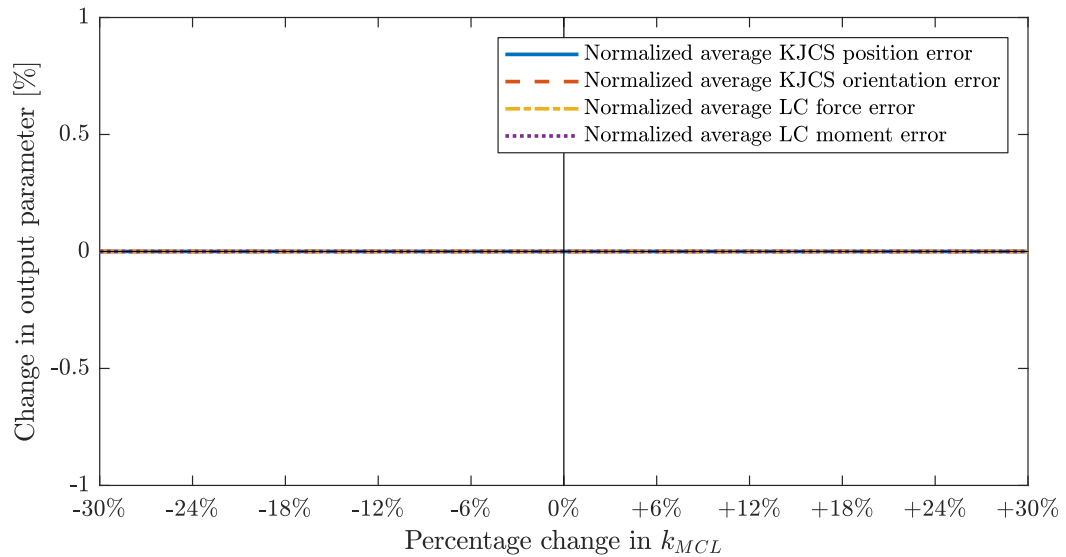


Figure D.3: Percentage change of output parameters relative to changes in MCL stiffness. Changes in MCL stiffness had no effect on model output.

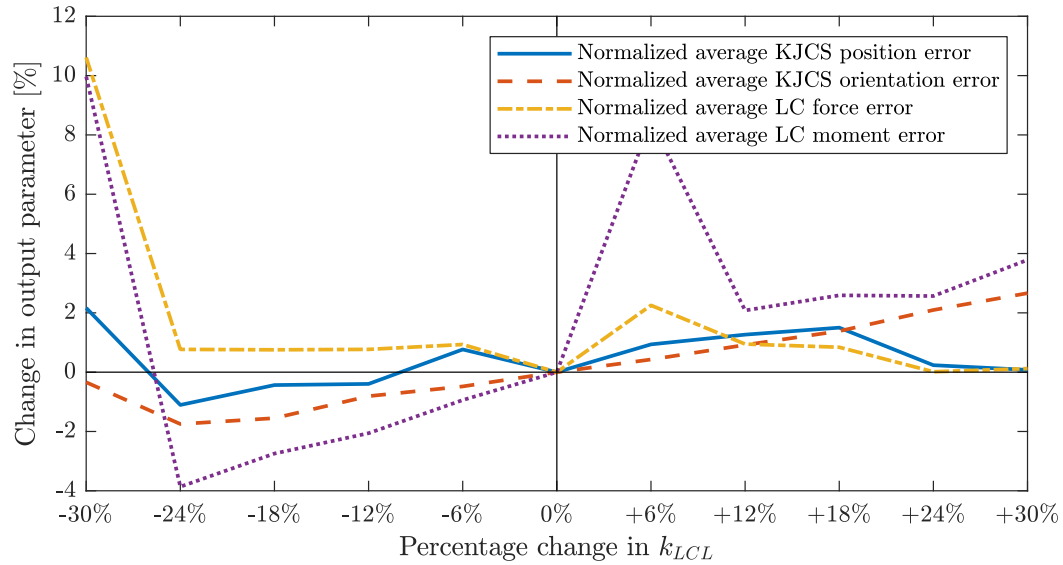


Figure D.4: Percentage change of output parameters relative to changes in LCL stiffness.

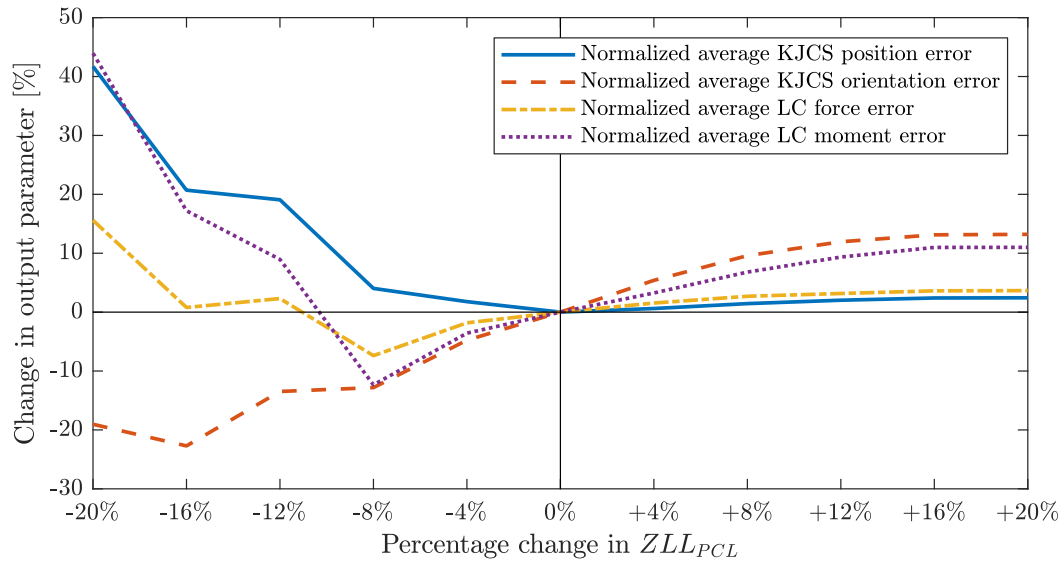


Figure D.5: Percentage change of output parameters relative to changes in PCL zero-load length.

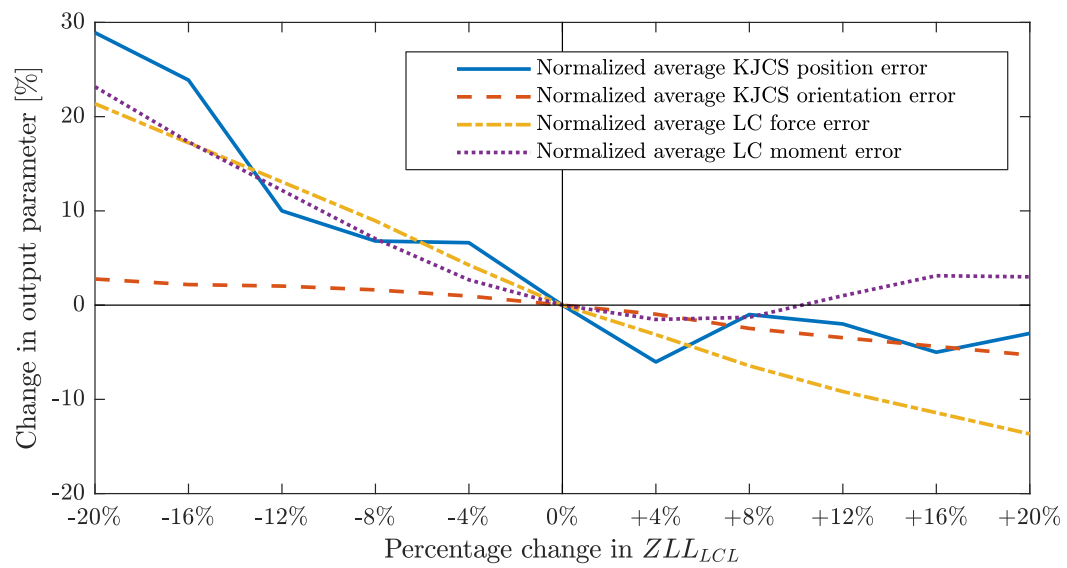


Figure D.6: Percentage change of output parameters relative to changes in LCL zero-load length.

List of References

- Abulhasan, J., Snow, M., Anley, C., Bakhsh, M. and Grey, M. (2016). An Extensive Evaluation of Different Knee Stability Assessment Measures: A Systematic Review. *Journal of Functional Morphology and Kinesiology*, vol. 1, no. 2, pp. 209–229.
- Ali, A.A., Shalhoub, S.S., Cyr, A.J., Fitzpatrick, C.K., Maletsky, L.P., Rullkoetter, P.J. and Shelburne, K.B. (2016). Validation of predicted patellofemoral mechanics in a finite element model of the healthy and cruciate-deficient knee. *Journal of Biomechanics*, vol. 49, no. 2, pp. 302–309. ISSN 18732380. 15334406.
Available at: <http://dx.doi.org/10.1016/j.jbiomech.2015.12.020>
- Amis, A.A. (2012). The functions of the fibre bundles of the anterior cruciate ligament in anterior drawer, rotational laxity and the pivot shift. *Knee Surgery, Sports Traumatology, Arthroscopy*, vol. 20, no. 4, pp. 613–620. ISSN 09422056.
- Arno, S., Bell, C.P., Uquillas, C., Borukhov, I. and Walker, P.S. (2015). Tibiofemoral contact mechanics following a horizontal cleavage lesion in the posterior horn of the medial meniscus. *Journal of Orthopaedic Research*, vol. 33, no. 4, pp. 584–590. ISSN 1554527X.
- Ateshian, G.A. (2009). The role of interstitial fluid pressurization in articular cartilage lubrication. *Journal of Biomechanics*, vol. 42, no. 9, pp. 1163–1176. ISSN 00219290.
- Baldwin, M.A., Clary, C.W., Fitzpatrick, C.K., Deacy, J.S., Maletsky, L.P. and Rullkoetter, P.J. (2012). Dynamic finite element knee simulation for evaluation of knee replacement mechanics. *Journal of Biomechanics*, vol. 45, no. 3, pp. 474–483. ISSN 00219290.
Available at: <http://dx.doi.org/10.1016/j.jbiomech.2011.11.052>
- Baldwin, M.A., Laz, P.J., Stowe, J.Q. and Rullkoetter, P.J. (2009). Efficient probabilistic representation of tibiofemoral soft tissue constraint. *Computer Methods in Biomechanics and Biomedical Engineering*, vol. 12, no. 6, pp. 651–659.
- Bei, Y. and Fregly, B.J. (2004). Multibody dynamic simulation of knee contact mechanics. *Medical Engineering & Physics*, vol. 26, no. 9, pp. 777–789.
- Bennetts, C.J., Chokhandre, S., Donnola, S.B., Flask, C.A., Bonner, T.F., Colbrunn, R.W. and Erdemir, A. (2015). Open Knee(s): magnetic resonance imaging for

- specimen-specific next generation knee models. In: *Summer Biomechanics, Bioengineering and Biotransport Conference*, pp. 3–4. Snowbird Resort, Utah, USA.
- Bertozi, L., Stagni, R., Fantozzi, S. and Cappello, A. (2007). Knee model sensitivity to cruciate ligaments parameters: A stability simulation study for a living subject. *Journal of Biomechanics*, vol. 40, no. SUPPL. 1, pp. 38–44. ISSN 00219290.
- Blankevoort, L. and Huiskes, R. (1991). Ligament-Bone Interaction in a Three-Dimensional Model of the Knee. *Journal of biomechanical engineering*, vol. 113, no. 3, pp. 263–269. ISSN 00219290.
- Blankevoort, L. and Huiskes, R. (1996). Validation of a three-dimensional model of the Knee. *Journal of Biomechanics*, vol. 29, no. 7, pp. 955–961.
- Blankevoort, L., Kuiper, J.H., Huiskes, R. and Grootenboer, H. (1991). Articular contact in a three-dimensional model of the knee. *Journal of Biomechanics*, vol. 24, no. 11, pp. 1019–1031.
- Bloemker, K.H., Guess, T.M., Maletsky, L. and Dodd, K. (2012). Computational Knee Ligament Modeling Using Experimentally Determined Computational Knee Ligament Determined Zero-Load Lengths Modeling Using Experimentally. *The Open Biomedical Engineering Journal*, vol. 6, pp. 33–41.
- Boeth, H., Duda, G.N., Heller, M.O., Ehrig, R.M., Doyscher, R., Jung, T., Moewis, P., Scheffler, S. and Taylor, W.R. (2013). Anterior cruciate ligament-deficient patients with passive knee joint laxity have a decreased range of anterior-posterior motion during active movements. *American Journal of Sports Medicine*, vol. 41, no. 5, pp. 1051–1057. ISSN 03635465.
- Bollen, S.R. (2010). Posteromedial meniscocapsular injury associated with rupture of the anterior cruciate ligament: A previously unrecognised association. *Journal of Bone and Joint Surgery - Series B*, vol. 92, no. 2, pp. 222–223. ISSN 0301620X.
- Bonner, T.F., Colbrunn, R.W., Chokhandre, S., Bennetts, C.J. and Erdemir, A. (2015). Open Knee(s): comprehensive tibiofemoral joint testing for specimen-specific next generation knee models. In: *Summer Biomechanics, Bioengineering, and Biotransport Conference, June 17-20, 2015*, pp. 3–4. Snowbird Resort, Utah, USA.
- Borotikar, B.S. (2009). *Subject specific computational models of the knee to predict anterior cruciate ligament injury*. Ph.D. thesis, Cleveland State University. Available at: http://sfx.scholarsportal.info/western?url{}_ver=Z39.88-2004-{}&rft{}_val{}_fmt=info:ofi/fmt:kev:mtx:dissertation{}&genre=dissertations+{}2526+theses{}&sid=ProQ:ProQuest+Dissertations+{}2526+Theses+Full+Text{}&atitle={}&title=Subject+specific+computational+models+of+the+knee
- Bull, A.M.J., Reilly, P., Wallace, A.L., Amis, A.A. and Emery, R.J.H. (2005). A novel technique to measure active tendon forces: Application to the subscapularis tendon. *Knee Surgery, Sports Traumatology, Arthroscopy*, vol. 13, no. 2, pp.

- 145–150.
Available at: <https://www.scopus.com/inward/record.uri?eid=2-s2.0-16344386264&doi=10.1007%7D2Fs00167-004-0556-y&partnerID=40&md5=6231d1177bc79d4605e01ada6c963912>
- Butler, D., Kay, M. and Stouffer, D. (1986). Comparison Of Material Properties In Fascicle-Bone Units From Human Patellar Tendon and Knee Ligaments. *Journal of Biomechanics*, vol. 19, no. 6, pp. 425–432.
- Butler, D.L., Noyes, F.R. and Grood, E.S. (1980). Ligamentous Restraints to Anterior-Posterior Knee in the Human. *J Bone Joint Surg Am*, vol. 62, no. 2, pp. 259–70.
- Caligaris, M. and Ateshian, G.A. (2008). NIH Public Access. *Osteoarthritis Cartilage*, vol. 16, no. 10, pp. 1220–1227.
- Cerulli, G., Placella, G., Sebastiani, E., Tei, M.M., Speziali, A. and Manfreda, F. (2013). ACL Reconstruction: Choosing the Graft. *Joints*, vol. 1, no. 1, pp. 18–24. ISSN 2512-9090.
Available at: <http://www.ncbi.nlm.nih.gov/pubmed/25606507>
<http://www.pubmedcentral.nih.gov/articlerender.fcgi?artid=PMC4295687>
- Chahla, J., Dean, C.S., Moatshe, G., Mitchell, J.J., Cram, T.R., Yacuzzi, C. and LaPrade, R.F. (2016). Meniscal Ramp Lesions: Anatomy, Incidence, Diagnosis, and Treatment. *Orthopaedic Journal of Sports Medicine*, vol. 4, no. 7, pp. 1–7. ISSN 23259671.
- Chappell, J.D., Creighton, R.A., Giuliani, C., Yu, B. and Garrett, W.E. (2007 feb). Kinematics and electromyography of landing preparation in vertical stop-jump: risks for noncontact anterior cruciate ligament injury. *The American journal of sports medicine*, vol. 35, no. 2, pp. 235–241. ISSN 0363-5465 (Print).
- Cignoni, P., Callieri, M., Corsini, M., Dellepiane, M., Ganovelli, F. and Ranzuglia, G. (2008). MeshLab : an Open-Source Mesh Processing Tool.
- Colbrunn, R.W., Bonner, T.F., Chokhandre, S.K., Bennetts, C.J., Halloran, J. and Erdemir, A. (2015). Open Knee(s): comprehensive patellofemoral joint testing for specimen-specific next generation knee models. In: *39th Annual Meeting of the American Society of Biomechanics*. Columbus, Ohio, USA.
- Crowninshield, R., Johnson, R.J. and Pope, M.H. (1976). AN ANALYTICAL MODEL OF THE KNEE. *Journal of Biomechanics*, vol. 9, pp. 397–405.
- Dargel, J., Gotter, M., Mader, K., Pennig, D., Koebke, J. and Schmidt-Wiethoff, R. (2007). Biomechanics of the anterior cruciate ligament and implications for surgical reconstruction. *Strategies in Trauma and Limb Reconstruction*, vol. 2, no. 1, pp. 1–12. ISSN 18288936.

- Delp, S.L., Anderson, F.C., Arnold, A.S., Loan, P., Habib, A., John, C.T., Guendelman, E. and Thelen, D.G. (2007). OpenSim: Open source to create and analyze dynamic simulations of movement. *IEEE transactions on bio-medical engineering*, vol. 54, no. 11, pp. 1940–1950. ISSN 0018-9294. 15334406.
- Draper, C.E., Besier, T.F., Gold, G.E., Fredericson, M., Fiene, A., Beaupre, G.S. and Delp, S.L. (2006). Is cartilage thickness different in young subjects with and without patellofemoral pain ? *OsteoArthritis and Cartilage*, vol. 14, no. 9, pp. 931–937.
- Duthon, V.B., Barea, C., Abrassart, S., Fasel, J.H., Fritschy, D. and Menetrey, J. (2006 mar). Anatomy of the anterior cruciate ligament. *Knee surgery, sports traumatology, arthroscopy : official journal of the ESSKA*, vol. 14, no. 3, pp. 204–213. ISSN 0942-2056 (Print).
- Eckstein, F., Cicuttini, F., Raynauld, J.P., Waterton, J.C. and Peterfy, C. (2006). Magnetic resonance imaging (MRI) of articular cartilage in knee osteoarthritis (OA): morphological assessment. *OsteoArthritis and Cartilage*, vol. 14, pp. A46–A75.
- Erdemir, A. (2016). Open Knee: Open Source Modeling & Simulation to Enable Scientific Discovery and Clinical Care in Knee Biomechanics. *Journal of Knee Surgery*, vol. 29, no. 2, pp. 107–116.
- Erdemir, A., Bennetts, C., Bonner, T., Chokhandre, S. and Colbrunn, R. (2015). Open Knee(s): Founding Data for Next Generation Knee Models.
- Eskinazi, I. and Fregly, B.J. (2015). Surrogate modeling of deformable joint contact using artificial neural networks. *Medical Engineering and Physics*, vol. 37, no. 9, pp. 885–891. ISSN 18734030.
Available at: <http://dx.doi.org/10.1016/j.medengphy.2015.06.006>
- Eskinazi, I. and Fregly, B.J. (2018). A computational framework for simultaneous estimation of muscle and joint contact forces and body motion using optimization and surrogate modeling. *Medical Engineering and Physics*, vol. 54, pp. 56–64. ISSN 1350-4533.
Available at: <https://doi.org/10.1016/j.medengphy.2018.02.002>
- Faber, S., Eckstein, F., Lukasz, S., Mühlbauer, R., Hohe, J., Englmeier, K.-H. and Reiser, M. (2001). Gender differences in knee joint cartilage thickness , volume and articular surface areas : assessment with quantitative three-dimensional MR imaging. *Skeletal Radiol*, vol. 30, pp. 144–150.
- Finni, T., Komi, P.V. and Lukkariniemi, J. (1998 feb). Achilles tendon loading during walking: application of a novel optic fiber technique. *European Journal of Applied Physiology and Occupational Physiology*, vol. 77, no. 3, pp. 289–291. ISSN 1439-6327.
Available at: <https://doi.org/10.1007/s004210050335>

- Fleming, B.C. and Beynnon, B.D. (2004). In Vivo Measurement of Ligament / Tendon Strains and Forces : A Review. *Annals of Biomedical Engineering*, vol. 32, no. 3, pp. 318–328.
- Fleming, B.C., Good, L., Peura, G.D. and Beynnon, B.D. (1999). Calibration and application of an intra-articular force transducer for the measurement of patellar tendon graft forces: An in situ evaluation. *Journal of Biomechanical Engineering*, vol. 121, no. 4, pp. 393–398.
Available at: <https://www.scopus.com/inward/record.uri?eid=2-s2.0-0032722082&doi=10.1115/1.2798336&partnerID=40&md5=eeee2afe5e72df0642ac97ffe3228153>
- Freeman, M.A. and Pinskerova, V. (2003). The movement of the knee studied by magnetic resonance imaging. *Clinical Orthopaedics and Related Research*, , no. 410, pp. 35–43. ISSN 15281132.
- Fregly, B.J., Besier, T.F., Lloyd, D.G., Delp, S.L., Banks, S.A., Pandy, M.G. and D’Lima, D.D. (2012). Grand Challenge Competition to Predict In Vivo Knee Loads. *Journal of Orthopaedic Research*, vol. 30, no. 4, pp. 503–513. ISSN 08966273. NIHMS150003.
- Fukubayashi, T., Torzilli, P.A., Sherman, M.F. and Warren, R.F. (1982 feb). An in vitro biomechanical evaluation of anterior-posterior motion of the knee. Tibial displacement, rotation, and torque. *The Journal of bone and joint surgery. American volume*, vol. 64, no. 2, pp. 258–264. ISSN 0021-9355 (Print).
- Gabriel, M.T., Wong, E.K., Woo, S.L.-y., Yagi, M. and Debski, R.E. (2004). Distribution of in situ forces in the anterior cruciate ligament in response to rotatory loads. *Journal of Orthopaedic Research*, vol. 22, pp. 8–12.
- Galbusera, F., Freutel, M., Dürselen, L., Aiuto, M.D., Croce, D., Villa, T., Sansone, V. and Innocenti, B. (2014). Material models and properties in the finite element analysis of knee ligaments : a literature review. *Frontiers in Bioengineering and Biotechnology*, vol. 2, no. November, pp. 1–11.
- Godest, A.C., Beaugonin, M., Haug, E., Taylor, M. and Gregson, P.J. (2002). Simulation of a knee joint replacement during a gait cycle using explicit finite element analysis. *Journal of Biomechanics*, vol. 35, pp. 267–275.
- Gollehon, D.L., Torzilli, P.A. and Warren, R.F. (1987 feb). The role of the posterolateral and cruciate ligaments in the stability of the human knee. A biomechanical study. *The Journal of bone and joint surgery. American volume*, vol. 69, no. 2, pp. 233–242. ISSN 0021-9355 (Print).
- Grood, E.S., Hefzy, M.S. and Lindenfield, T.N. (1989). Factors affecting the region of most isometric femoral attachments: Part I: The posterior cruciate ligament. *The American Journal of Sports Medicine*, vol. 17, no. 2, pp. 197–207.
Available at: <https://doi.org/10.1177/036354658901700209>

- Grood, E.S., Noyes, F.R., Butler, D.L. and Suntay, W.J. (1981 oct). Ligamentous and capsular restraints preventing straight medial and lateral laxity in intact human cadaver knees. *The Journal of bone and joint surgery. American volume*, vol. 63, no. 8, pp. 1257–1269. ISSN 0021-9355 (Print).
- Grood, E.S., Stowers, S.F. and Noyes, F.R. (1988 jan). Limits of movement in the human knee. Effect of sectioning the posterior cruciate ligament and posterolateral structures. *The Journal of bone and joint surgery. American volume*, vol. 70, no. 1, pp. 88–97. ISSN 0021-9355 (Print).
- Grood, E.S. and Suntay, W.J. (1983). A Joint Coordinate System for the Clinical Description of Three-Dimensional Motions: Application to the Knee.
Available at: <http://biomechanical.asmedigitalcollection.asme.org/article.aspx?articleid=1396188>
- Guess, T.M., Liu, H., Bhashyam, S. and Thiagarajan, G. (2013). A multibody knee model with discrete cartilage prediction of tibio-femoral contact mechanics. *Computer Methods in Biomechanics and Biomedical Engineering*, vol. 16, no. 3, pp. 256–270.
- Guess, T.M. and Razu, S. (2017). Loading of the medial meniscus in the ACL deficient knee: A multibody computational study. *Medical Engineering and Physics*, vol. 41, pp. 26–34. ISSN 18734030.
- Guess, T.M., Razu, S., Jahandar, H. and Stylianou, A. (2015). Predicted loading on the menisci during gait: The effect of horn laxity. *Journal of Biomechanics*, vol. 48, no. 8, pp. 1490–1498. ISSN 18732380. 15334406.
Available at: <http://dx.doi.org/10.1016/j.jbiomech.2015.01.047>
- Guess, T.M., Razu, S.S., Kuroki, K. and Cook, J.L. (2018 jan). Function of the Anterior Intermeniscal Ligament. *The journal of knee surgery*, vol. 31, no. 1, pp. 68–74. ISSN 1938-2480 (Electronic).
- Guess, T.M. and Stylianou, A. (2012). Simulation of anterior cruciate ligament deficiency in a musculoskeletal model with anatomical knees. *The open biomedical engineering journal*, vol. 6, no. 816, pp. 23–32. ISSN 1874-1207.
Available at: <http://www.pubmedcentral.nih.gov/articlerender.fcgi?artid=3314869&tool=pmcentrez&rendertype=abstract>
- Guess, T.M., Thiagarajan, G., Kia, M. and Mishra, M. (2010). A subject specific multibody model of the knee with menisci. *Medical Engineering and Physics*, vol. 32, no. 5, pp. 505–515. ISSN 13504533.
- Halloran, J., Ackermann, M., Erdemir, A. and van den Bogert, A. (2010). Concurrent musculoskeletal dynamics and finite element analysis predicts altered gait patterns to reduce foot tissue loading. *J Biomech*, vol. 43, no. 14, pp. 2810–5. ISSN 1873-2380. NIHMS150003.
Available at: <http://www.pubmedcentral.nih.gov/articlerender.fcgi?artid=2946980&tool=pmcentrez&rendertype=abstract>

- Halloran, J.P., Easley, S.K., Petrella, A.J. and Rullkoetter, P.J. (2005 oct). Comparison of deformable and elastic foundation finite element simulations for predicting knee replacement mechanics. *Journal of biomechanical engineering*, vol. 127, no. 5, pp. 813–818. ISSN 0148-0731 (Print).
- Halloran, J.P., Erdemir, A. and van den Bogert, A.J. (2009). Adaptive Surrogate Modeling for Efficient Coupling of Musculoskeletal Control and Tissue Deformation Models. *Journal of Biomechanical Engineering*, vol. 131, no. 1, p. 011014. ISSN 01480731.
- Halloran, J.P., Sibole, S., Van Donkelaar, C.C., Van Turnhout, M.C., Oomens, C.W., Weiss, J.A., Guilak, F. and Erdemir, A. (2012). Multiscale mechanics of articular cartilage: Potentials and challenges of coupling musculoskeletal, joint, and microscale computational models. *Annals of Biomedical Engineering*, vol. 40, no. 11, pp. 2456–2474. ISSN 00906964.
- Harris, M.D., Cyr, A.J., Ali, A.A., Fitzpatrick, C.K., Rullkoetter, P.J., Maletsky, L.P. and Shelburne, K.B. (2016). A Combined Experimental and Computational Approach to Subject-Specific Analysis of Knee Joint Laxity. *Journal of Biomechanical Engineering*, vol. 138, no. 8, p. 081004. ISSN 0148-0731.
Available at: <http://biomechanical.asmedigitalcollection.asme.org/article.aspx?doi=10.1115/1.4033882>
- Hefzy, M.S. and Grood, E.S. (1983). An analytical technique for modeling knee joint stiffness-Part II: Ligamentous geometric nonlinearities. *Journal of Biomechanical Engineering*, vol. 105, no. 2, pp. 145–153.
Available at: <https://www.scopus.com/inward/record.uri?eid=2-s2.0-0021070645&doi=10.1115%7D2F1.3138398&partnerID=40&md5=68f810b32f97f5ba0e24a7d153b57552>
- Hefzy, M.S., Grood, E.S. and Noyes, F.R. (1989). Factors affecting the region of most isometric femoral attachments: Part II: The anterior cruciate ligament. *The American Journal of Sports Medicine*, vol. 17, no. 2, pp. 208–216.
Available at: <https://doi.org/10.1177/036354658901700210>
- Holden, J. and Stanhope, S. (1998 jan). The effect of variation in knee center location estimates on net knee joint moments. *Gait & posture*, vol. 7, no. 1, pp. 1–6. ISSN 1879-2219 (Electronic).
- Holden, J.P., Grood, E.S. and Cummings, J.F. (1995). Factors affecting sensitivity of a transducer for measuring anterior cruciate ligament force. *Journal of Biomechanics*, vol. 28, no. 1, pp. 99–102.
Available at: <https://www.scopus.com/inward/record.uri?eid=2-s2.0-0028958365&doi=10.1016%7D2F0021-9290%7D2895%7D2980011-5&partnerID=40&md5=7493309111e24442f395493cb893d3b9>
- Holden, J.P., Grood, E.S., Korvick, D.L., Cummings, J.F., Butler, D.L. and Bylski-Austrow, D.I. (1994). In vivo forces in the anterior cruciate ligament: Direct measurements during walking and trotting in a quadruped. *Journal of*

- Biomechanics*, vol. 27, no. 5, pp. 517–519, 521–526.
Available at: <https://www.scopus.com/inward/record.uri?eid=2-s2.0-0028434083&doi=10.1016%7D2F0021-9290%7D2894%7D2990063-9%7DpartnerID=40%7Dmd5=5baec92eb0b290ef5a812ed66a4d978d>
- Hosseini, A., Qi, W., Tsai, T.Y., Liu, Y., Rubash, H. and Li, G. (2015). In vivo length change patterns of the medial and lateral collateral ligaments along the flexion path of the knee. *Knee Surgery, Sports Traumatology, Arthroscopy*, vol. 23, no. 10, pp. 3055–3061. ISSN 14337347.
- Kanamori, A., Woo, S.L.-Y., Ma, C.B., Zeminski, J., Rudy, T.W., Li, G. and Livesay, G.A. (2000). The forces in the anterior cruciate ligament and knee kinematics during a simulated pivot shift test: A human cadaveric study using robotic technology. *Arthroscopy*, vol. 16, no. 6, pp. 633–639. ISSN 07498063.
- Kia, M., Schafer, K., Lipman, J., Cross, M., Mayman, D., Pearle, A., Wickiewicz, T. and Imhauser, C. (2016). A Multibody Knee Model Corroborates Subject-Specific Experimental Measurements of Low Ligament Forces and Kinematic Coupling During Passive Flexion. *Journal of Biomechanical Engineering*, vol. 138, no. 5, p. 051010. ISSN 0148-0731.
Available at: <http://biomechanical.asmedigitalcollection.asme.org/article.aspx?doi=10.1115/1.4032850>
- Kiapour, A., Kiapour, A.M., Kaul, V., Quatman, C.E., Wordeman, S.C. and Hewett, T.E. (2014). Finite Element Model of the Knee for Investigation of Injury Mechanisms : Development and Validation. *Journal of Biomechanical Engineering*, vol. 136, no. January, pp. 1–14.
- Kluess, D., Souffrant, R., Mittelmeier, W., Wree, A., Schmitz, K.-p. and Bader, R. (2009). A convenient approach for finite-element-analyses of orthopaedic implants in bone contact : Modeling and experimental validation. *Computer Methods and Programs in Biomedicine*, vol. 5, pp. 23–30.
- Knoll, Z., Kocsis, L. and Kiss, R.M. (2004 jan). Gait patterns before and after anterior cruciate ligament reconstruction. *Knee surgery, sports traumatology, arthroscopy : official journal of the ESSKA*, vol. 12, no. 1, pp. 7–14. ISSN 0942-2056 (Print).
- Lin, Y.-c., Haftka, R.T., Queipo, N.V. and Fregly, B.J. (2010a). Surrogate articular contact models for computationally efficient multibody dynamic simulations. *Medical Engineering and Physics*, vol. 32, no. 6, pp. 584–594. ISSN 1350-4533.
Available at: <http://dx.doi.org/10.1016/j.medengphy.2010.02.008>
- Lin, Y.C., Walter, J.P., Banks, S.A., Pandy, M.G. and Fregly, B.J. (2010b). Simultaneous prediction of muscle and contact forces in the knee during gait. *Journal of Biomechanics*, vol. 43, no. 5, pp. 945–952. ISSN 00219290.
Available at: <http://dx.doi.org/10.1016/j.jbiomech.2009.10.048>

- Lohmander, L.S., Englund, P.M., Dahl, L.L. and Roos, E.M. (2007 oct). The long-term consequence of anterior cruciate ligament and meniscus injuries: osteoarthritis. *The American journal of sports medicine*, vol. 35, no. 10, pp. 1756–1769. ISSN 1552-3365 (Electronic).
- Macaulay, A.A., Perfetti, D.C. and Levine, W.N. (2012). Anterior cruciate ligament graft choices. *Sports Health*, vol. 4, no. 1, pp. 63–68. ISSN 19417381.
- Machado, M., Flores, P., Claro, J.C., Ambrósio, J., Silva, M., Completo, A. and Lankarani, H.M. (2010). Development of a planar multibody model of the human knee joint. *Nonlinear Dynamics*, vol. 60, no. 3, pp. 459–478. ISSN 0924090X.
- Marieswaran, M., Jain, I., Garg, B., Sharma, V. and Dinesh, K. (2018). A review on biomechanics of anterior cruciate ligament and materials for reconstruction. *Applied Bionics and Biomechanics*, vol. 2018, pp. 1–38. ISSN 1176-2322.
- Markolf, K., Burchfield, D., Shapiro, M., Shepard, M., Finerman, G. and Slauterbeck, J. (1995). Combined knee loading states that generate high anterior cruciate ligament forces. *Journal of Orthopaedic Research*, vol. 13, no. 6, pp. 930–935. Available at: <https://www.ncbi.nlm.nih.gov/pubmed/8544031>
- Markolf, K.L., Bargar, W.L., Shoemaker, S.C. and Amstutz, H.C. (1981). The role of joint load in knee stability. *Journal of Bone and Joint Surgery - Series A*, vol. 63, no. 4, pp. 570–585. Available at: <https://www.scopus.com/inward/record.uri?eid=2-s2.0-0019498846&doi=10.2106%2F00004623-198163040-00007&partnerID=40&md5=4dc3d7350a2705733a743a2910b49173>
- Markolf, K.L., Feeley, B.T., Tejwani, S.G., Martin, D.E. and McAllister, D.R. (2006). Changes in Knee Laxity and Ligament Force After Sectioning the Posteromedial Bundle of the Posterior Cruciate Ligament. *Arthroscopy - Journal of Arthroscopic and Related Surgery*, vol. 22, no. 10, pp. 1100–1106. ISSN 07498063.
- Markolf, K.L., Mensch, J.S. and Amstutz, H.C. (1976). Stiffness and laxity of the knee: the contributions of the supporting structures. A quantitative in vitro study. *Journal of Bone and Joint Surgery - Series A*, vol. 58, no. 5, pp. 583–594. Available at: <https://www.scopus.com/inward/record.uri?eid=2-s2.0-0017130024&doi=10.2106%2F00004623-197658050-00001&partnerID=40&md5=e4799d31acd22fd26debae497aa8d4b6>
- Markolf, K.L., O’Neill, G., Jackson, S.R. and McAllister, D.R. (2004). Effects of applied quadriceps and hamstrings muscle loads on forces in the anterior and posterior cruciate ligaments. *American Journal of Sports Medicine*, vol. 32, no. 5, pp. 1144–1149. ISSN 03635465.
- Markolf, K.L., Park, S., Jackson, S.R. and McAllister, D.R. (2008). Contributions of the Posterolateral Bundle of the Anterior Cruciate Ligament to Anterior-Posterior Knee Laxity and Ligament Forces. *Arthroscopy - Journal of Arthroscopic and Related Surgery*, vol. 24, no. 7, pp. 805–809. ISSN 07498063.

- Martini, F.H., Timmons, M.J. and Tallitsch, R.B. (2012). *Human Anatomy Seventh Edition*. 7th edn. Pearson Education Inc. ISBN 9780321688156.
- Nasab, S.H.H., List, R., Oberhofer, K., Fucentese, S.F., Snedeker, J.G. and Taylor, W.R. (2016). Loading patterns of the posterior cruciate ligament in the healthy knee: A systematic review. *PLoS ONE*, vol. 11, no. 11, pp. 1–28. ISSN 19326203.
- Nielsen, S. and Helmig, P. (1986a). Posterior instability of the knee joint - An experimental study. *Archives of Orthopaedic and Traumatic Surgery*, vol. 105, no. 2, pp. 121–125.
Available at: <https://www.scopus.com/inward/record.uri?eid=2-s2.0-0023003412&doi=10.1007%2F00455846&partnerID=40&md5=de69e3401a0c848de451222df1e6eece>
- Nielsen, S. and Helmig, P. (1986b). The static stabilizing function of the popliteal tendon in the knee - An experimental study. *Archives of Orthopaedic and Traumatic Surgery*, vol. 104, no. 6, pp. 357–362.
Available at: <https://www.scopus.com/inward/record.uri?eid=2-s2.0-0022640251&doi=10.1007%2F00454430&partnerID=40&md5=a55e40707e89c611a8c024ec354defbc>
- Noble, L.D., Colbrunn, R.W., Lee, D.G., Van Den Bogert, A.J. and Davis, B.L. (2010). Design and validation of a general purpose robotic testing system for musculoskeletal applications. *Journal of Biomechanical Engineering*, vol. 132, no. 2. ISSN 01480731.
- Noyes, F.R., Huser, L.E. and Levy, M.S. (2017). Rotational Knee Instability in ACL-Deficient Knees. *The Journal of Bone and Joint Surgery*, vol. 99, no. 4, pp. 305–314. ISSN 0021-9355.
- Ohori, T., Mae, T., Shino, K., Tachibana, Y., Fujie, H., Yoshikawa, H. and Nakata, K. (2017). Varus-valgus instability in the anterior cruciate ligament-deficient knee: effect of posterior tibial load. *Journal of Experimental Orthopaedics*, vol. 4, no. 1.
- Oungoulian, S.R., Durney, K.M., Jones, B.K., Ahmad, C.S., Clark, T. and Ateshian, G.A. (2016). Oungoulian et al 2015 _Wear and damage of articular cartilage with friction against orth implant mater.pdf. *J Biomech*, vol. 48, no. 10, pp. 1957–1964.
- Pandy, M.G. and Andriacchi, T. (2010). Muscle and Joint Function in Human Locomotion. *Annual review of biomedical engineering*, vol. 12, pp. 401–433.
- Papageorgiou, C.D., Gil, J.E., Kanamori, A., Fenwick, J.A., Woo, S.L.-Y. and Fu, F.H. (2001). The Biomechanical Interdependence between the Anterior Cruciate Ligament Replacement Graft and the Medial Meniscus. *The American Journal of Sports Medicine*, vol. 29, no. 2, pp. 226–231.
Available at: <https://doi.org/10.1177/03635465010290021801>
- Park, S.E., DeFrate, L.E., Suggs, J.F., Gill, T.J., Rubash, H.E. and Li, G. (2005). The change in length of the medial and lateral collateral ligaments during in vivo knee flexion. *The Knee*, vol. 12, no. 5, pp. 377–382. ISSN 0968-0160.

- Available at: <http://www.sciencedirect.com/science/article/pii/S0968016005000190>
- Piazza, S.J. and Delp, S.L. (2001 jul). Three-Dimensional Dynamic Simulation of Total Knee Replacement Motion During a Step-Up Task. *Journal of Biomechanical Engineering*, vol. 123, no. 6, pp. 599–606. ISSN 0148-0731.
Available at: <http://dx.doi.org/10.1115/1.1406950>
- Platt, D., Wilson, A.M., Timbs, A., Wright, I.M. and Goodship, A.E. (1994). Novel force transducer for the measurement of tendon force in vivo. *Journal of Biomechanics*, vol. 27, no. 12, pp. 1489–1493.
Available at: <https://www.scopus.com/inward/record.uri?eid=2-s2.0-0028630508&doi=10.1016%7D2F0021-9290%7D2894%7D2990198-8%7DpartnerID=40%7Dmd5=1b12a10c863e31e94bfa2383997c1b04>
- Race, A. and Amis, A.A. (1994). The mechanical properties of the two bundles of the human posterior cruciate ligament. *Journal of Biomechanics*, vol. 27, no. 1, pp. 13–24. ISSN 00219290.
- Roriz, P., Carvalho, L., Frazão, O. and Luís, J. (2014). From conventional sensors to fibre optic sensors for strain and force measurements in biomechanics applications : A review. *Journal of Biomechanics*, vol. 47, no. 6, pp. 1251–1261. ISSN 0021-9290.
Available at: <http://dx.doi.org/10.1016/j.jbiomech.2014.01.054>
- Sakane, M., Livesay, G.A., Fox, R.J., Rudy, T.W., Runco, T.J. and Woo, S.L.-Y. (1999). Relative contribution of the ACL, MCL, and bony contact to the anterior stability of the knee. *Knee Surgery, Sports Traumatology, Arthroscopy*, vol. 7, no. 2, pp. 93–97. ISSN 0942-2056.
- Schmitz, A. and Piovesan, D. (2016a). Development of an open-source cosimulation method of the knee. *Proceedings of the Annual International Conference of the IEEE Engineering in Medicine and Biology Society, EMBS*, vol. 2016-October, pp. 6034–6037. ISSN 1557170X.
- Schmitz, A. and Piovesan, D. (2016b). Development of an Open-Source, Discrete Element Knee Model. *IEEE Transactions on Biomedical Engineering*, vol. 63, no. 10, pp. 2056–2067. ISSN 15582531.
- Seering, W.P., Piziali, R.L., Nagel, D.A. and Schurman, D.J. (1980). The function of the primary ligaments of the knee in varus-valgus and axial rotation. *Journal of Biomechanics*, vol. 13, no. 9, pp. 785–794. ISSN 0021-9290.
Available at: <http://www.sciencedirect.com/science/article/pii/0021929080902407>
- Seth, A., Sherman, M., Eastman, P. and Delp, S. (2010). Minimal formulation of joint motion for biomechanisms. *Nonlinear Dynamics*, vol. 62, pp. 291–303.

- Shelburne, K.B., Torry, M.R. and Pandy, M.G. (2005). Muscle, ligament, and joint-contact forces at the knee during walking. *Medicine and Science in Sports and Exercise*, vol. 37, no. 11, pp. 1948–1956. ISSN 01959131. 1207.7235.
- Shimokochi, Y. and Shultz, S.J. (2008). Mechanisms of noncontact anterior cruciate ligament injury. *Journal of Athletic Training*, vol. 43, no. 4, pp. 396–408. ISSN 10626050.
- Shoemaker, S.C. and Markolf, K.L. (1985 jan). Effects of joint load on the stiffness and laxity of ligament-deficient knees. An in vitro study of the anterior cruciate and medial collateral ligaments. *The Journal of bone and joint surgery. American volume*, vol. 67, no. 1, pp. 136–146. ISSN 0021-9355 (Print).
- Shultz, S.J., Schmitz, R.J., Benjaminse, A., Collins, M., Ford, K. and Kulas, A.S. (2015). ACL research retreat VII: An update on anterior cruciate ligament injury risk factor identification, screening, and prevention March 19-21, 2015; Greensboro, nc. *Journal of Athletic Training*, vol. 50, no. 10, pp. 1076–1093. ISSN 10626050. NIHMS150003.
- Smith, C.R., Lenhart, R.L., Kaiser, J., Vignos, M. and Darryl, G. (2017). Influence of Ligament Properties on Knee Mechanics in Walking. vol. 29, no. 2, pp. 99–106.
- Smith, J.P. and Barrett, G.R. (2001). Medial and Lateral Meniscal Tear Patterns in Anterior Cruciate Ligament-Deficient Knees: A Prospective Analysis of 575 Tears. *The American Journal of Sports Medicine*, vol. 29, no. 4, pp. 415–419. Available at: <https://doi.org/10.1177/03635465010290040501>
- Stephen, J.M., Halewood, C., Kittl, C., Bollen, S.R., Williams, A. and Amis, A.A. (2016). Posteromedial Meniscocapsular Lesions Increase Tibiofemoral Joint Laxity With Anterior Cruciate Ligament Deficiency, and Their Repair Reduces Laxity. *The American Journal of Sports Medicine*, vol. 44, no. 2, pp. 400–408. Available at: <https://doi.org/10.1177/0363546515617454>
- Thelen, D.G., Schmitz, A.M. and Choi, K.W. (2014). Co-Simulation of Neuromuscular Dynamics and Knee Mechanics During Human Walking. *Journal of Biomechanical Engineering*, vol. 136, no. February, pp. 1–8.
- Tillman, M.D., Smith, K.R., Bauer, J.A., Cauraugh, J.H., Falsetti, A.B. and Patishall, J.L. (2002 feb). Differences in three intercondylar notch geometry indices between males and females: a cadaver study. *The Knee*, vol. 9, no. 1, pp. 41–46. ISSN 0968-0160 (Print).
- Trad, Z., Barkaoui, A., Chafra, M. and Tavares, J.M.R.S. (2018). *FEM Analysis of the Human Knee Joint A Review*. 1st edn. Springer International Publishing. ISBN 9783319741574.
- Vedi, V., Williams, A., Tennant, S.J., Spouse, E., Hunt, D.M. and Gedroyc, W.M.W. (1999). Meniscal movement. *The Journal of Bone and Joint Surgery*, vol. 81, no. 1, pp. 37–41. ISSN 0301620X.

- Walker, P.S., Arno, S., Bell, C., Salvadore, G., Borukhov, I. and Oh, C. (2015). Function of the medial meniscus in force transmission and stability. *Journal of Biomechanics*, vol. 48, no. 8, pp. 1383–1388. ISSN 18732380. Available at: <http://dx.doi.org/10.1016/j.jbiomech.2015.02.055>
- Walter, J.P. and Pandy, M.G. (2017). Dynamic simulation of knee-joint loading during gait using force-feedback control and surrogate contact modelling. *Medical Engineering and Physics*, vol. 48, pp. 196–205. ISSN 18734030.
- Weiss, J.A. and Gardiner, J.C. (2001). Computational Modeling of Ligament Mechanics. *Critical Reviews in Biomedical Engineering*, vol. 29, no. 3, pp. 303–371. ISSN 0278-940X. arXiv:1011.1669v3. Available at: <http://www.dl.begellhouse.com/journals/4b27cbfc562e21b8,60a599ed4591de34,4df7cd705d560f83.html>
- Wetters, N., Weber, A.E., Wuerz, T.H., Schub, D.L. and Mandelbaum, B.R. (2015). Mechanism of Injury and Risk Factors for Anterior Cruciate Ligament Injury. *Operative Techniques in Sports Medicine*, vol. 24, no. 1, pp. 2–6. ISSN 1060-1872. Available at: <http://dx.doi.org/10.1053/j.otsm.2015.09.001>
- Wismans, J., Veldpaus, F. and Janssen, J. (1980). A THREE-DIMENSIONAL MATHEMATICAL OF THE KNEE-JOINT. *Journal of Biomechanics*, vol. 13, pp. 677–685.
- Woo, S.L.-Y., Debski, R.E., Withrow, J.D. and Janaushek, M.A. (1999). Biomechanics of Knee Ligaments. *American Journal of Sports Medicine*, vol. 27, no. 4, pp. 533–543.
- Woo, S.L.-Y., Kanamori, A., Zeminski, J., Yagi, M., Papageorgiou, C. and Freddie H. Fu (2002). Journal of bone and joint surgery. American volume. *The Journal of bone and joint surgery*, p. 8. ISSN 0021-9355.
- Wouda, F.J., Giuberti, M., Bellusci, G., Maartens, E., Reenalda, J., Beijnum, B.-j.F.V. and Veltink, P.H. (2018). Estimation of Vertical Ground Reaction Forces and Sagittal Knee Kinematics During Running Using Three Inertial Sensors. *Frontiers in Physiology*, vol. 9, no. March, pp. 1–14.
- Xu, Z., Luo, Z., Ren, L., Wang, K. and Hu, D. (2017). Three-dimensional human modeling and dynamics simulation based on ADAMS. In: *Proceedings - 9th International Conference on Intelligent Human-Machine Systems and Cybernetics, IHMSC 2017*, vol. 2, pp. 354–358. ISBN 9781538630228.
- Yang, Z., Wickwire, A.C. and Debski, R.E. (2010). Development of a subject-specific model to predict the forces in the knee ligaments at high flexion angles. *Medical and Biological Engineering and Computing*, vol. 48, no. 11, pp. 1077–1085. ISSN 01400118.
- Zavatsky, A.B. (1997). A kinematic-freedom analysis of a flexed-knee-stance testing rig. *Journal of Biomechanics*, vol. 30, no. 3, pp. 277–280. ISSN 0021-9290.

Available at: <http://www.sciencedirect.com/science/article/pii/S002192909600142X>